Instituto Tecnológico y de Estudios Superiores de Monterrey

Campus Monterrey

School of Engineering and Sciences

Self-Assembly Behavior of Amphiphilic Janus Dendrimers in Water: A Combined Experimental and Coarse-Grained Molecular Dynamics Simulation Approach

A dissertation presented by

Mariana Estefanía Elizondo García

Submitted to the
School of Engineering and Sciences
in partial fulfillment of the requirements for the degree of

Doctor

in

Biotechnology

Monterrey Nuevo León, May 14th, 2018

Dedication

Dedicated to my parents. Thank you for your love, patience and unconditional support. This work could not have been possible without you.

Acknowledgments

To my principal advisor, Dr. Jesús Ángel Valencia Gallegos, for trust in me for the development of this work. The freedom that he gave me to carry out the research made me grow as a student and a researcher.

To my co-advisor, Dr. Marcelo Videa Vargas, for accepting to collaborate on this project and for your help and advice during the thermal analysis studies.

To the dissertation committee members, Dr. Janet Gutierrez Uribe and Dr. Jorge Cortés Ramirez, for their guidance, suggestions, and comments, which helped in the improvement of this thesis work. Also, for the patience and availability, they always had with me.

To Dr. Fernando Danilo González Nilo for his support in advising, reviewing and improving this project. Also, for giving me the opportunity to make a research stay at the Center for Bioinformatics and Integrative Biology (CBIB) and allowing me to meet his great group and learn from them. To all the CBIB community for their kindness and hospitality during my stay in Chile. To Ingrid Araya, Camila Navas, and Valeria Marquez, for their support and guidance in the molecular dynamics simulations.

I would like to express my gratitude to Dr. Luis Elizalde Herrera from Centro de Investigación en Química Aplicada, for his help running the NMR spectra; MSc. Gloria Macedo Raygoza and Dr. Miguel J. Beltrán García from Universidad Autónoma de Guadalajara, for their help in the measuring of MALDI-TOF mass spectra; MSc. Luis Montes de Oca, MSc. Maricela Rodríguez Nieto and Jorge Luis Menchaca from Universidad Michoacana de San Nicolás de Hidalgo and Universidad Autónoma de Nuevo León, for their collaboration in microfluidics experiments and their help with the

Self-Assembly Behavior of Amphiphilic Janus Dendrimers in Water: A Combined Experimental and Coarse-Grained Molecular Dynamics Simulation Approach

by

Mariana Estefanía Elizondo García

Abstract

Amphiphilic Janus dendrimers (JDs) are repetitively branched molecules with hydrophilic and hydrophobic components that self-assemble in water to form a variety of morphologies, including vesicles analogous to liposomes with potential pharmaceutical and medical application. To date, the self-assembly of JDs has not been fully investigated thus it is important to gain insight into its mechanism and dependence on JDs' molecular structure. In this study, a series of amphiphilic JDs with variations in their core and branching pattern was synthesized and its aggregation behavior in water was evaluated using experimental and computational methods. JDs were obtained from 2,2-bis(hydroxymethyl)propionic acid, myristic acid and different glycols. Dispersions of JDs in water were carried out using the thin-film hydration, solvent injection methods and by microfluidics, using double emulsion drops with ultrathin shells as templates. Furthermore, a coarse-grained molecular dynamics (CG-MD) simulation was performed to study the mechanism of JDs aggregation. The resulting assemblies were characterized by optical microscopy, dynamic light scattering, confocal microscopy, and atomic force microscopy. The obtaining of assemblies in water with no interdigitated bilayers was confirmed by the experimental characterization and CG-MD simulation for one of the dendrimers. Assemblies with dendrimersome characteristics were obtained using the solvent injection method. Also, monodisperse nanometric assemblies were obtained by this method. The use of microfluidics enables the production of giant dendrimersomes from highly hydrophobic JDs, even when the dendrimers did not form vesicles using the thin-film hydration method. The results of this study establish a relationship between the molecular structure of the JDs and the properties of its aggregates in water. These results could be relevant for the design of novel JDs with tailored assemblies suitable for drug delivery systems. In addition, this study offers an approach to produce dendrimersomes in a more controlled way.

Keywords: Janus dendrimers; amphiphilic; self-assembly; dendrimersome; coarse-grained molecular dynamics; microfluidics; thin-film hydration method; solvent injection method.

Contents

List of Figures

List of Tables

List of Equations

List of Abbreviations and Units of Measurement

[G-1]	First generation
[G-2]	Second generation
[G-3]	Third generation
°C	Celsius
^{13}C-NMR	Carbon nuclear magnetic resonance
^{1}H-NMR	Proton nuclear magnetic resonance
AFM	Atomic force microscopy
ANOVA	Analysis of variance
Bis-MPA	2,2-bis(hydroxymethyl)propionic acid
CDCl$_3$	Deuterated chloroform
CG-MD	Coarse-grained molecular dynamics
cm^2	Square centimeters
CuAAc	Copper-catalyzed alkyne-azide cycloaddition
DCC	*N,N'*-dicyclohexylcarbodiimide
DCM	Dichloromethane
DD	1,10-decanediol
DLS	Dynamic light scattering
DPTS	4-(dimethylamino)pyridinium *p*-toluenesulfonate
DSC	Differential scanning calorimetry
EG	Ethylene glycol
ESEM	Environmental scanning electron microscopy
EtOAc	Ethyl acetate
fs	Femtoseconds
g	Grams
Gly	Glycine
h	Hours
HLB	Hydrophilic-lipophilic balance
JDs	Janus dendrimers
K	Kelvins

kDa	Kilodaltons
kJ/mol	Kilojoules per mole
kJ/mol°C	Kilojoules per mole celsius
kJ/(mol nm)	Kilojoules per mole per nanometer
L-Ala	L-Alanine
L-Asp	L-Aspartate
L-Glu	L-Glutamate
LCTEM	Liquid-cell transmission electron microscopy
MALDI-TOF	Matrix assisted laser desorption/ionization time-of-flight
MeOH	Methanol
mg/mL	Milligram per milliliter
MHz	Megahertz
mL	Milliliters
mM	Millimolar
mmol	Millimole
mV	Millivolts
MS	Mass spectrometry
MW	Molecular weight
MΩ.cm	Megaohms centimeter
N	Newtons
nm	Nanometer
Pd/C	Palladium on carbon
PAMAM	Polyamidoamine
PDI	Polydispersity index
PEG	Poly(ethylene glycol)
ppm	Parts per million
PVA	Poly(vinyl alcohol)
Ref.	Reference
s	Seconds
SASA	Solvent accessible surface area

TEG	Triethylene glycol
TEM	Transmission Electron Microscopy
Tg	Glass transition temperature
THF	Tetrahydrofuran
TLC	Thin Layer Chromatography
Tm	Melting temperature
v/v	Volume by volume
w/w	Weight by weight
W/O/W	Water-in-oil-in-water
µL	Microliters
µL/h	Microliters per hour
µm	Micrometers
µs	Microseconds

Chapter 1

Introduction

In recent years, interest in the development of new materials for drug delivery, and other therapeutic and diagnostic applications has been increased. This interest is motivated mainly by the problematic properties of potentially useful low-weight drug candidates, such as low solubility in water and bioavailability, rapid elimination, high toxicity and side effects [1]. Drug delivery systems offer an alternative to optimize the pharmacokinetics and pharmacodynamics of these kinds of compounds.

Amphiphilic Janus dendrimers (JDs) are molecules composed of polar (hydrophilic) and non-polar (hydrophobic) dendritic blocks [2]. This characteristic is the key factor that favors the spontaneous self-assembly of JDs in water into complex supramolecular structures [3]. Variations in the molecular structure of JDs allows achieving a rich palette of morphologies in water, among which are bilayered vesicles termed as dendrimersomes [4].

Dendrimersomes possess characteristics that make them ideal vehicles for drug delivery and as diagnostic or theranostic agents. They are monodisperse, stable up to one year in various media and can encapsulate both hydrophilic and/or hydrophobic species [5–9]. In addition, they exhibit mechanical properties as good as their analogous polymersomes and cholesterol stabilized liposomes [10].

Despite these advantages, the information about dendrimersomes is still limited and is mainly focused on one type of JDs (Percec-type). Recent alternatives to Percec-type structures involve dendrimers obtained from click chemistry reactions, which incorporate more complex, and in some cases, more flexible molecules as cores, in comparison

with Percec-type dendrimers [3,11,12]. Thus, it is important to evaluate if these variations in the core of the amphiphilic JDs influences in their self-assembly ability in aqueous media, as well as in the generation of stable vesicles; and if this core effect has an interaction with the branching pattern of the hydrophobic and hydrophilic blocks of the dendrimer. Previous studies reported that the incorporation of molecules that can form hydrogen bonds (amino acids) to the core of the JDs generate changes in bilayer thickness, size, and lamellarity of the assemblies [13,14]. Nevertheless, the effect of the core length and its polarity has not been studied. This information could be relevant for the design of novel JDs with tailored assemblies suitable for drug delivery systems.

Therefore, the aim of this work was to establish a relationship between the molecular structure of JDs and the properties of their assemblies in water. In order to study the impact of the molecular structure of the JDs in the self-assembly structures, a series of dendrimers with variations in the core and the number of generation were synthesized and characterized. These dendrimers were obtained from 2,2-bis(hydroxymethyl)propionic acid (bis-MPA), myristic acid, and different glycols. The self-assembly behavior of JDs in water was evaluated using experimental and computer simulation methods. In addition, the morphology, physical properties, and stability as a function of time and temperature of the self-assembly structures were evaluated.

Chapter 2

Theoretical Framework

2.1 Dendrimers

Dendrimers (Figure 2.1) are geometric polymeric structures that are prepared through the consecutive addition of monomeric multifunctional units around a central core with the aim to form tree-like structures (dendrimer from the Greek dendron that means tree). The core can be formed by any functional monomer and by at least two functional groups that allow the union of additional layers or generations, which constitute the majority of the dendrimer. The step-wise synthesis of dendrimers affords a high degree of control over the positioning of chemical functionalities at the nanoscale [9].
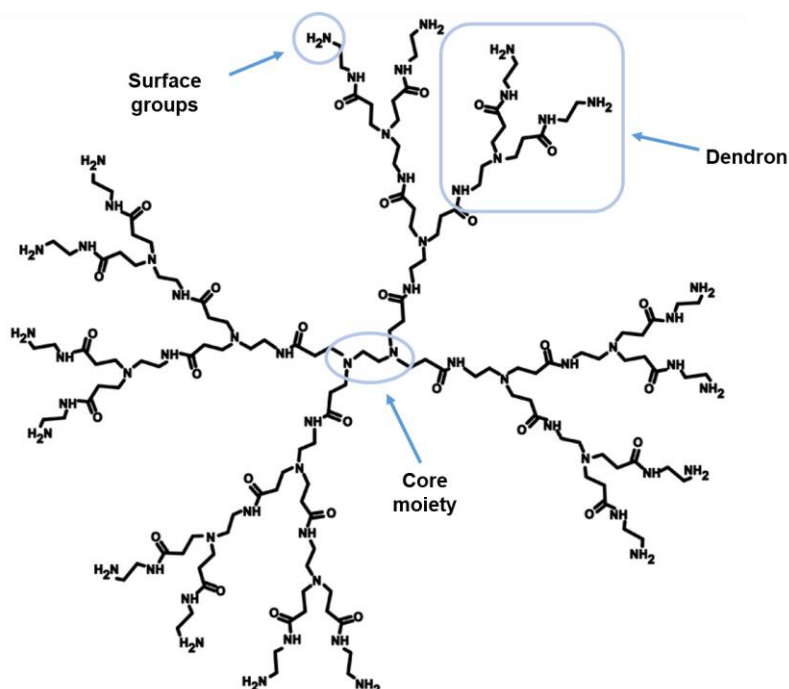
Figure 2.1 Second generation polyamidoamine (PAMAM) dendrimer.

Dendrimers are constructed iteratively step-by-step by either divergent or convergent growth approach (Figure 2.2) [15]. Divergent synthesis is a widely adopted method for dendrimer obtaining, where the molecule is growth radially from a multifunctional core through sequential activation and condensation reactions [16,17]. A significant feature of a divergent method that makes it the preferred commercial approach is that the molecular weight and the number of reactive end groups rapidly increase in each reaction step [18,19]. Nonetheless, this leads to potential problems like the incomplete reaction coupling that causes branching defects in the final products [17–19], and the need of large excess amounts of reagents to prevent side reactions and to force reactions to completion that causes difficulties in purification of final products [18,19]. On the other hand, convergent synthesis consists of the coupling of individual branched segments (dendrons) to a multifunctional core [17]. The convergent method offers some advantages over the divergent method: the more control over the synthesis due to the small number of coupling reactions per generation, the minimization of possible failure sequences, and the avoidance of the use of a large excess of reagents which simplifies purification [18]. Nevertheless, it has been reported that the construction of high generation dendrimers using this synthetic approach is difficult due to the presence of steric hindrance during the coupling of dendrons to the core. In addition, the convergent method suffers from low reaction yields [19].
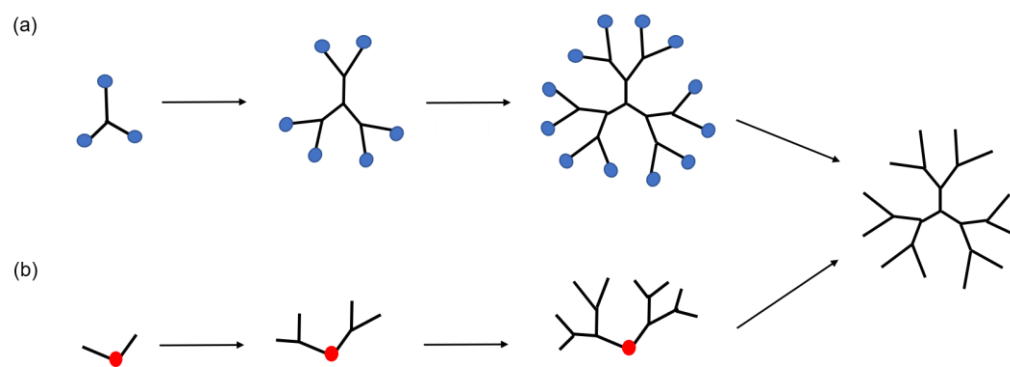
Figure 2.2 Different dendrimer synthesis approaches: (a) divergent and (b) convergent growth.

2.2 Amphiphilic Janus Dendrimers

2.2.1 Structure

Janus dendrimers (JDs, Figure 2.3), also called "bow-tie" dendrimers, surface-block dendrimers or diblock co-dendrimers, are macromolecules formed by the union of two chemically distinct dendritic building blocks, which break with the traditional roughly spherical symmetry of the dendrimers [4]. When they are synthesized with hydrophobic and hydrophilic dendrons, JDs can act as powerful structure-directing amphiphiles. Due to each dendron in the JDs can be precisely and reproducibly tuned, JDs have more versatility than simple lipids, surfactants or block copolymers [4,20,21].
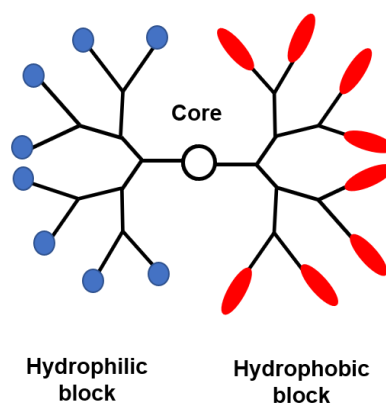
Figure 2.3 Structure of an amphiphilic Janus dendrimer.

2.2.2 Synthesis

For the synthesis of JDs is necessary to combine the conventional divergent and convergent approaches with new synthetic procedures to allow the incorporation of dendrons of different functionalities into one molecule [5,3]. Three main methods of JDs synthesis have been reported [21] (Figure 2.4): chemoselective coupling [3,12], heterogeneous double exponential growth [22] and mixed modular approach [23,9,4,24,1].
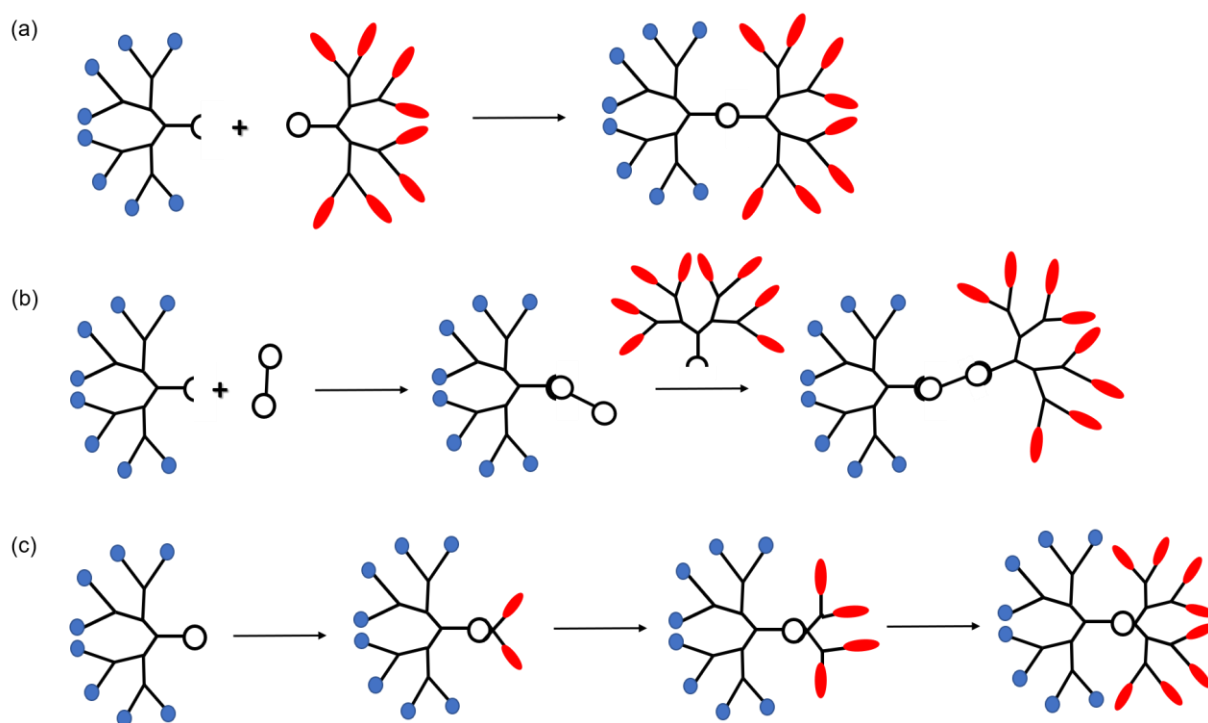
Figure 2.4 Main methods for Janus dendrimers synthesis. (a) Chemoselective coupling. (b) Heterogeneous double exponential growth. (c) Mixed modular approach. Modified from Ref. [21].

2.2.2.1 Chemoselective Coupling

The chemoselective method consists in reacting two dendrons, synthesized by the convergent approach, with complementary functions as the core. This is the simplest method to obtain JDs, and mainly involve the use of click chemistry [5,21]. The click chemistry reaction most widely used is the Cu(I)-catalyzed 1,3-dipolar cycloaddition between an alkyne and azide groups (CuAAC). Although this reaction is an efficient and high yielding method for the synthesis of JDs, the complete removal of Cu from the final products can be difficult and can interfere with their subsequent applications [5].

Fedeli et al. [3] employed click chemistry for the synthesis of amphiphilic JDs derived from 2,2-bis(hydroxymethyl)propionic acid (bis-MPA) and stearic acid (Figure 2.5a). The hydrophilic block of these dendrimers consisted of bis-MPA dendrons with free terminal hydroxyl groups. The hydrophobic block also consisted in bis-MPA dendrons, in this case, functionalized with the stearic acid. The hydrophilic and hydrophobic blocks were functionalized in their focal point with a hexamethyl azide group and alkyne group, respectively. Dendrons were obtained by the divergent method, using Steglich esterification and protection/deprotection of acetonide protecting groups. Final dendrimers were obtained by the combination of equal or different generations of hydrophilic/hydrophobic blocks ([G-1] to [G-3]), which were linked together via CuAAC.

Nummelin et al. [12] synthesized six amphiphilic JDs from gallate ether-type [G-1] dendrons with two generation ([G-1] and [G-2]) of hydrophilic blocks consisted in bis-MPA dendrons with free hydroxyl groups (Figure 2.5b). The hydrophilic block was functionalized with a propargyl moiety, while the hydrophobic block with an azide moiety. No spacer between the construction blocks was used. The growth of hydrophilic

dendrons and the obtaining of the final dendrimers were carried as Fedeli et al. [3]. It is important to note that Nummelin et al. [12] reported the concentration of copper residues in the final products (below 35 ppm). According to the authors, this concentration is within the acceptable levels for future biological applications.

(a)   Fedeli et al., 2015

Hydrophobic block   **Core**   **Hydrophilic block**

(b)   Nummelin et al., 2017

Hydrophobic block   **Core**   **Hydrophilic block**
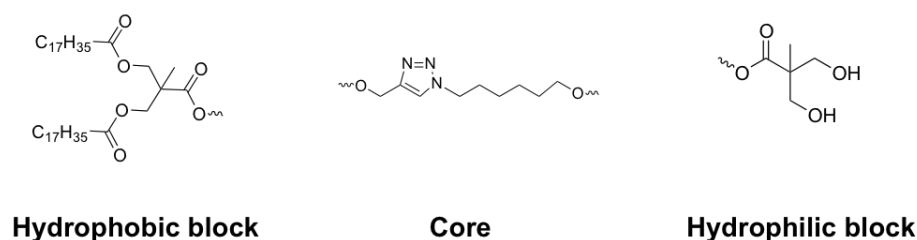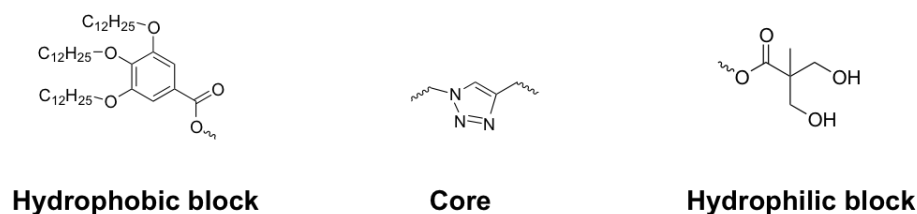
Figure 2.5 Components of amphiphilic Janus dendrimers obtained by the chemoselective method. Dendrimers synthesized by (a) Fedeli et al. [3] and (b) Nummelin et al. [12].

2.2.2.2 Heterogeneous Double Exponential Growth

Heterogeneous double exponential growth consists in the reaction of a first dendron to a multifunctional core (at least difunctional); then a second dendron is coupled to the remaining functions of the core. This method of synthesis was used by Pan et al. [22] to obtain a series of JDs, which consisted of multiple polar L-Asp or L-Glu and multiple nonpolar model drug (naproxen) (Figure 2.6). The synthetic procedure involved two steps: the synthesis of the hydrophilic and hydrophobic dendrons through a convergent

approach and the coupling of these two dendrons together after activating the focal functionality of the hydrophobic dendron. Hydrophilic dendron presented an amine focal point in its structure, and hydrophobic dendron a carboxylic acid that was activated by debenzylation. The authors reported a significant problem to produce [G-2] JDs with this method of synthesis, due to steric hindrance.

Pan et al., 2012

Hydrophobic block   **Core**   **Hydrophilic block**
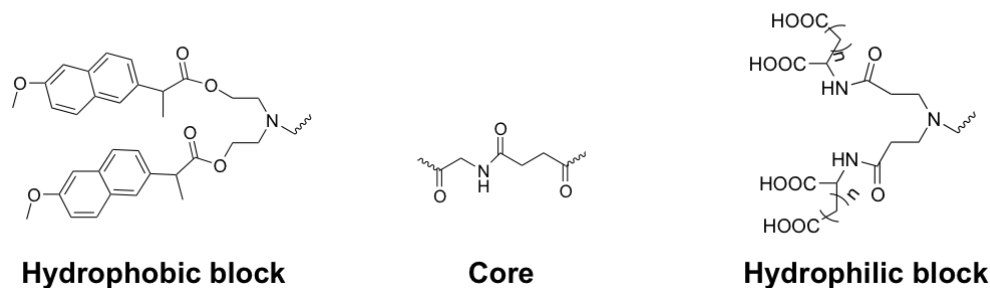
Figure 2.6 Components of amphiphilic Janus dendrimers obtained by the heterogeneous double exponential growth. Dendrimers synthesized by Pan et al. [22].

2.2.2.3 Mixed Modular Approach

The mixed modular approach consists in the combination of convergent and divergent methods. First, a dendron is prepared using the convergent method and then, a second dendron grows by the divergent method on a focal point of the first dendron [5,21,24]. An example of this approach has been reported by Ropponen et al. [24]. These authors synthesized [G-1] and [G-2] JDs from nonpolar aromatic monodendrons (gallate ether moieties) and bis-MPA hydrophilic dendrons, using pentaerythritol as the core (Figure 2.7). The hydrophilic dendron and JDs were growth using Steglich esterification. First, acetonide protected bis-MPA units were added to the protected core molecule (monobenzal-pentaerythritol). Then, core molecule was deprotected by catalytic hydrogenolysis and gallate ether monodendrons were coupled. Finally, the acetonide

protecting groups were removed in acid media from the compounds to generate [G-1] dendrimers. [G-2] dendrimers were obtained after the esterification of [G-1] dendrimers with acetonide protected bis-MPA units and their posterior deprotection in acid media. All the involved reactions were reported with high yields.

Ropponen et al., 2004

| **Hydrophobic block** | **Core** | **Hydrophilic block** |
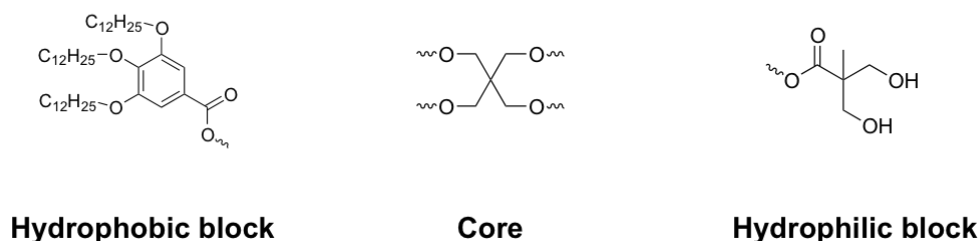
Figure 2.7 Components of amphiphilic Janus dendrimers obtained by the mixed modular approach. Dendrimers synthesized by Ropponen et al. [24].

2.2.3 Applications

The self-assembly properties of amphiphilic molecules have allowed them to be applied in technological applications ranging from nanomedicine to its use in cosmetics, food, and agriculture [25]. In recent years, a variety of amphiphilic JDs backbones have been investigated, including poly(propyl ether imine) [26], polyester [23,6–8,4,3,12,24,1,25,27–31], poly(alkyl ether) [32], polyamidoamine [11,33] and polyamide [22]. Their potential applications are mainly focused on the pharmaceutical and biomedical areas and can be divided into two major approaches, conjugation and vesicular formation [5].

2.2.4 Self-Assembly of JDs

Percec et al. [4] synthesized a wide variety of amphiphilic JDs (Figure 2.8) and studied their self-assembly in aqueous media. They found that through structural modifications

of dendrimers and the variation of their generations, it was possible to obtain supramolecules with a wide variety of morphologies in water, such as cubosomes, disks, tubular vesicles, helical ribbons and bilayered vesicles, termed as dendrimersomes [4]. The authors demonstrated that the obtained dendrimersomes exhibited mechanical properties as good as their analogous polymersomes and cholesterol stabilized liposomes [10]. Therefore, attention over these vesicles has been recently increasing.

The libraries of amphiphilic JDs generated by Percec et al. [4] have been used as starting point for other studies, related to the physical properties and applications of dendrimersomes [6–8,10,29–31]. However, only a few of these reports propose the design and synthesis of new dendrimeric structures.
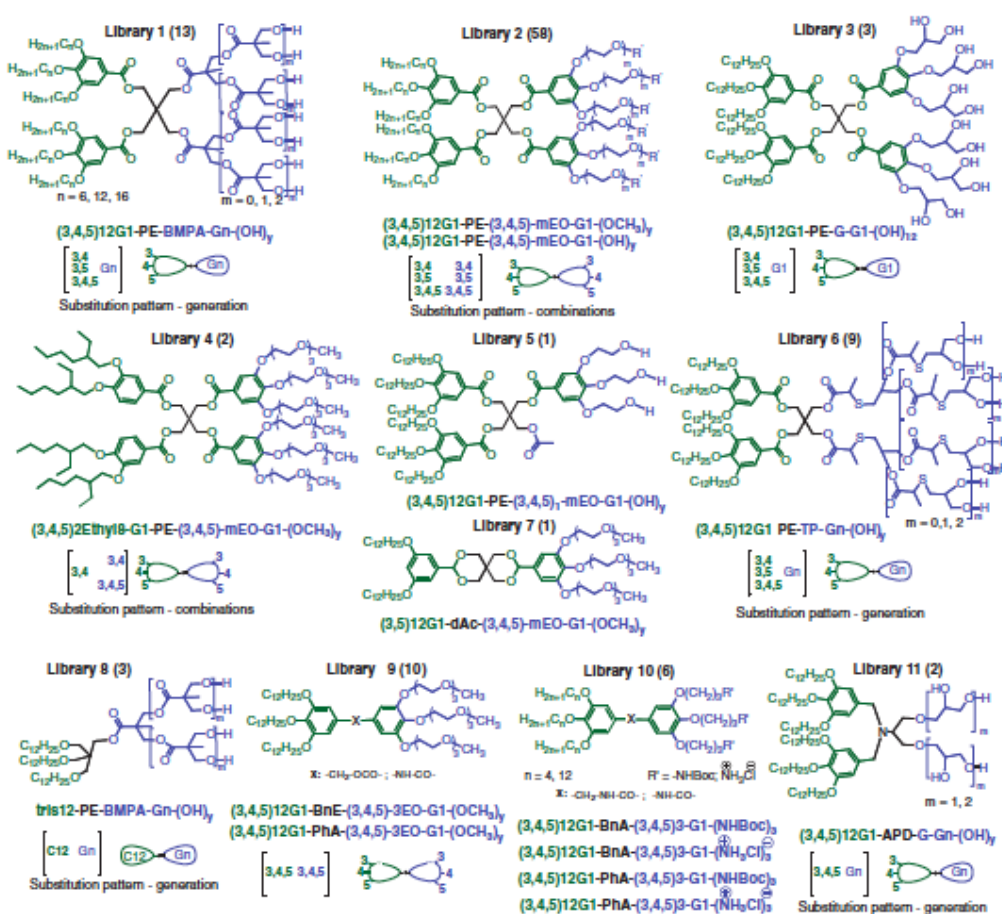
Figure 2.8 Libraries of Percec-type Janus dendrimers. Reproduced from Ref. [4].

Fedeli et al. [3] synthesized and evaluated the self-assembly of six symmetric and asymmetric bis-MPA JDs (described in section 2.2.2.1). They found that all dendrimers (excluding the lowest generation [G-1] dendrimer) formed supramolecular architectures in water. [G-3]-[G-3] (hydrophobic-hydrophilic block generation) dendrimer generated dendrimersomes; [G-2]-[G-2] dendrimer generated aggregates; and [G-2]-[G-3], [G-1]-[G-2] and [G-1]-[G-3] dendrimers generated elongated micelles. All aggregates showed the ability to encapsulate a hydrophobic drug.

Nummelin et al. [12] presented the synthesis of six JD composed by bis-MPA moieties and Percec-type hydrophobic dendrons (described in section 2.2.2.1). These low generation dendrimers generated unilamellar and multilamellar dendrimersomes with narrow size distribution. Dendrimers encapsulated the hydrophobic dye Nile red and the small-molecule drug propranolol. Dendrimers with (3,5) and (3,4,5)-hydrophobic pattern presented a robust shelf-life (> 4 months).

Zhang et al. [13] reported the obtaining and self-assembly of 29 amphiphilic JDs. They proposed the simplification of Percec-type dendrimers by the designing of "single-single" dendrimers that were synthesized from a "single" hydrophilic and a "single" hydrophobic dendron, interconnected with L-Ala, Gly and L-propanediol cores (Figure 2.9). With this structure simplification, the time required for the synthesis and the number of reaction steps were reduced. In addition, JDs were produced with the half of the molar mass of their Percec-type JDs homologs. The single-single JDs produced a diversity of complex structures in water, including dendrimersomes.
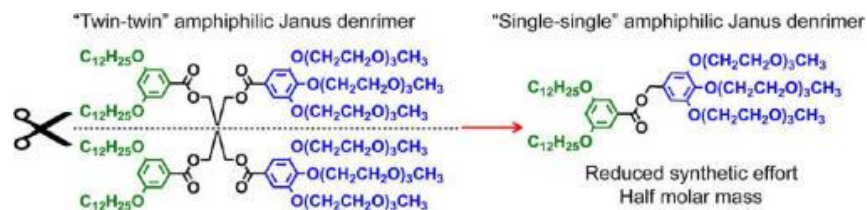
Figure 2.9 Comparison between Percec-type dendrimers and single-single dendrimers. Reproduced from Ref. [13].

Zhang et al. [14] generated six new single-single JD structures that self-assemble into onion-like dendrimersomes (multilamellar vesicles) in water. The structures of these JDs were designed from previous dendrimer libraries [13,34] with variations in their cores.

As mentioned above, Percec-type dendrons have been modified to obtain JDs and therefore dendrimersomes tailored to specific applications. Recent reports include dendrimersomes with photodegradable membranes [9], glycodendrimersomes [34] and gadoteridol dendrimersomes [6–8] for biomedical applications.

2.2.4.1 Relationship Between JD Structure and Dendrimersome Properties

The mechanism of vesicle formation, including dendrimersomes, is not completely elucidated. Therefore, any methodology that can predict the size, physical properties and polydispersity of vesicles from the primary structure of their precursors, even using empirical rules, would provide an advance in this field [25].

Some reports [3] apply the critical packing parameter *p*, that is commonly used to predict the self-assembly morphologies of lipids, to JDs. However, the molecular complexity of JDs makes difficult to apply conventional geometric models for predicting their self-assembly into dendrimersomes and other structures [4].

Peterca et al. [25] reported the first attempt to correlate the size and physical properties of monodispersed dendrimersomes, with the molecular structure of the JDs and with the

morphology of their periodic arrays self-organized in bulk state. The authors found that the self-assembly in water follows pathways that preserve the surface curvature of the assemblies formed in bulk. In addition, they found a direct correlation between the branching pattern of the hydrophobic block of dendrimers and the thickness of the layers formed in the lamellar phases in bulk. This trend is also valid for the membrane thickness of the dendrimersomes. (3,5)-hydrophobic pattern of the gallate ether moiety of JDs favored the dendrimer interdigitation, which caused a lower membrane thickness in bulk and in water, in comparison with the (3,4) and (3,4,5)-hydrophobic patterns. Likewise, more interdigitated membranes generated tougher and larger vesicles (Figure 2.10). Peterca et al. study is limited to Percec-type JDs and their dendrimersomes self-assembled by the ethanol injection method.
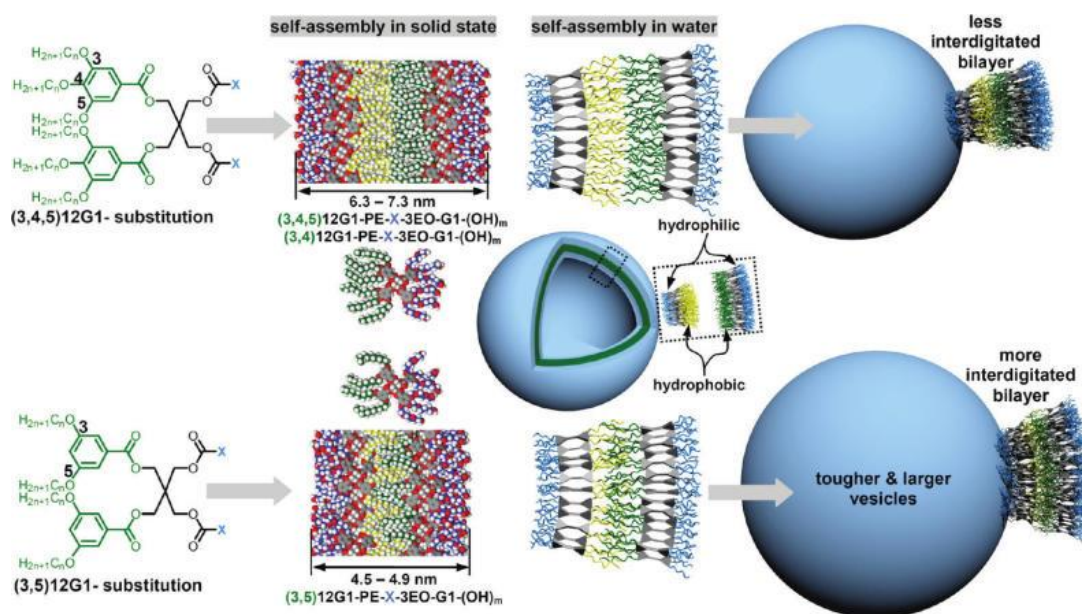
Figure 2.10 Schematic of the self-assembly of Percec-type dendrimers into vesicles. The substitution pattern of hydrophobic block controls the size and mechanical properties of dendrimersomes. Reproduced from Ref. [25]**.**

Zhang et al. [13] carried out studies related to the self-assembly of single-single JDs in aqueous media, obtained by ethanol injection method. The structural variations in the hydrophobic, hydrophilic and core blocks generated a large diversity of structures in water, such as soft and hard dendrimersomes, cubosomes, solid lamellae, and rod-like micelles. A relationship between the variation of the primary structure of dendrimers and their effects on the properties of the dendrimersomes was established. According to the hydrophilic block of the JDs played an important role in the formation of dendrimersomes, being the (3,4,5)-hydrophilic pattern in the gallate ether moiety with triethylene glycol which favors the self-assembly. The hydrophobic block and the core influenced the melting point or glass transition temperatures of dendrimers and therefore, the formation of soft or hard dendrimersomes at room temperature. Soft dendrimersomes were produced from JDs with a melting point or glass transition below room temperature and hard assemblies from those with higher temperature transitions. Dendrimers with (3,5) and (3,4,5)-hydrophobic patterns in the gallate ether moiety and propylene glycol as the core, presented lower transition temperatures, while (3,4)-hydrophobic patter and amide cores presented higher transition temperatures. In agreement with the results reported by Peterca et al. [25], Zhang et al. [13] reported that the substitution pattern of the hydrophobic block influences in the size of the dendrimersomes, being the JDs with (3,5)-hydrophobic pattern and ester core which presented a smaller lattice parameter and formed larger dendrimersomes. On the other hand, JDs with amide cores generated dendrimersomes with smaller size and larger lattice parameter due to the formation of hydrogen bonds between the cores during the

formation of JDs monolayer. These hydrogen bonds align and prevent the interdigitation of dendrimers (Figure 2.11).
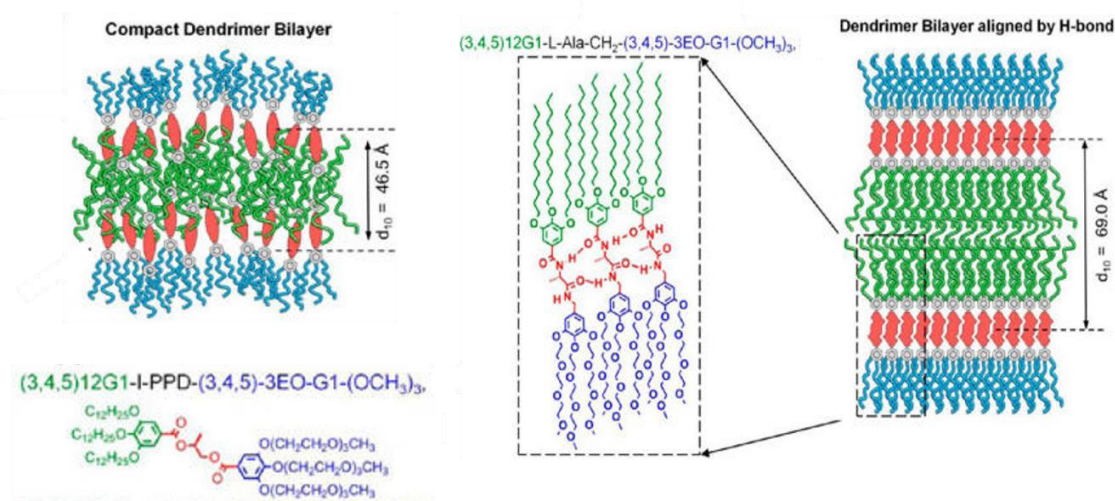
Figure 2.11 Differences in lattice parameter due to the formation of hydrogen bonds between the cores. Modified from Ref. [13].

Both, Peterca et al. [25] and Zhang et al. [13] studies established a methodology to predict the size of dendrimersomes from JD concentration and parameters taken from a reference JD structure. Furthermore, Zhang et al. [14] related the concentration of JDs with the distance between bilayers in multilamellar onion-like dendrimersomes.

Most of the reported studies focus on the prediction of dendrimersomes size, shape, and stability using experimental methods. Moreover, these studies are based on a single type of JDs (Percec-type with gallate ether moieties) and require the full characterization of a reference structure [10,13,14]. A deep exploration of other JD structures using theoretical tools is required to understand the role of the molecular architecture in the assembly formation and molecular properties [5]. Molecular simulation can be a useful tool to gain insight into JDs self-assembly mechanism. Also,

other important properties of their aggregates, difficult to evaluate via experimental methods, could be studied.

Mesoscopic molecular dynamics technologies, such as coarse-grained molecular dynamics (CG-MD), are popular alternatives to study the self-assembly of amphiphilic molecules since they reduce the computational costs when handling with large molecules and long timescales of simulation [35]. CG modeling consists of the simplification of molecular structure by mapping several atoms as single interactions sites reducing the number of degrees of freedom and maintaining the essential molecular features [36,37]. CG-MD simulation has already been applied to Percec-type JDs that formed dendrimersomes [4] and to other amphiphilic dendrimers [38].

2.2.4.2 Methods for Dendrimersomes Preparation

The preparation procedure of assemblies with complex geometries, such as dendrimersomes, plays an important role in the final morphology. Usually, the preparation of self-assembled molecules follows two different kinds of approaches: bottom-up, when the molecule is dissolved in a good solvent and forced to assemble by a solvent switch; and the top-down, where a precursor phase is induced to rearrange in solution [39]. The top-down approach is generally used for the preparation of giant vesicles (size > 1 µm) through the thin-film hydration method [40]. On the other hand bottom-up approach is applied to the production of nanovesicles [41], for example using the method of solvent injection.

Thin-film hydration and solvent injection methods have been widely applied for the obtaining of dendrimersomes [9,4,14,42]. The solvent injection method represents the simplest method to produce dendrimersomes. In this technique, JDs are first dissolved

in an organic solvent, such as diethyl ether or ethanol, and then injected through a thin needle into an excess aqueous medium [41,43]. When ethanol is used, dendrimersomes are formed spontaneously as soon as the organic solution is in contact with the aqueous phase, but vigorous agitation is needed to obtain narrow size distribution [10]. This method generally allows the formation of unilamellar vesicles with diameters below 300 nm [43]. The production of unilamellar and multilamellar dendrimersomes with narrow size distribution by the solvent injection method, have been reported [4,12].

Other reported procedure for the formation of dendrimersomes is the oil-in-water method applied by Fedeli et al. [3] and Nazemi et al. [28]. In this method, JDs are dissolved in a volatile non-water-miscible solvent and then aqueous media is added and the mixture stirred rapidly until the complete evaporation of the organic fraction.

A common problem, which arises with the previously mentioned methods, is the difficulty of upscaling toward their production in large quantities with high reproducibility, a necessary condition for drug delivery applications in the biomedical field.

The use of microfluidic techniques for the formation of vesicles and microcapsules, and for the encapsulation of drugs, offer several advantages over the traditional techniques, such as the ability to produce large amounts of highly monodisperse microcapsules and to achieve control of the concentrations and molecular composition into the cores and shells of these microcapsules. An advantageous use of microfluidics in the pharmaceutical industry is the capability to reduce the waste of precious material during encapsulation, and the consequent reduction of costs in the elaboration process [44–46].

Thin-film hydration method consists in the hydration of stacked dendrimer bilayers that separate and self-close, forming the assemblies [47]. The solvent injection method is performed by the injection of a solution of dendrimers in a water-miscible organic solvent through a thin needle, into an aqueous solution while stirring [48]. Assemblies are formed instantaneously [49] with particle sizes smaller than the obtained by thin-film hydration method.

Chapter 3

Materials and Methods

3.1 General Information

All chemicals were purchased from Sigma-Aldrich (St. Louis, MO, USA) and used without any further purification except where noted otherwise. Ethyl acetate (EtOAc), dichloromethane (DCM), and hexane (all reagent grade) were purchased from CTR scientific (Monterrey, Mexico) and distilled prior to use. Ultrapure water (18.2 MΩ.cm) was obtained from a Milli-Q system from Millipore (Billerica, MA, USA). The catalyst 4-(dimethylamino)pyridinium *p*-toluenesulfonate (DPTS) was synthesized according to Moore et al. [50]. Isopropylidene-2,2-bis(methoxy)propionic acid and benzyl-2,2-bis(methylol)propionate were obtained following the procedure reported by Ihre et al. [15]. Isopropylidene-[G-2]-benzyl ester and its deprotected product OH-[G-2]-benzyl ester were obtained according to the procedure reported by Appel et al. [51]. Isopropylidene-[G-2]-COOH was obtained from isopropylidene-[G-2]-benzyl ester hydrogenolysis, following the procedure reported by Ihre et al. [15]. Preparative flash column chromatographies were carried out using silica-gel with a particle size of 40–63 µm (SiliaFlash® P60, SiliCycle, Quebec City, Canada). Analytical thin layer chromatographies (TLC) were performed on silica gel plastic plates (TLC Silica gel 60 F$_{254}$, Merck, Darmstadt, Germany).

3.2 Instruments for Dendrimers Characterization

3.2.1 Nuclear Magnetic Resonance (NMR)

^{1}H- and ^{13}C-NMR spectra were recorded at 500.13 and 125.76 MHz, respectively, on a Bruker Advance III spectrometer (Billerica, MA, USA), using *d*-chloroform (CDCl$_3$) as a solvent. The solvent signal was used as an internal standard.

3.2.2 Mass Spectra

Mass spectra were obtained using an Autoflex II MALDI-TOF mass spectrometer (Bruker Daltonics, Bremen, Germany). Measures were performed in linear positive mode, using a nitrogen laser (337 μm) at 50 Hz frequency. The acceleration voltage was 19.50 kV, with delay time acquisition. The analytical samples were obtained by the dry-droplet method. Briefly, 1 μL of an analyte solution in methanol (1 mg/mL) was loaded on the MALDI plate (MTP 384 target plate polished steel BC, Bruker Daltonics, Bremen, Germany) and allowed to dry at 23 °C. Each sample was covered with 2 μL of matrix (α-cyano-4-hydroxycinnamic acid) solution (10 mg/mL, 50% acetonitrile, water 47.5% and 2.5% trifluoroacetic acid) and allowed to dry at 23 °C before the plate was inserted into the vacuum chamber of the MALDI instrument. Data analysis was carried in FlexAnalysis 3.0 software (Bruker Daltonics, Bremen, Germany).

3.2.3 Differential Scanning Calorimetry (DSC)

Thermal behavior of dendrimers **5A-C** and **10A-C** was determined using a Diamond DSC (PerkinElmer, Shelton, USA) equipped with an intra-cooling system. The measures were carried out under a constant dry nitrogen flow. The samples were analyzed using 50 μL sealed aluminum pans (PerkinElmer, Shelton, USA). An empty pan was used as a reference in all cases. Sample weights of 3-6mg were used on the

measurements. Typically, the following temperature profile was used for each sample: (1) Heat from 30 °C to 60 °C at 10 °C/min; (2) Cool from 60 °C to -45 °C at 70 °C/min; (3) Hold for 3 minutes at -45 °C; (4) Heat from -45 °C to 60 °C at 10 °C/min; (5) Cool from 60 °C to -20 °C at 10 °C/min and (6) Heat from -20 °C to 60 °C at 10 °C/min. DSC curves were analyzed using OriginPro Evaluation 2018b b9.5.5.409 (Northampton, MA, USA). The melting transition temperatures were taken at the onset of the peaks. The glass transition temperature was taken as half ΔCp extrapolated.

3.3 Synthesis of Amphiphilic Janus Dendrimers

In general, the growth of dendrimers was performed via Steglich esterifications, which involve the use of *N,N'*-dicyclohexylcarbodiimide (DCC) and DPTS as activating agents. The reaction schemes are presented in Figures 4.1, 4.2, 4.6 and 4.7.

Dendron 1 and General Esterification Procedure

Benzyl-2,2-bis(methylol)propionate (0.5 g, 2.32 mmol), myristic acid (1.6 g, 6.96 mmol) and DPTS (0.41 g, 0.139 mmol) were dissolved in dichloromethane (15 mL). To this, a solution of *N,N'*-dicyclohexylcarbodiimide (DCC, 1.66 g, 8.04 mmol) in dichloromethane (3 mL) was added dropwise. The reaction mixture was stirred for 24 h at 23 °C. Once the reaction was complete, the white precipitate (*N,N'*-dicyclohexylurea, DCU) was filtered off using a glass filter and washed with dichloromethane (5 mL). The organic solvent was removed with a rotary evaporator. The crude product was precipitated in ethanol (68 mL) at 4 °C.

Dendron 2 and General Procedure for Removal of Benzyl Ester Group

Pd/C (10%, 0.42 g), was added to a solution of dendron **1** (4 g, 6.02 mmol) in a mixture of EtOAc and dichloromethane (5:1, 30 mL). The apparatus for catalytic hydrogenolysis was evacuated of air and filled with H_2 (40 psi). After 5 h of shaking at 23 °C, the reaction was complete. The catalyst was filtered off and carefully washed with EtOAc (5 mL). The solvent of the filtrate was eliminated with a rotary evaporator. This product was used without further purification.

Dendron 3A

Dendron **2** (1.02 g, 1.8 mmol), ethylene glycol (0.569 g, 9.17 mmol), DPTS (0.116 g, 0.394 mmol), and DCC (0.450 g, 2.18 mmol) were allowed to react for 24 h in DCM (10 mL) following the general esterification procedure. The crude product was purified by flash column chromatography using a mixture of 20:80 EtOAc/hexane, increasing to 100% EtOAc, to give compound **3A**.

Dendron 3B

Compound **2**, 1.03 g (1.9mmol), and 1.36 g (9.06 mmol) of triethylene glycol, 0.122 g (0.414 mmol) of DPTS, and 0.472 g (2.29 mmol) of DCC were allowed to react following the general esterification procedure in 12 mL of DCM for 24 h. The crude product was purified by flash column chromatography using a mixture of 20:80 EtOAc/hexane, increasing to 100% EtOAc, to give compound **3B**.

Dendron 3C

Compound **2**, 1.04 g (1.87 mmol), and 0.677 g (3.88 mmol) of 1,10-decanediol, 0.106 g (0.36 mmol) of DPTS, and 0.456 g (2.21 mmol) of DCC were allowed to react following the general esterification procedure in 10 mL of DCM for 24 h. The crude product was purified by flash column chromatography using a mixture of 20:80 EtOAc/hexane, to give compound **3C**.

Dendrimer 5A and General Procedure for Removal of the Acetonide Protective Group

Dendron **3A** (0.900 g, 1.5 mmol), isopropylidene-2,2-bis(methoxy)propionic acid (0.530 g, 3.04 mmol), DPTS (0.185 g, 6.28 mmol), and DCC (0.748 g, 3.63 mmol) were allowed to react for 24 h in DCM (15 mL) following the general esterification procedure. The crude product was purified by flash column chromatography using a mixture of 30:70 EtOAc/hexane. Deprotected dendrimer was obtained following the procedure described by Tuutila et al. [30]. Briefly, a fraction of the purified solid (0.200 g, 0.265 mmol) was solubilized in DCM (5 mL) and diluted with methanol (5 mL). One teaspoon of Dowex® 50WX8 resin was added, and the reaction mixture was stirred at 55 °C for 24 h. After this time, the resin was filtered off and washed with dichloromethane (5 mL). The organic solvent was removed with a rotary evaporator to give the compound **5A**.

Dendrimer 5B

Compound **3B**, 0.973 g (1.4 mmol), and 0.494 g (2.83 mmol) of isopropylidene-2,2-bis(methoxy)propionic, 0.168 g (0.57 mmol) of DPTS, and 0.707 g (3.43 mmol) of DCC were allowed to react following the general esterification procedure in 15 mL of DCM for

24 h. The crude product was purified by flash column chromatography using a mixture of 50:70 EtOAc/hexane. Purified solid, 0.206 g (0.244 mmol) was deprotected following the general procedure for the acetonide protective group.

Dendrimer 5C

Compound **3C**, 0.694 g (0.98 mmol), and 0.342 g (1.96 mmol) of isopropylidene-2,2-bis(methoxy)propionic, 0.117 g (0.397 mmol) of DPTS, and 0.483 g (2.34 mmol) of DCC were allowed to react following the general esterification procedure in 15 mL of DCM for 24 h. The crude product was purified by flash column chromatography using a mixture of 20:80 EtOAc/hexane. The purified compound, 0.200 g (0.231 mmol) was deprotected following the general procedure for the acetonide protective group.

Dendron 6

Isopropylidene-[G-2]-benzyl ester (0.409 g, 0.896 mmol), myristic acid (1 g, 4.38 mmol) and DPTS (0.113 g, 0.384 mmol) were allowed to react for 24 h in DCM (12 mL) following the general esterification procedure. The crude product was precipitated in ethanol (68 mL) at 4 °C.

Dendron 7

Dendron **6** (2.88 g, 2.22 mmol) was dissolved in a mixture of EtOAc and dichloromethane (5:1, 30 mL) and Pd/C (10%, 0.29 g) was added. Dendron 7 was deprotected according to the general procedure for removal of benzyl ester group. This product was used without further purification.

Dendron 8A

Dendron **7** (1.022 g, 0.846 mmol), ethylene glycol (0.269 g, 4.33 mmol), DPTS (0.049 g, 0.166 mmol), and DCC (0.209 g, 1.01 mmol) were allowed to react for 24 h in DCM (12 mL) following the general esterification procedure. The crude product was purified by flash column chromatography using a mixture of 20:80 EtOAc/hexane, increasing to 100% EtOAc, to give compound **8A**.

Dendron 8B

Compound **7**, 1.007 g (mmol), and 0.642 g (mmol) of triethylene glycol, 0.054 g (mmol) of DPTS, and 0.268 g (mmol) of DCC were allowed to react following the general esterification procedure in 12 mL of DCM for 24 h. The crude product was purified by flash column chromatography using a mixture of 20:80 EtOAc/hexane, increasing to 100% EtOAc, to give compound **8B**.

Dendron 8C

Compound **7**, 1.009 g (0.836 mmol), and 0.291 g (1.67 mmol) of 1,10-decanediol, 0.050 g (0.170 mmol) of DPTS, and 0.218 g (1.06 mmol) of DCC were allowed to react following the general esterification procedure in 12 mL of DCM for 24 h. The crude product was purified by flash column chromatography using a mixture of 20:80 EtOAc/hexane, to give compound **8C**.

Dendrimer 10A

Dendron **8A** (0.781 g, 0.624 mmol), isopropylidene-[G-2]-COOH (0.563 g, 1.26 mmol), DPTS (0.076 g, 0.258 mmol), and DCC (0.335 g, 1.62 mmol) were allowed to react for 24 h in DCM (18 mL) following the general esterification procedure. The crude product

was purified by flash column chromatography using a mixture of 30:70 EtOAc/hexane. The purified solid (0.210 g, 0.124 mmol) was deprotected following the general procedure for the acetonide protective group.

Dendrimer 10B

Compound **8B**, 0.624 g (0.353 mmol), and 0.710 g (1.59 mmol) of Isopropylidene-[G-2]-COOH, 0.063 g (0.214 mmol) of DPTS, and 0.261 g (1.26 mmol) of DCC were allowed to react following the general esterification procedure in 20 mL of DCM for 24 h. The crude product was purified by flash column chromatography using a mixture of 50:70 EtOAc/hexane. The purified solid [0.111 g (0.062 mmol)] was deprotected following the general procedure for the acetonide protective group.

Dendrimer 10C

Compound **8C**, 0.544 g (0.400 mmol), and 0.356 g (0.798 mmol) of Isopropylidene-[G-2]-COOH, 0.080 g (0.272 mmol) of DPTS, and 0.206 g (0.998 mmol) of DCC were allowed to react following the general esterification procedure in 20 mL of DCM for 24 h. The crude product was purified by flash column chromatography using a mixture of 30:70 EtOAc/hexane. The purified compound [0.212 g (0.118mmol)] was deprotected following the general procedure for the acetonide protective group.

3.4 Formation and Characterization of Assemblies (Experimental Method)

To assess different properties of aggregation behavior in water, two sizes of assemblies were created through different methods. Giant assemblies (size ≥ 1 µm) were used to evaluate the morphology of the assemblies and to identify hydrophobic and hydrophilic domains in their structure. While small assemblies (size ≤ 100 nm) were produced to

evaluate the size, polydispersity index (PDI), ζ-potential, stability and morphology of the assemblies. Aqueous dispersions of JDs were carried out using the dendrimersomes preparation protocols of thin-film hydration (for giant assemblies), and solvent injection (for small assemblies) previously reported by Percec et al. [4]. In addition, microfluidics was used as an alternative to the thin-film hydration method to produce giant dendrimersomes, using double emulsion drops with ultrathin shells as templates.

3.4.1 Thin-Film Hydration Method

Procedure 1: A 10 mg/mL solution of dendrimer in chloroform (200 µL) and a 3 mg/mL solution of Nile Red (10 µL) in the same solvent were mixed and deposited on a 2 cm^2 roughened Teflon plate. After solvent evaporation, the Teflon plate was placed in a vial and continued drying under reduced pressure for 2 h. Addition of 4 mL of ultrapure water and subsequent hydration at 60 °C for 1 h followed by hydration at 23 °C for 12 h, led to the formation of the aggregates.

Procedure 2: The solution of dendrimer and Nile Red in chloroform was deposited on a glass vial. The solvent was evaporated at 80 °C under reduced pressure for 2 h. Addition of 2 mL of ultrapure water and subsequent hydration at 80 °C for 1 h followed by hydration at 23 °C for 12 h, led to the formation of the aggregates.

Assemblies were characterized by confocal microscopy using a Leica TCS SP5 confocal microscope (Leica Microsystems, Wetzlar, Germany), equipped with an HCX PL APO CS 20.0×/0.70 IMM UV objective (Leica Microsystems, Wetzlar, Germany). Nile Red was excited at 488 nm with an argon laser and emission spectra collected at 600–700 nm. Confocal images of 512 × 512 pixels were acquired in the XYZ scan mode at a scan speed of 400 Hz. Optical sections were taken at 1.98 µm intervals. Images

were digitalized at a resolution of 8 bits. The digital images of the confocal stacks were processed using Fiji software (ImageJ, National Institutes of Health, Bethesda, MD, USA) [52].

3.4.2 Microfluidics

3.4.2.1 Fabrication of the Microfluidic Device.

Monodisperse water-in-oil-in-water (W/O/W) double emulsion drops with ultra-thin shells were produced using a glass capillary microfluidic device, following a procedure similar to that reported by Kim et al. [53]. These drops were utilized as templates to form the dendrimersomes. The microfluidic device consisted of two tapered cylindrical capillaries of the outer diameter of 1.00 mm. These cylindrical capillaries were inserted oppositely into each end of a cylindrical capillary, whose inner diameter was slightly larger (1.05 mm) than the outer diameter of the inner capillaries; this configuration enabled to accurately align the axes of the cylindrical capillaries under the microscope, as illustrated schematically in Figure 3.1. The tip of the capillary on the left (injector capillary) was about 50-80 µm in diameter, and the tip of the capillary on the right (collection capillary) was about 120-160 µm. The separation distance between them was the same as the tip size of the injection capillary. These cylindrical capillaries were tapered to a diameter of 20 µm with a micropipette puller (P-30, Sutter Instrument, Novato, CA, USA) and then were carefully sanded to the desired final diameter. The middle injection capillary was coated with n-octadecyl-trimethoxysilane to render its surface hydrophobic; to prevent wetting of the aqueous phase on the external capillary wall and enhance the formation of a water-in-oil emulsion. Also, the collector capillary was coated with (3-mercaptopropyl)trimethoxysilane for rendering its surface hydrophilic,

to prevents wetting of the middle oil phase of the double emulsion drops on its walls. A third cylindrical capillary was stretched with a burner to obtain a long conical tip with an outer diameter of approximately 200 µm to be used for the infusion of the inner phase. This hand-stretched capillary was inserted into the left cylindrical capillary.
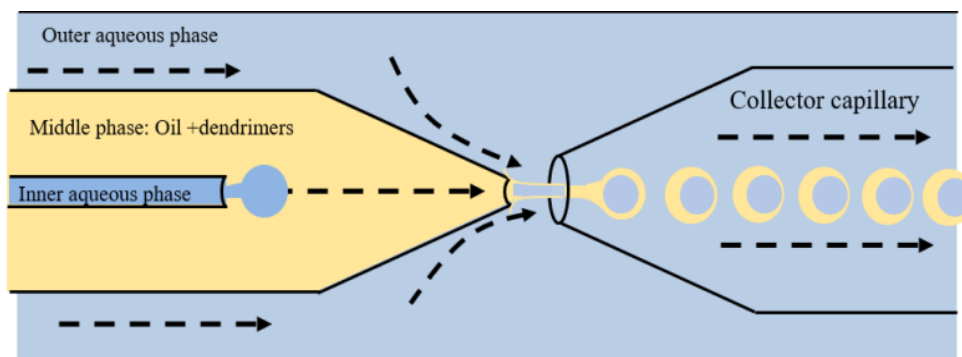
Figure 3.1 Schematic illustration of the microfluidic device for preparation of monodisperse double-emulsion drops.

3.4.2.2 Operation of the Microfluidic Device

The inner capillary provides the inlet to inject the innermost aqueous phase. This phase was prepared by the dissolution of 8% w/w poly(ethylene glycol) (PEG, MW = 6 kDa) and 2% w/w poly(vinyl alcohol) (PVA, MW = 13–23 kDa, 87-89% hydrolyzed) in ultrapure water. In the first explorative experiments with dendrimer **10A-C**, the middle oil phase was composed of a solution of 5 mg/ml of dendrimers, dissolved in a mixture of 36% chloroform and 64% hexane (v/v). For the second set of experiments with dendrimer **10B**, the middle oil phase was composed of a solution of 12 mg/ml of dendrimers, dissolved in a mixture of 44% chloroform and 56% hexane (v/v). The middle oil phase was injected through the left capillary in the same direction as the inner

aqueous phase. The outer aqueous phase, composed of 10% w/w PVA solution was injected through the interstices between the left capillary and the outer capillary, and it flows in the same direction on the inner and middle phases. The PVA in the outer phase enhanced this phase viscosity and the stability of double emulsion drops. With this device, a water drop is forced to be re-emulsified into the oil phase forming a W/O/W double emulsion drops, pulled downstream into the collection capillary, as shown in Figure 3.1. The innermost aqueous phase and the middle oil phase were injected at a flow rate of 498 µL/h and the outer phase at a flow rate of 3000 µL/h.

The double emulsion drops were produced as templates for the formation of dendrimersomes in the dripping regime which enhance the monodispersity of the samples [54]. The resultant double emulsion drops were collected in a glass vial containing a solution of 100 mM sucrose water, having the same osmolarity of the inner aqueous cores to prevent osmotic stresses. Once in the vial, the solvents contained in the middle oil phase of the double emulsions start to diffuse to the outer continuous aqueous phase [54]. The collector vial was maintained uncovered for 1 h, during the collection process, to allow the solvents in the outer aqueous phase to evaporate. All experiments were performed at room temperature. The production of double emulsion drops in the microfluidic device was recorded using a 10x objective on an inverted microscope (Axio Observer Z1, Zeiss, Göttingen, Germany) equipped with a high-speed camera (Phantom Miro EX2-2048MM, Vision Research, Wayne, NJ, USA). The time of collection was 1 h in all experiments. The values reported on the shell thickness and radius of the dendrimersomes were measured from bright field images with the use of ImageJ (NIH) software [55] in combination with MATLAB codes for their posterior

analysis. Hydrophilic-lipophilic balance (HLB) value was calculated with the MarvinSketch 17.27 program (ChemAxon Ltd., Cambridge, MA, USA), using the Griffin method [56,57].

3.4.3 Solvent Injection Method

A dendrimer solution (10 mg/mL, 100 µL) in absolute ethanol, acetone or tetrahydrofuran (THF), was injected into ultrapure water (1.9 mL) and vortex mixed for 5 s to obtain a final dendrimer concentration of 0.5 mg/mL. The size, PDI, and ζ-potential of the assemblies were determined by triplicate (independent samples from each treatment) at 23 °C, using dynamic light scattering (DLS) with a Malvern Zetasizer ZS ZEN3600 (Malvern Instruments Ltd., Malvern, UK) following the procedure described by Percec et al. [4]. Morphology of the assemblies was evaluated using atomic force microscopy (AFM). For this analysis, samples obtained from ethanol injection experiments were diluted 1:2 with ultrapure water. 10 µL of the sample were placed on a glass coverslip and then allowed to air dry for approximately 15 h. Samples were observed in a NT-MDT NTEGRA Prima AFM (Moscow, Russia) at 23 °C, with a RTESPA probe (Bruker, Billerica, MA, USA) of spring constant k = 40 N/m in semicontact mode. Height and phase images were simultaneously obtained with a scan rate of 1.61 µm/s over a selected area of 1 × 1 µm. Images were processed and analyzed using NOVA 3.1. (NT-MDT). The height and diameter of assemblies were measured from the profile section of AFM line scans analyzing height images.

3.5 Coarse-Grained Molecular Dynamic Simulation

CG-MD simulation was made using the MARTINI CG model [58]. The parameters of this model were adapted to use with the dendrimer composed of 2 [G-2] bis-MPA

dendrons with 4 OH terminal groups and 4 C_{13} alkyl chains. These parameters are available at http://www.cgmartini.nl/images/parameters/ITP/martini_v2.0_polymers.itp. The simplification of this structure to CG model resulted in the use of three types of beads: three C1 beads and a Na bead for each myristoyl group, six Na beads corresponding to the methyl formate blocks, and four SP2 beads for the hydroxymethyl groups. Bis-MPA methyl substituents were not considered. The dendrimer structure and its bead mapping are shown in Figure 3.2.
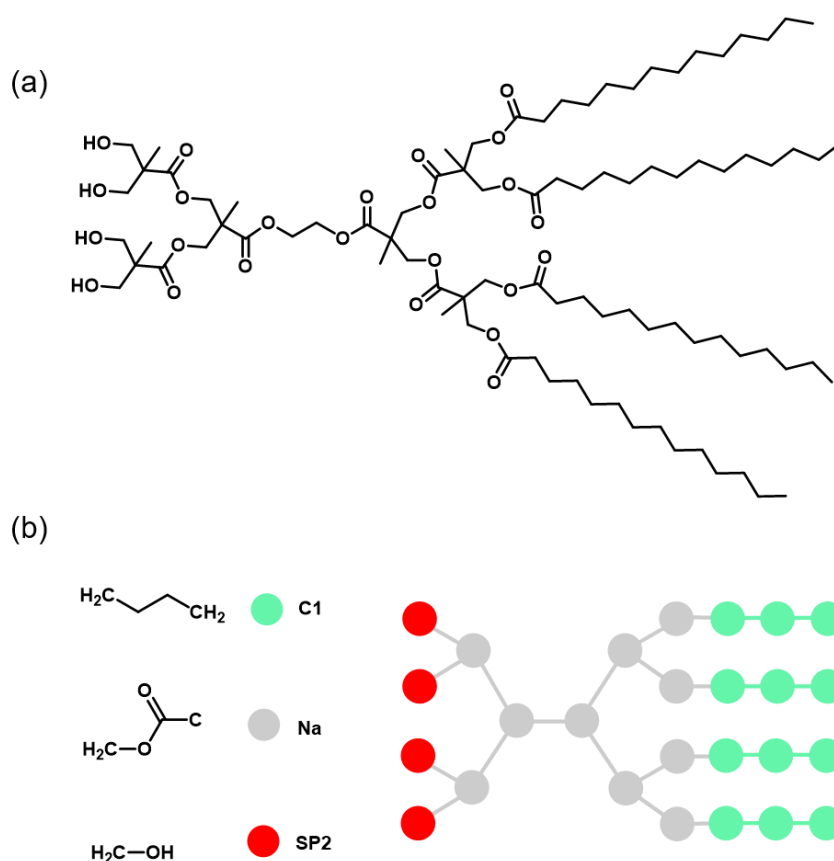
Figure 3.2. Mapping between the molecular structure and coarse-grained (CG) model for the amphiphilic Janus dendrimer. (a) Dendrimer molecular structure (full-atom); (b) The simplified structure using CG beads. Bis-MPA methyl substituents were not considered.

Angle and bond parameters for CG model were obtained from a full atomistic simulation of a single molecule of dendrimer in explicit water and transformed to CG resolution using the mapping technique described previously and following the procedure described by Marquez-Miranda et al. [38], and following Marrink et al. [59,60] criteria to obtain parameters for known bead types. Furthermore, radii of gyration for the full atomistic model was similar to CG model.

Simulation system was built with 1700 CG-dendrimers placed randomly into a 37.6 nm × 37.4 nm × 37 nm non-polarized MARTINI water box, representing a dendrimer concentration of 76 mM.

The CG simulation was performed using GROMACS simulation package 5.0.3 (SciLifeLab, Stockholm, Sweden). Steepest descent method was used for energy minimization with a force tolerance of 10 kJ/(mol nm). After, a molecular dynamics simulation in the isobaric-isothermal ensemble was performed under periodic boundary conditions with a temperature of 310 K and pressure of 1 bar. The temperature was maintained by the velocity rescaling thermostat (modifies Berendsen) [61] and pressure by the Parrinello-Rahman scheme. Lennard-Jones potentials and short-range electrostatics were shifted from 0.9 and 0.0 nm, respectively, to the cut-off distance (1.2 nm) using the standard shift function in GROMACS [62]. Long-range electrostatics were calculated using particle mesh Ewald summation [63]. An integration time step of 30 fs and Verlet algorithm were considered. The total simulation length was 13 μs. Analysis and visualization of simulation results were performed using Tcl homemade-scripts, VMD 1.9.3 (University of Illinois, Urbana, IL, USA) [64] and GROMACS programs.

3.6 Statistical Analysis

Data were expressed as a mean ± standard deviation. Data were analyzed using analysis of variance (ANOVA), followed by Tukey's honestly significantly different test. Mean differences were evaluated by paired Student's *t*-test or when appropriate unpaired *t*-test. The accepted level of significance was *p*-value ≤ 0.05. Statistical analysis was performed with MINITAB 15 (Minitab Inc., Champaign, IL, USA).

Chapter 4

Results and Discussion

4.1 Synthesis and Characterization of Amphiphilic JDs

4.1.1 First Generation Dendrimers

The hydrophobic building block of [G-1] dendrimers (Figure 4.1), (myristoyl)$_2$-[G-1]-benzyl ester (dendron **1**) was synthesized in 82% yield by the condensation of benzyl-2,2-bis(methylol)propionate (**EB**) and myristic acid, in a 1:3 molar ratio. Taking advantage of the differences in solubility of the reactants and the product of interest, dendron **1** was obtained by precipitation in ethanol at 4 °C, without the need of column chromatography for its isolation. Then, dendron **1** was deprotected from the benzyl group by low pressure (40 psi) catalytic hydrogenolysis with palladium on carbon, to give dendron **2** with a reaction yield of 98%.
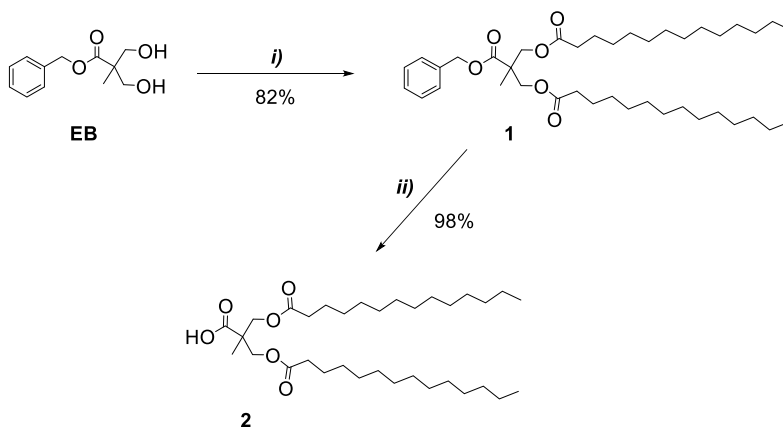
Figure 4.1. Synthesis of hydrophobic building block of [G-1] dendrimers. Reagents and conditions: *i)* Myristic acid, DCC, DPTS, DCM; *ii)* Pd/C, H$_2$ (40 psi), EtOAc: DCM.

Dendron **2** was used to couple the different cores. Ethylene glycol (**A**), triethylene glycol (**B**) and 1,10-decanediol (**C**) were coupled directly to the deprotected hydrophobic dendron, without the use of hydroxyl protective groups (Figure 4.2). This was achieved using an excess of the glycols in the condensation reaction and allowed us to reduce the number of synthetic steps. Ethylene glycol and triethylene glycol cores were coupled to dendron **2** in a 5:1 molar ratio. Due to the lower solubility of 1,10-decanediol in the reaction solvent, in comparison with the other cores, this glycol was used in a 2:1 molar ratio. Dendrons **3A**, **3B,** and **3C** were obtained in 91, 91 and 61% yield, respectively, after column chromatography purification.
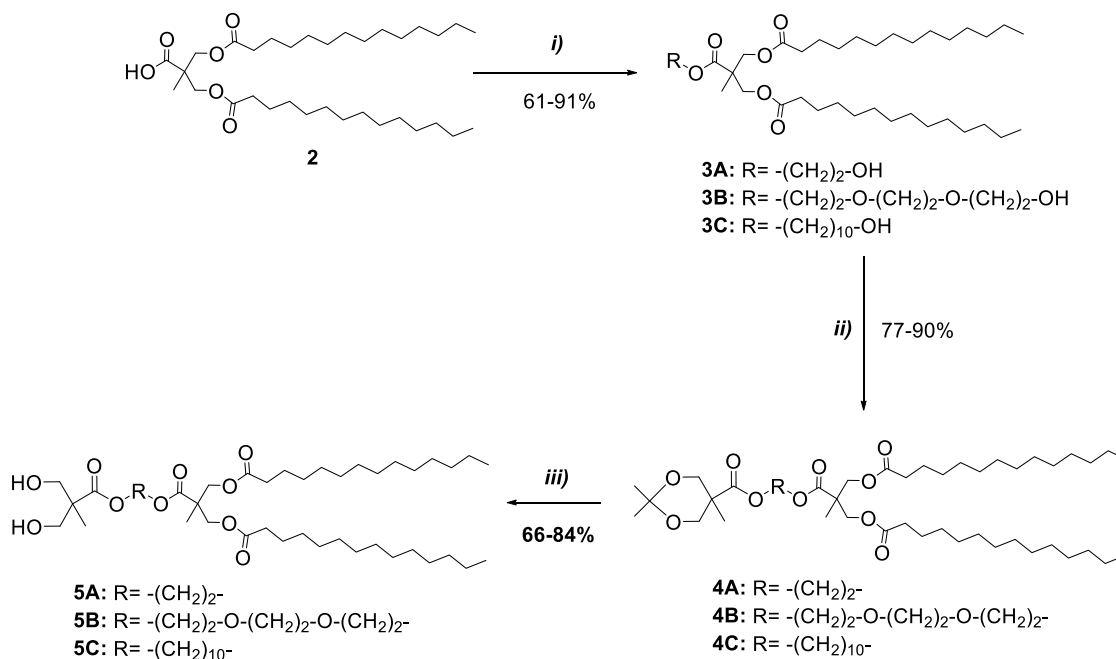
Figure 4.2 Synthesis of hydrophobic building block of [G-1] dendrimers. Reagents and conditions: *i)* Ethylene glycol, triethylene glycol or 1,10-decanediol, DCC, DPTS, DCM; *ii)* isopropylidene-2,2-bis(methoxy)propionic acid, DCC, DPTS, DCM; *iii)* DOWEX® H, MeOH: DCM, 55°C.

To obtain the [G-1] dendrimers **4A-C** (Figure 4.2) compounds **3A-C** were coupled to the hydrophilic dendron isopropylidene-2,2-bis(methoxy)propionic acid in a 1:2 molar ratio, and purified by column chromatography, in 84 (**4A**), 77 (**4B**) and 90% (**4C**) yield. Afterward, the acetonide protective group was effectively removed in presence of an acidic Dowex 50WX8 resin at 55 °C, as described by Tuuttila *et al*. [30], obtaining dendrimers **5A-B** in 84 (**5A**), 66 (**5B**) and 70% (**5C**) yields. We tried other unsuccessful approaches to remove acetonide group. First, we used the ion-exchange resin at room temperature, but the reaction was incomplete probably due to too mild conditions. We also tried the procedure described by Ropponen et al. [24] that involves the use of HCl 6 N but was ineffective leading to the formation of byproducts probably due to the ester hydrolysis.

The structures of the [G-1] dendrimers and their precursors were fully characterized by ^{1}H NMR, ^{13}C NMR, and MALDI-TOF MS, and the detailed information is described in the Appendix A. Particularly, ^{1}H NMR and ^{13}C NMR were very useful to monitoring the coupling and deprotection reactions to obtain the final dendrimers. Examination of the ^{1}H NMR spectra of reveals signals attributed to the bis-MPA units in the hydrophilic and hydrophobic building blocks around 1.1, 3.6-3.9, 4.0-4.3 and 4.4 ppm, and the signals of the myristic chains in the hydrophobic block at 0.88, 1.2-1.4, 1.5-1.6 and 2.3 ppm, as shown in the ^{1}H NMR spectra of dendrimers (Figures 4.3-4.5). In addition, signals around 4.2-4.3 ppm for **5A** (Figure 4.3); 3.5-3.7 and 4.2-4.3 ppm for **5B** (Figure 4.4); and 1.2-1.4, 1.4-1.7 and 4.1-4.3 ppm for **5C** (Figure 4.5), revealed the coupling of dendrons to the respective core molecule. The ^{1}H NMR spectra integration of all dendrimer was consistent with the expected results. ^{13}C NMR spectra of the final

dendrimers did not show the signals corresponding to the acetonide protective group around 113 and 26 ppm, confirming the effective deprotection of the dendrimers.
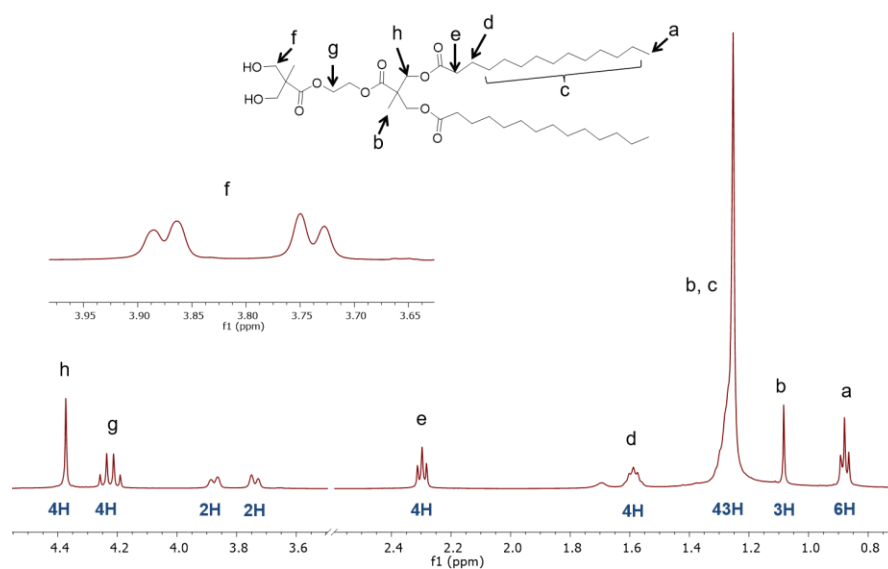
Figure 4.3 ¹H-NMR spectra (500 MHz, CDCl₃) of 5A, integrals and peak assignments.
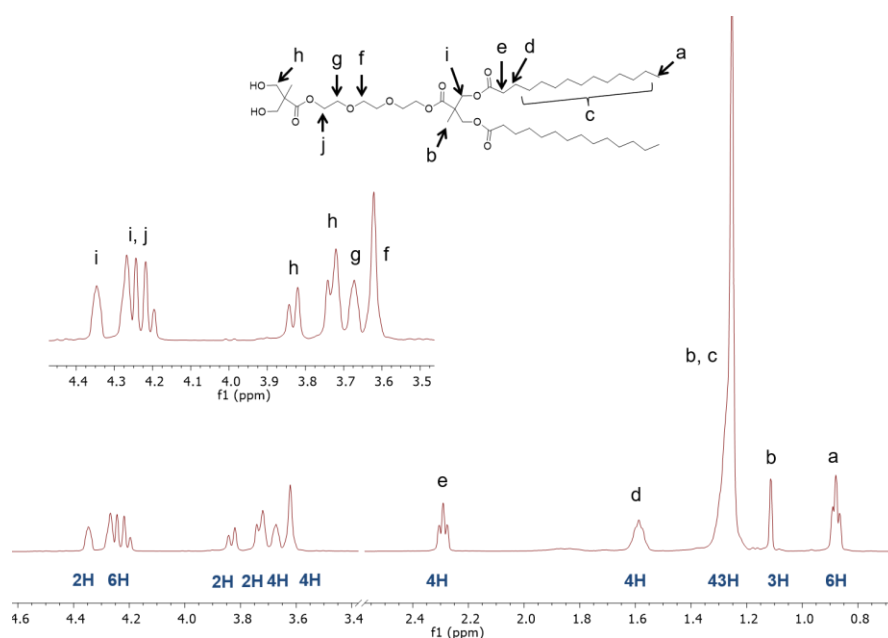
Figure 4.4 ¹H-NMR spectra (500 MHz, CDCl₃) of 5B, integrals and peak assignments.
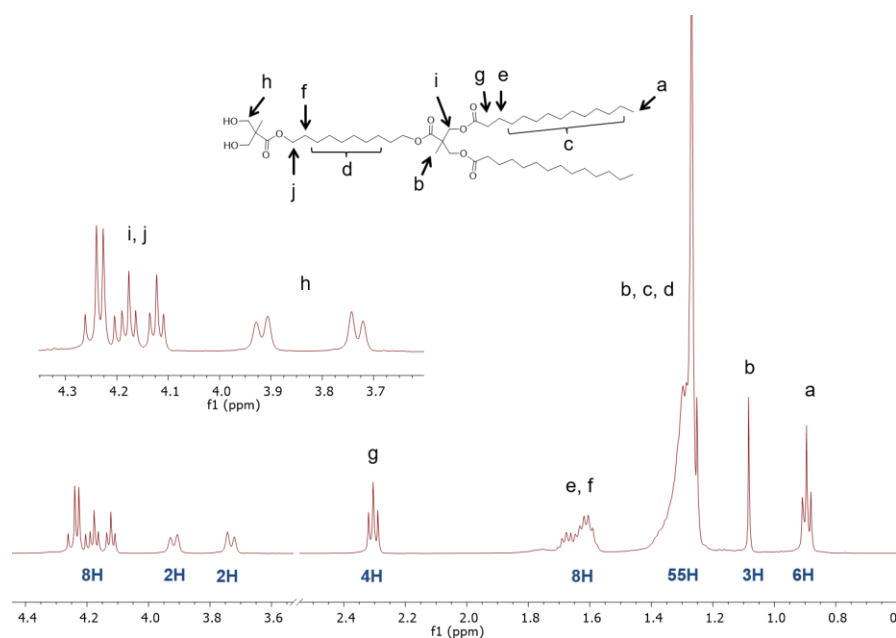
Figure 4.5 ^{1}H-NMR spectra (500 MHz, CDCl$_3$) of 5C, integrals and peak assignments.

4.1.2 Second Generation Dendrimers

The [G-2] dendrimers were prepared using the same procedures previously described, varying the starting dendrons. In this case, the hydrophobic building block, (myristoyl)$_4$-[G-2]-benzyl ester (dendron **6**), was obtained in 79% yield after the esterification of dendron (OH)$_4$-[G-2]-benzyl ester (**EB-2**) and myristic acid in a 1:5 molar ratio (Figure 4.6). Dendron **6** was deprotected from the benzyl group to give dendron **7** with a reaction yield of 99%.
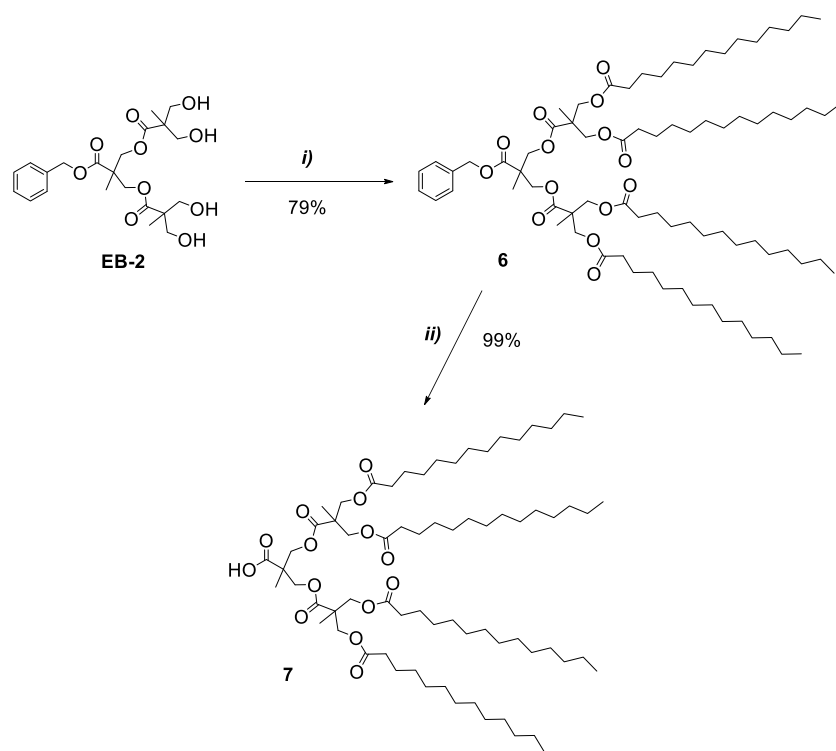
Figure 4.6 Synthesis of hydrophobic building block of [G-2] dendrimers. Reagents and conditions: *i)* **Myristic acid, DCC, DPTS, DCM;** *ii)* **Pd/C, H$_2$ (40 psi), EtOAc: DCM.**

The hydrophilic building block was obtained from (isopropylidene)$_4$-[G-2]-COOH. Coupling reactions between the hydrophobic building group and the different cores in a 1:5 molar ratio (except for 1,10-decanediol where a 1:2 molar ratio was used), generated dendrons **8A-C** in 75 (**8A**), 75 (**8B**) and 45% (**8C**) yield (Figure 4.7). These dendrons were attached to the hydrophilic block in a 1:2 molar ratio, to produce dendrimers **9A-C** in 81 (**9A**), 44 (**9B**) and 68% (**9C**) yield. Finally, dendrimers **10A-C** were obtained in 78 (**10A**), 79 (**10B**) and 31% (**10C**) yield, after the elimination of isopropylidene protecting group from dendrimers **9A-C.**
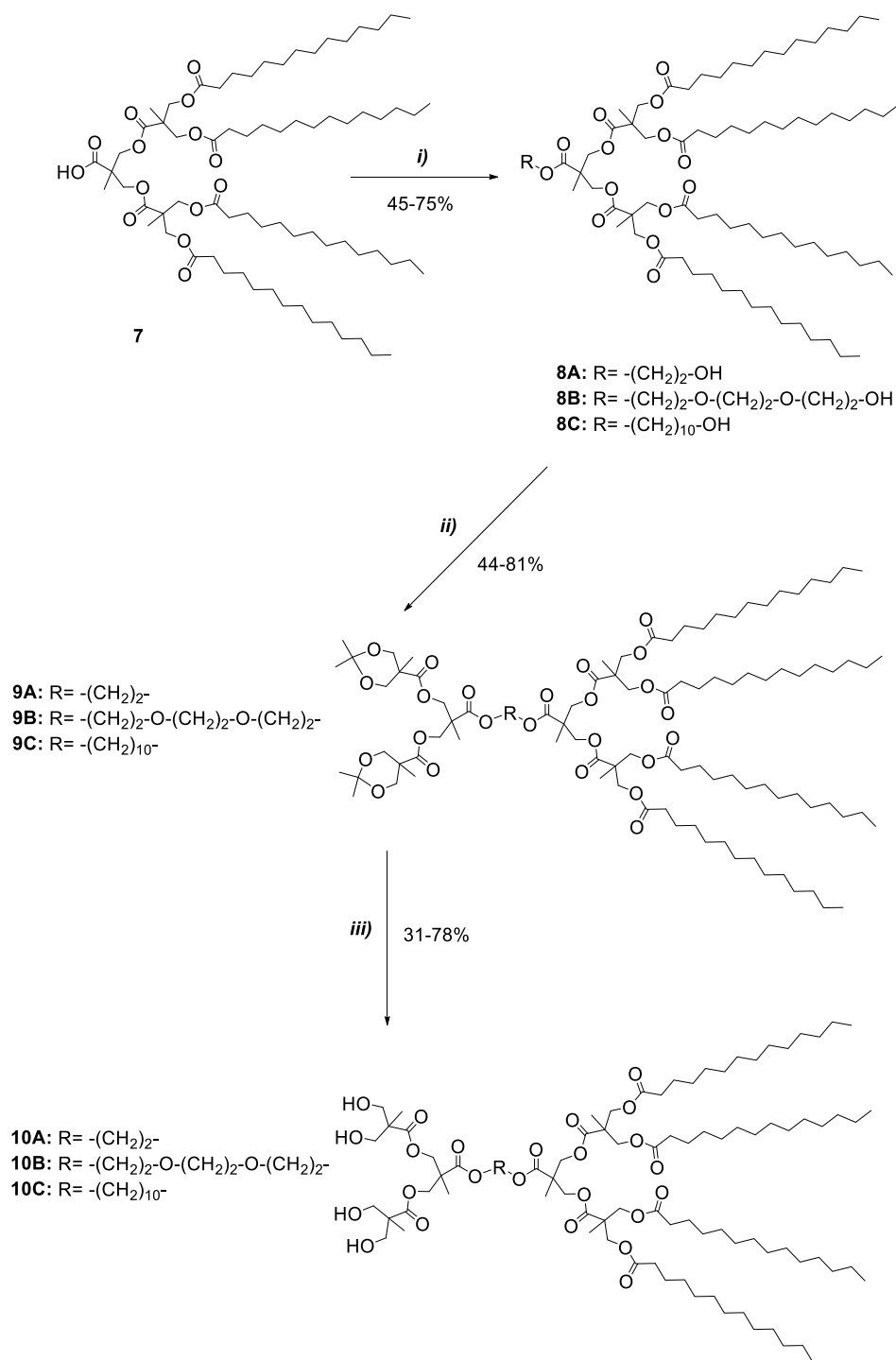
Figure 4.7 Synthesis of hydrophobic building block of [G-1] dendrimers. Reagents and conditions: *i)* **Ethylene glycol, triethylene glycol or 1,10-decanediol, DCC, DPTS, DCM;** *ii)* **(isopropylidene)₄-[G-2]-COOH, DCC, DPTS, DCM;** *iii)* **DOWEX® H, MeOH: DCM, 55°C.**

The structures of the [G-2] dendrimers and their precursors were fully characterized by ^{1}H NMR, ^{13}C NMR, and MALDI-TOF MS, and the detailed information is described in the Appendix A. In the same way that with [G-1] dendrimers, NMR was used to monitoring the coupling and deprotection reaction involved in the synthesis of dendrimers **10A-C**. In general, ^{1}H NMR spectra of [G-1] and [G-2] dendrimers present the same signals attributed to the respective core in the molecule around 4-4.4 ppm for **10A** (Figure 4.8); 3.6, 3.5-3.8 and 4.2-4.3 ppm for **10B** (Figure 4.9); and 1.1-1.4, 1.4-1.7 and 4-4.4 for **10C** (Figure 4.10). These signals confirm the coupling of the dendrons to the respective core. The signals attributed to the bis-MPA units in the hydrophilic and hydrophobic dendrons were also present at 3.6-3.9, 4.0-4.3, and 4.4 ppm. In comparison with [G-1] dendrimers, the signals around 4-4.5 for [G-2] dendrimers were more complex due to the addition of the second layer of bis-MPA units. The signals of the myristic chains in the hydrophobic block at 0.88, 1.2-1.4, 1.5-1.6 and 2.3 ppm, were also present (Figures 4.8-4.10). The ^{1}H NMR spectra integration of all dendrimers was consistent with the expected results and is presented in Figures 4.8-4.10. In addition, ^{13}C NMR spectra of the final dendrimers did not show the signals corresponding to the acetonide protective group around 113 and 26 ppm, confirming the effective deprotection of the dendrimers.
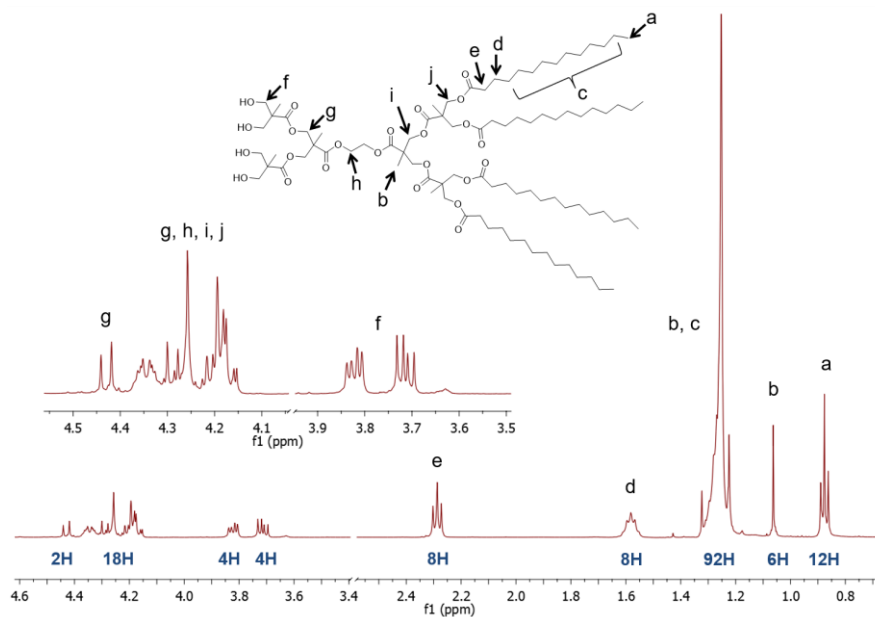
Figure 4.8 ¹H-NMR spectra (500 MHz, CDCl₃) of 10A, integrals and peak assignments.
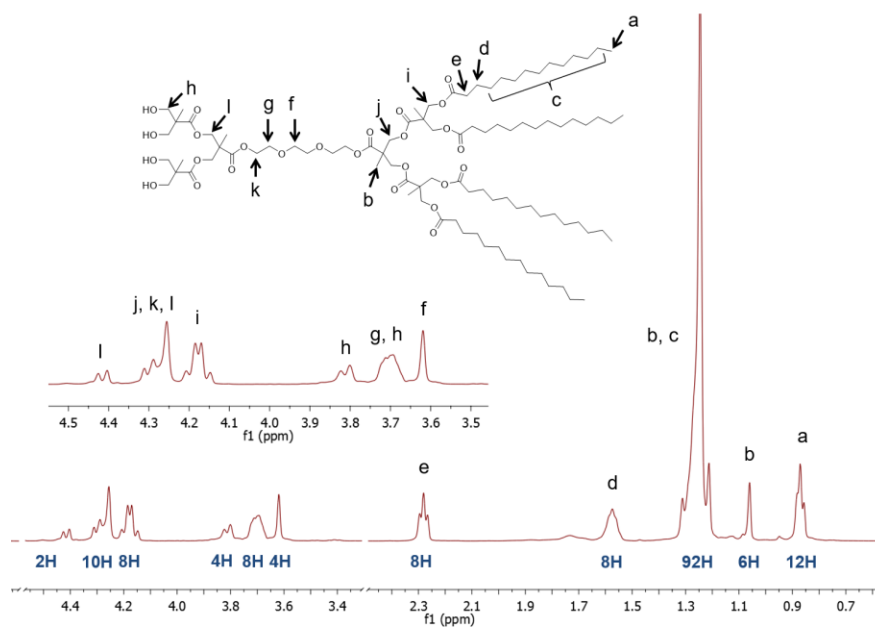
Figure 4.9 ¹H-NMR spectra (500 MHz, CDCl₃) of 10B, integrals and peak assignments.
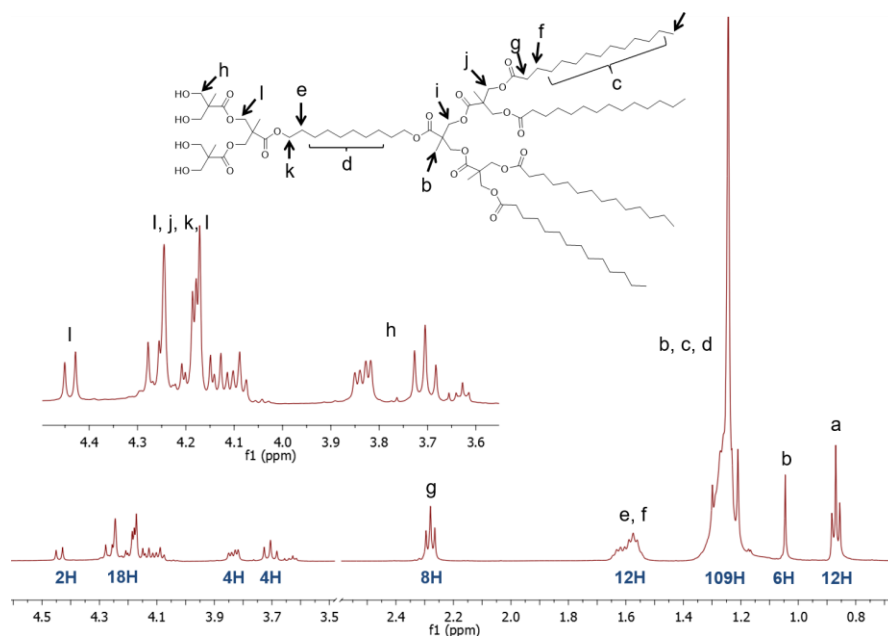
Figure 4.10 ^{1}H-NMR spectra (500 MHz, CDCl$_3$) of 10C, integrals and peak assignments.

4.2 Thermal Behavior of Amphiphilic JDs

The thermal behavior of the dendrimers was determined using differential scanning calorimetry (DSC). Results of DSC measurements are summarized in Table 4.1, and the DSC curves are presented in Figures 4.11 and 4.12.

Due to the waxy consistency of the dendrimers, an initial heating scan from 30 to 60 °C was applied to increase the contact surface between the samples and the bottom of the aluminum pans where the measures were conducted. In this range of temperatures only melting transitions (Tm) were observed for all dendrimers. In general, the shape of these melting transitions peaks was broad and presented high enthalpy values (66-230 kJ/mol) (Figure 4.11). These values were in the order of magnitude of melting process enthalpies of similar dendrimers [3]. The [G-2] dendrimer with ethylene glycol core (compound **10A**) presented the highest melting temperature. On the other hand, [G-2] dendrimer with 1,10-decanediol as core (compound **10C**) presented the highest

enthalpy value. Enthalpies of [G-2] dendrimers were higher than those of the [G-1]. In addition, it was observed a trend between the enthalpy values and the type of core in the dendrimer structures, being the dendrimers with 1,10-decanediol as core (denoted with letter C in the nomenclature of the compounds) those that presented higher enthalpy values compared to the other dendrimers in the same generation. This suggests that the long hydrocarbon chain in the 1,10-decanediol core increase the van der Waals interactions between dendrimer molecules, increasing the total heat required for the phase transition [65].

Table 4.1 Thermal properties of amphiphilic Janus dendrimers.

Generation	Core	Dendrimer	MW (g/mol)	Thermal transitions (°C) and their corresponding enthalpy and/or heat capacity changes [kJ/mol] (kJ/mol°C)
[G-1]	EG	5A	714.53	1° Heating Tm 32.22 [66.09] 2° Heating Tm_1 13.34 [123.58], Tm_2 28.18 [27.70]
	DD	5C	827.24	1° Heating Tm 38.64 [135.70] 2° Heating Tm 35.13 [118.43]
[G-2]	EG	10A	1600.21	1° Heating Tm 48.23 [155.8] 2° Heating Tm 10.93 [63.58]
	TEG	10B	1687.17	1° Heating Tm 31.77 [165.39] 2° Heating Tm 14.7 [71.89]
	DD	10C	1711.24	1° Heating Tm_1 33.74 [230.18], Tm_2 40.87 [11.99] 2° Heating Tg -26.10 (1.04), Tm 5.086 [65.76]

[G-1]: first generation; [G-2]: second generation; EG: ethylene glycol core: TEG: triethylene glycol core; DD: 1,10-decanediol core. 1° Heating from 30 to 60 °C; 2° Heating from -45 to 60 °C. Tm: melting temperature; Tg: glass transition temperature.
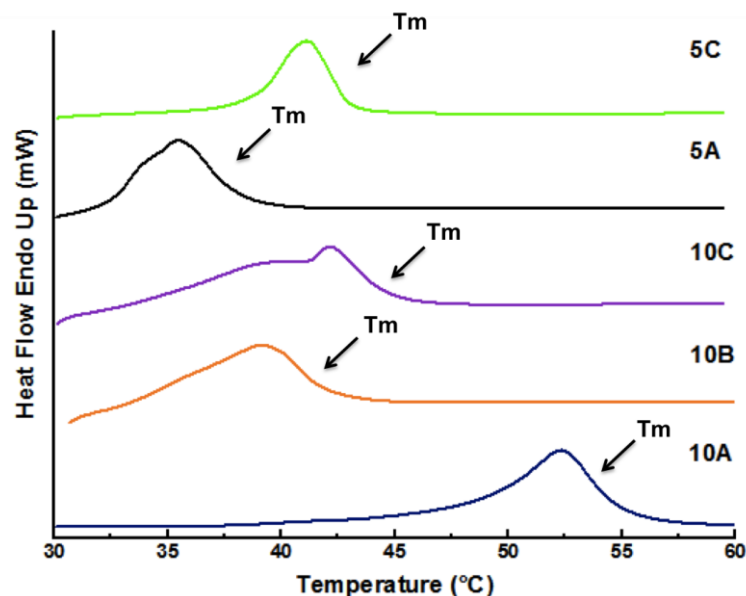
Figure 4.11 First heating DSC curves of amphiphilic Janus dendrimers.

In the second heating scan, it was observed a displacement of the fusion transitions to lower temperatures, for all dendrimers (Figure 4.12). This behavior is due to the formation of metastable phases via crystallization or cold crystallization [30]. This effect was more pronounced in the [G-2] dendrimers, probably because of the size of their structure that difficult the rapid arrangement of the dendrimer molecules into more stable phases. Dendrimers **5A**, **5B** and **10C** exhibited more complex thermal behavior in the second heating. In dendrimer **5A**, it was observed two melting transitions in DSC curves, indicating the presence of polymorphism [29]. In the case of dendrimer **5B**, a crystallization peak was observed during the heating. This behavior is observed when an amorphous material tends to crystallize or a semicrystalline material does not crystallize to the limit of its ability when cooled [66]. Only dendrimer **10C** exhibit a glass transition at -26.1 °C in addition to the melting transition.

It is important to note that all dendrimers presented crystallization in the cooling scans (data not shown).
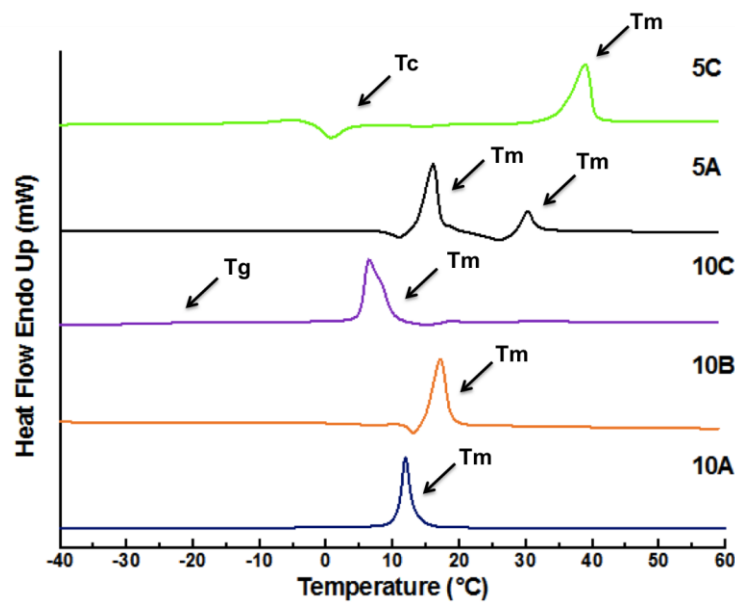
Figure 4.12 Second heating DSC curves of amphiphilic Janus dendrimers.

4.3 Self-Assembly of JDs in Water

4.3.1 Formation and Characterization of Giant Assemblies

4.3.1.1 Thin-Film Hydration Method

The hydration of dried lipid films is a method generally used to obtain giant vesicles [40,67]. In previous reports, giant unilamellar dendrimersomes have been formed by the gentle hydration (natural swelling) of JD films JD films [6–8,4,12]. Herein, we adapted the method reported by Percec et al. [4] to obtain the hydration structures of the synthesized dendrimers. Two procedures were used for the thin-film hydration: (1) temperature of hydration at 60 °C, using a roughened Teflon surface as support of the film; and (2) at 80 °C using glass as support. In general, both procedures generated polydisperse dendrimer assemblies with spherical morphology (Figure 4.13). In addition, a low production of assemblies and the incomplete dispersion of the JD films in water

were observed for all dendrimers (Figure 4.13a). The procedure 1 generated fewer assemblies than procedure 2. Also, this procedure generated assemblies of smaller size.

(a)   (b)   (c)
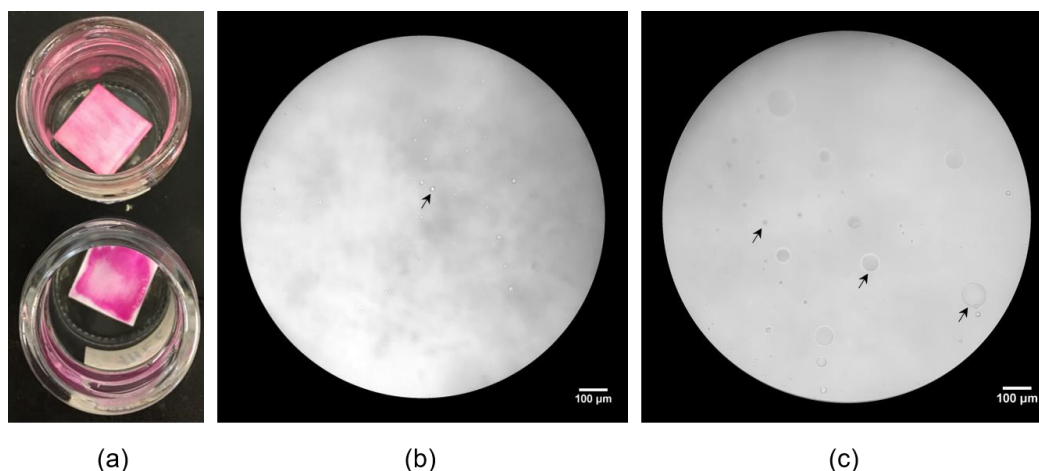
Figure 4.13 Production of assemblies using the thin-film hydration method. (a) Residual dendrimer/Nile Red films after 12 h of hydration. (b) Optical micrograph showing assemblies obtained by procedure 1. (c) Optical micrograph showing assemblies obtained by procedure 2.

The JDs were able to encapsulate the hydrophobic dye Nile Red as confirmed by confocal microscopy (Figure 4.14). Optical sections of assemblies showed the accumulation of the dye within the whole structure of the assemblies. No presence of water inside the structures was observed, except for some of the assemblies of dendrimer **5A** that presented solvent sections. However, these sections represent a small proportion of the assemblies. Figure 4.14 shows optical sections of dendrimers assemblies, taken from the center of their structures. The results of dye encapsulation experiments indicate that the dendrimer assemblies are mainly composed of hydrophobic domains, without water entrapped inside, discarding the presence of dendrimersomes (vesicle-like morphology). Multiple layers of dendrimers could form the

obtained assemblies. No formation of dendrimersomes can be attributed to the poorly hydration of the dendrimer film caused by the insufficient electrostatic repulsion between the adjacent lamellae, as seen in neutral phospholipids [40,67]. Moreover, the preparation methodology adopted used heat to promote the lamellae hydration. According to Ianiro et al. [39], this condition causes the loss of the hydrogen bonds between the water and hydrophilic domains, reducing the overall solubility of the amphiphile. It is necessary to explore other preparation procedures, varying the temperature of thin-films rehydration or using other production techniques for giant vesicles, such as microfluidics.

(a)   (b)   (c)
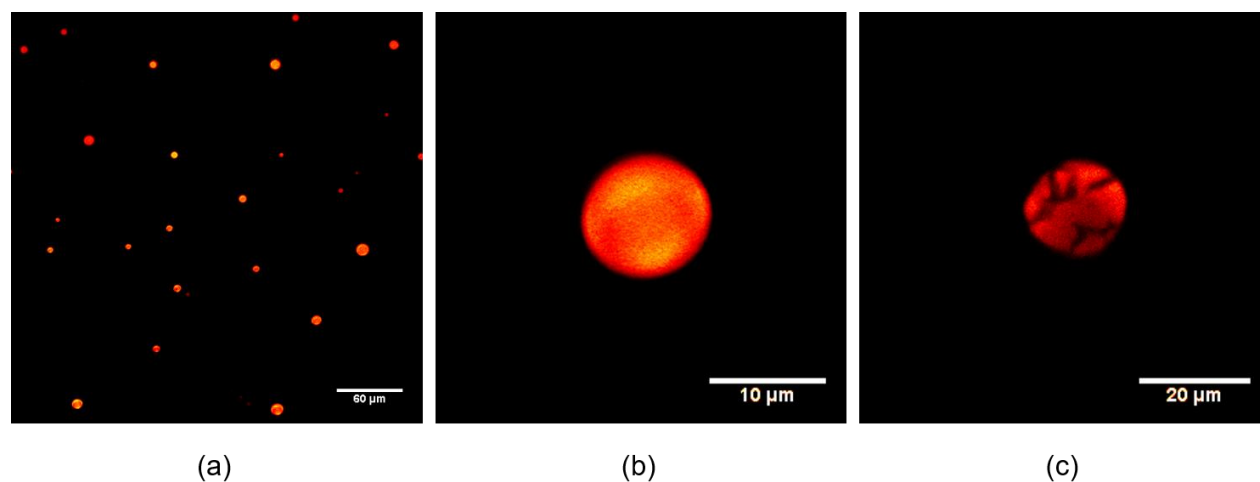
Figure 4.14 (a) Confocal microscopy images of dendrimer 10A assemblies formed by the thin-film hydration method and encapsulating Nile Red (hydrophobic dye). Optical sections of individual assemblies of (a) 10A and (b) 5A, taken from the center of their structure.

4.3.1.2 Microfluidics

Due to the low efficiency for dendrimersomes formation using the thin-film hydration method, the microfluidic approach was employed as an alternative for vesicle production. Monodisperse double emulsion drops with ultrathin shells were used as templates for the fabrication of dendrimersomes from [G-2] JDs (compounds **10A-C**). The election of these dendrimers was arbitrary. However, the molecular structure of [G-2] dendrimers could be interesting for further applications due to the higher number of functionalizable hydroxyl groups. Figure 4.15 shows a typical image of the double emulsion production in the glass microfluidic devices employed.

Figure 4.15 Optical micrograph showing a typical production of monodisperse double emulsion drops containing dendrimers in the oil phase.

First explorative experiments were conducted using the conditions described by Arriaga et al. [54]. The oil phase for these experiments was composed of a mixture of 36% chloroform and 64% hexane (v/v), and a JD concentration of 5 mg/mL. With the addition of dendrimers in the oil middle phase in the microfluidic devices, two different flow

behaviors were observed. For dendrimers **10A** and **10C**, the flow followed a discontinuous regime, in which single-emulsion drops and double-emulsion drops were produced intermittently [54]. For dendrimer **10B**, double-emulsion drops were obtained in a stable continuous regime during 1 h of sample collection. It is known that surfactant molecules do not affect the surface tension during the drop production in microchannels when their diffusion times are higher than the time of drop formation [68]. This is an evidence that dendrimer **10B** must have a low diffusion time.

Due to the precise control over the flow ratios in the microfluidic device, in experiments with dendrimer **10B,** the resultant double emulsion drops were highly monodispersed, with radius 30 ± 3 μm, as shown in Figure 4.16. The small drop with high optical contrast (indicated in a circle) in Figure 4.16a was an oil-in-water single emulsion drop. Since the double emulsion drops with dendrimer **10B** were obtained in the continuous regime, these single emulsion drops must come from destabilized double-emulsion drops and represent 14% of the total sample.
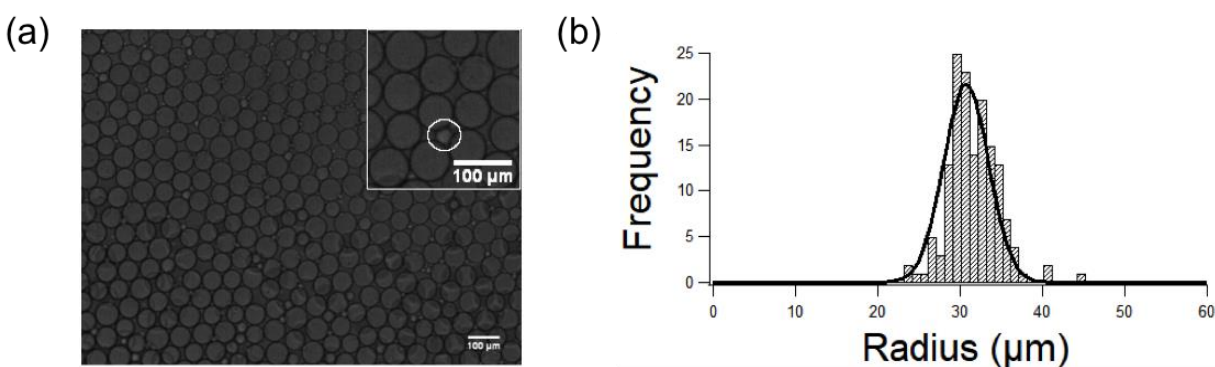
Figure 4.16 (a) Optical micrograph of a population of double emulsion drops containing dendrimer B. The inset shows a single emulsion drop formed by the destabilization of a double emulsion drop (white circle). (b) Radius distribution of double emulsion drops. The mean radius is 30 ± 3 μm.

The mean value of the radii R_o of these single emulsion drops was used to determine the thickness of the middle oil phase of the double emulsion drops: since the total volume of the double emulsion drop (V_T) must be equal to the sum of the volume of the aqueous phase (V_{aq}) plus the volume of the oil phase (V_o) (Equation 1), the expression for the thickness (t) of the double emulsion drops can be formulated as Equation 2, where R_T is the external radius of the double emulsion drop and R_o is the radius of the single emulsion [53].

$$V_T = V_{aq} + V_o \qquad \text{Equation 1}$$

$$t = R_T - \sqrt[3]{R_T^3 - R_o^3} \quad \text{Equation 2}$$

By this calculation, the shell thickness was 140 nm, considering an uncertainty of 6% from the optical resolution limit of microscopy images. This value was similar to previously reported works with this method, being around 200-600 nm for double emulsion drops made with SPAN 80 surfactant in hexadecane [53,69]. In fact, the oily shell of the double emulsion drops made with this method was less than a micron thick, smaller than in double emulsion templates obtained with other methods. This feature is important in double emulsion drops because under the appropriate conditions enables the formation of vesicles after the oil phase evaporation [54], due to the minimal amount of residual solvent within their shells. However, double emulsions obtained with this experiment did not precipitate into bilayered structures.

As mentioned above, double emulsions made with dendrimers **10A** and **10C** were obtained with a discontinuous regime. The resulting double emulsions made with these dendrimers destabilize in some minutes after their production. Even though, in the case

of dendrimer **10A**, the presence of polydisperse vesicle-like structures was observed among several drops of oil in water (**Figure 4.17a**). In the case of the sample made with dendrimer **10C**, no evidence of stable double emulsion drops was observed (data not shown).

The different behavior of the JD assembly could be attributed to the difference in the hydrophilicity of each dendrimer. Following this idea, the HLB balance for dendrimers was calculated. The resulting values were 6.36 for dendrimer **10A**, 7.07 for **10B**, and 5.94 for **10C**; being the dendrimer **10C** the less hydrophilic. Samples of double emulsions obtained from dendrimers **10B** were stable at least for 20 days, stored at room temperature. It was considered that the polydisperse vesicle-like structures observed in the dendrimer **10A** sample were driven by the self-assembly of this dendrimer into vesicles next to destabilization of the double emulsion drops.

(a)   (b)
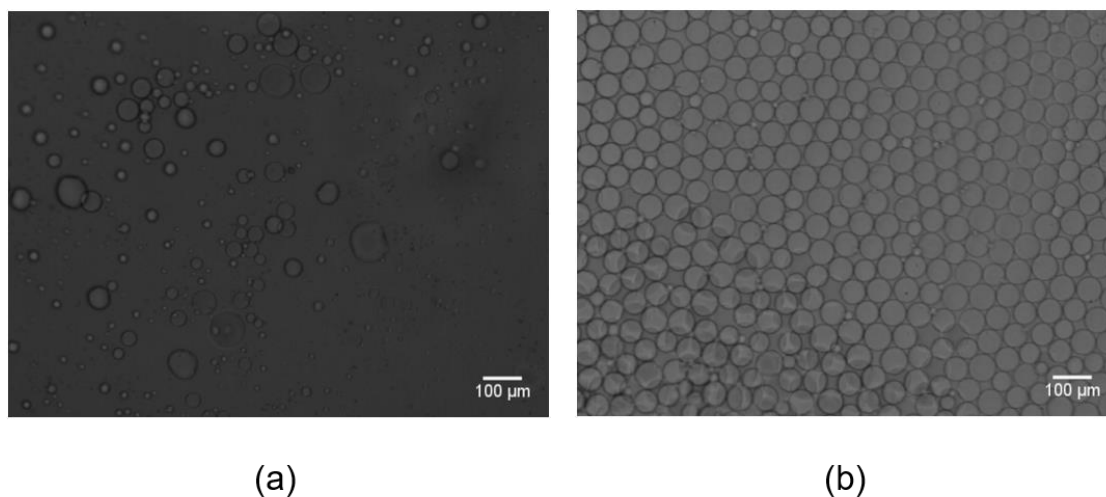
Figure 4.17 Bright field microscopy images showing the samples resulting from double emulsion drops made with: (a) dendrimer 10A, image was taken 4 days after production, polydisperse vesicle-like structures are observed; (b) dendrimer 10B, image was taken 12 days after production, monodisperse double emulsion drops continue presently.

Since dendrimer **10B** was the only dendrimer that formed stable double emulsions suitable for dendrimersomes production, this dendrimer was used in a second experiment. For the second experiment, dendrimer concentration was increased to 12 mg/mL and the oil phase mixture was modified 44% chloroform and 56% hexane (v/v). With the flow ratios and the solvent mixture used in this experiment, the microfluidic device worked in a discontinuous regime. In addition, with the solvent mixture and dendrimer concentration employed, the double emulsion drops produced precipitated into dendrimersomes, as shown in Figure 4.18. In the obtained dendrimersomes, it was observed the formation of the small dendritic reservoirs (Figure 4.18b). This reservoirs of surfactant molecules had been observed previously in liposomes obtained with this method [54], in which, the formation of vesicle-like structures was promoted by the ultrathin oily shell of the double emulsion templates made in the microfluidic devices used. A careful selection of the oil mixture in the middle phase, with a volatile solvent (chloroform) capable of a fast evaporation and a less volatile solvent that promotes the precipitation of dendrimers (hexane), lead the formation of bilayers through a hydrodynamic fluctuation after the evaporation of solvents, in a process known as dewetting [54,70,71]. Nevertheless, the samples of dendrimersomes produced were polydisperse due to difficulties related to the control of the dripping regime in the double emulsion formation. The formed dendrimersomes (Figure 4.18c) started to destabilize upon three days after their production. In spite of the short time of stability of the dendrimersomes, the results show the ability of the microfluidic method to assemble these JDs into vesicle structures.
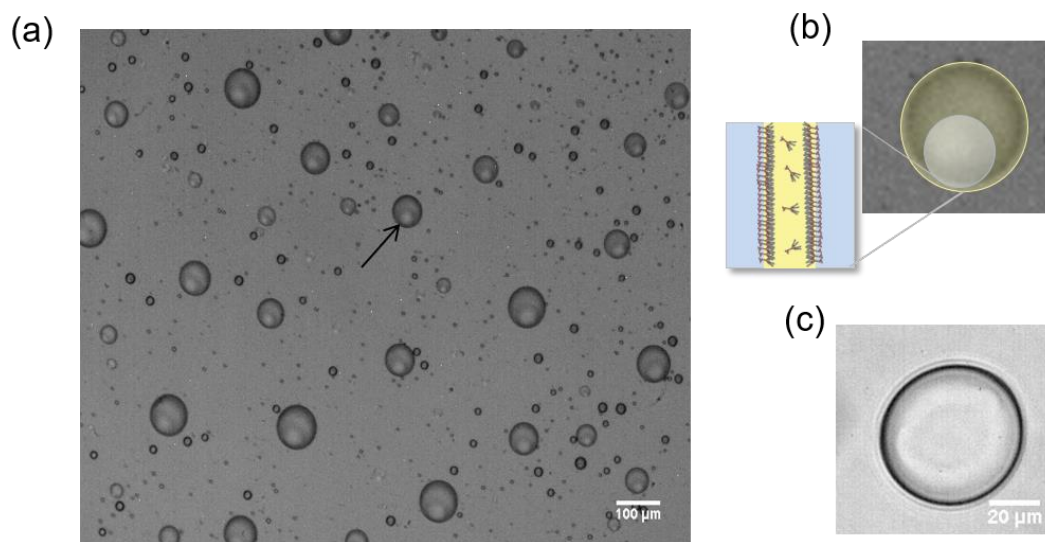
Figure 4.18 (a) Optical micrograph showing the population of double emulsion drops after their transition to dendrimersomes. (b) Scheme showing the formation of dendritic reservoirs. (c) Dendrimersome formed after solvent evaporation.

4.3.2 Formation and Characterization of Small Assemblies

All synthesized dendrimers were soluble in acetone, ethanol, and THF. These solvents are commonly used for the preparation of dendrimersomes through the injection method. As an explorative experiment, small assemblies of dendrimer **10A** were prepared by the injection of dendrimer solutions in each of these solvents into ultrapure water. Small assemblies were analyzed using dynamic light scattering (DLS) to determine their size distribution. Injection of an ethanol solution of dendrimer **10A** generated assemblies with a Z-average of 69.6 ± 1.92 nm (diameter) and PDI of 0.14 ± 0.01. On the other hand, an acetone solution of dendrimer **10A** produced assemblies with a larger Z-average of 141.3 ± 5.6 nm and PDI of 0.163 ± 0.05. THF solutions of dendrimer **10A** generated assemblies with Z-average of 221.8 ± 39 nm and PDI of 0.335 ± 0.01. Samples from THF solution injection were not stable, and the precipitation

of dendrimer was observed. It is important to note that ethanol and acetone solutions of dendrimer formed assemblies with PDI values that were below the threshold of 0.2 that is considered monodisperse for vesicles [12]. However, the following experiments with all dendrimers were conducted using ethanol as solvent. One of the major drawbacks of solvent injection method for future biomedical applications is the presence of organic solvent traces in the final vesicle solution that can be toxic and hazardous to human health. Ethanol is a biocompatible solvent that is widely used in pharmaceutical formulations [72].

Injection of ethanol solutions of dendrimers **5A-C** and **10B-C** into ultrapure water produced slightly cloudy dispersions, indicative of the formation of dendrimer assemblies (Figure 4.19). Dendrimers with ethylene glycol (**5A** and **10A**) core presented greater turbidity.

(a)　　　　　　　　　(b)　　　　　　　　　(c)
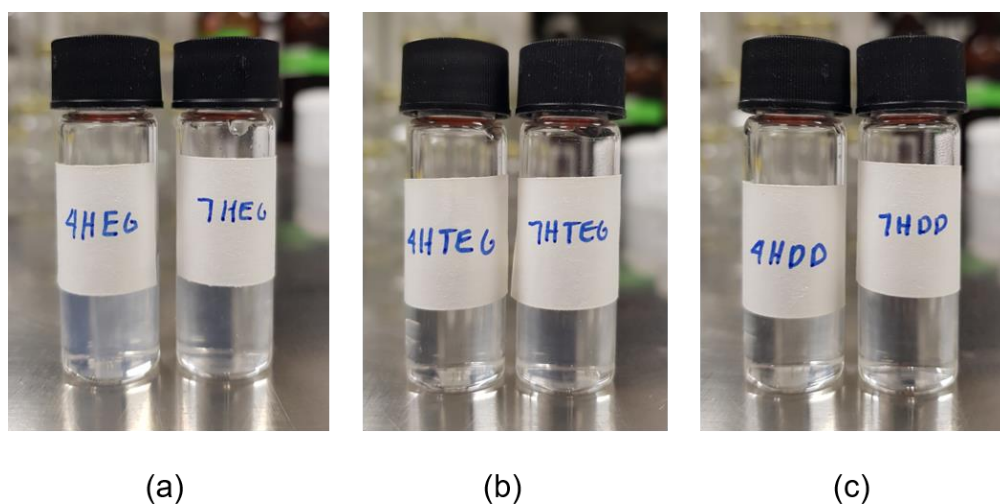
Figure 4.19 Cloudy dispersions of dendrimers with (a) ethylene glycol core (5A and 10A), (b) triethylene glycol core (5B and 10B), and (c) 1,10-decanediol core (5C and 10C), indicative of the formation of assemblies in water.

According to DLS measures, dendrimers generated assemblies with Z-average sizes in a range from 42 to 64 nm with narrow size distribution (PDI from 0.08 to 0.21) (Table 4.2). The analysis of variance (ANOVA) for Z-average values showed significant evidence (*p*-value < 0.05) of effects of the dendrimer branching pattern (generation) and the type of core in the size of the assemblies, being the type of core the factor that had a major impact in this parameter. In addition, an interaction between the generation and the type of core was found. On the other hand, ANOVA for PDI values showed significant evidence (*p*-value < 0.05) of an effect of the type of core in the PDI. An interaction between the generation and the type of core was also found. Detailed information of these analyses is described in Appendix B and C.

Table 4.2 Small assemblies size and PDI (by DLS) obtained by the injection of ethanol.

Generation	Core	Dendrimer	Z-Average (diameter, nm) *	PDI *
	EG	5A	63.8 ± 2.33^B	0.08 ± 0.02^C
[G-1]	TEG	5B	50.1 ± 2.42^D	$0.12 \pm 0.04^{B,C}$
	DD	5C	48.1 ± 3.15^D	0.21 ± 0.05^A
	EG	10A	69.6 ± 1.92^A	$0.14 \pm 0.01^{B,C}$
[G-2]	TEG	10B	56.5 ± 2.41^C	$0.13 \pm 0.06^{B,C}$
	DD	10C	41.7 ± 1.02^E	0.15 ± 0.03^B

[G-1]: first generation; [G-2]: second generation; EG: ethylene glycol core: TEG: triethylene glycol core; DD: 1,10-decanediol core. *Dendrimer Z-averages and PDI not connected by the same letter are significantly different by Tukey test at p-value ≤ 0.05.

In general, JDs with ethylene glycol as core generated the largest assemblies (compounds **5A** and **10A**), followed by dendrimers with triethylene glycol (compounds **5B** and **10B**). Dendrimers with 1,10-decanediol as core (compounds **5C** and **10C**) formed the smallest assemblies. According to the results obtained by DSC, dendrimers with 1,10-decanediol as core presented more interactions between their molecules in

bulk than dendrimers with another type of core. This may be influenced in the arrangement of the membrane dendrimers in the water assemblies, generating less interdigitated and less flexible bilayers, and thus smaller assemblies [25,13]. Dendrimers with ethylene glycol and triethylene glycol as cores present a similar hydrophobic fraction in their structure. Differences in the size of their assemblies may be also influenced by the interaction between the bilayer dendrimers. Figure 4.20 shows a schematic image of the possible arrangement of dendrimers in the membrane of the assemblies.

(a)   (b)   (c)
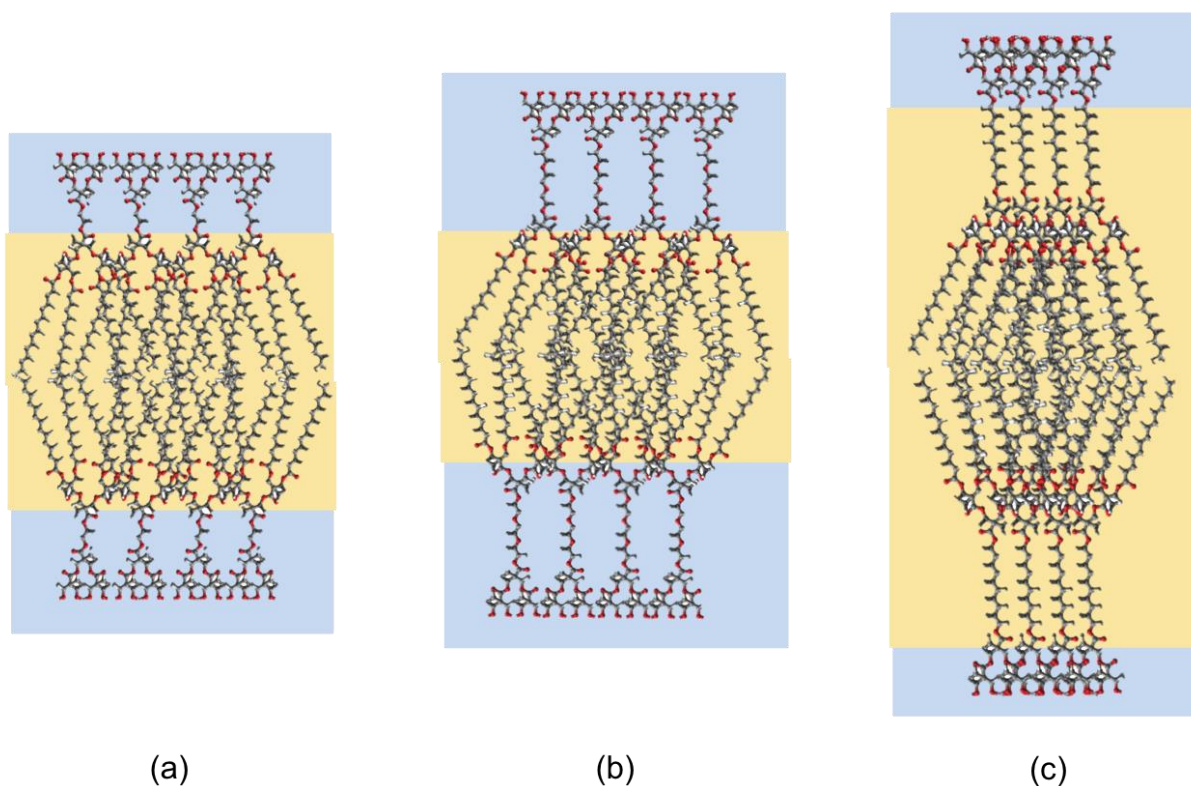
Figure 4.20 Schematic representation of the possible arrangement of dendrimers in the membrane of formed assemblies. Dendrimers with (a) ethylene glycol, (b) triethylene glycol and (c) 1,10-decanediol. Color code: yellow, hydrophobic part of the membrane; blue, hydrophilic part of the membrane.

In the case of PDI, dendrimer **5C** with 1,10-decanediol as core presented the largest PDI value, and there was not observed a trend related with the type of core and PDI, as was observed in the Z-average results. The assemblies of all dendrimers presented negative ζ-potentials ranging from −30 to -46 mV. In agreement with our results, Nummelin et al. [12] obtained negative ζ-potentials values for neutral JDs (hydroxyl-terminated).

The stability of the assemblies to time and temperature was also explored. Only assemblies from dendrimers **5C** and **10A** did not show significant differences in Z-average size after 20 days at 25 °C (p-value > 0.05, Figure 4.21a). However, all dendrimer samples maintained their Z-average sizes below 100 nm. Furthermore, the PDI values decreased after 20 days. This behavior could be due to the equilibration of the assemblies to form more stable structures. With the bottom-up approach (solvent injection method) the hydrophobic chains need time to organize into a stable conformation. When the solvent switch is too fast, the hydrophobic chains tend to collapse forming spherical objects, to reduce their interfacial area. These structures are metastable and are not the most stable conformation that the system can adopt [73].

Dendrimers **5B-C** and **10A-C** showed thermal stability in a temperature range of 25-70 °C (Figure 4.22). Their Z-average size did not vary more than 6% and the PDI maintained below 0.2 in this temperature range. Dendrimer **5A** ([G-1] with ethylene glycol as core) showed a size variation greater than 10%, indicating the merging of the assemblies. In DSC measurements results, dendrimer **5A** presented a low melting temperature with low enthalpies values. These thermal properties could be generated

more mobility of the molecules of the membrane, thus generating instability of the assemblies.
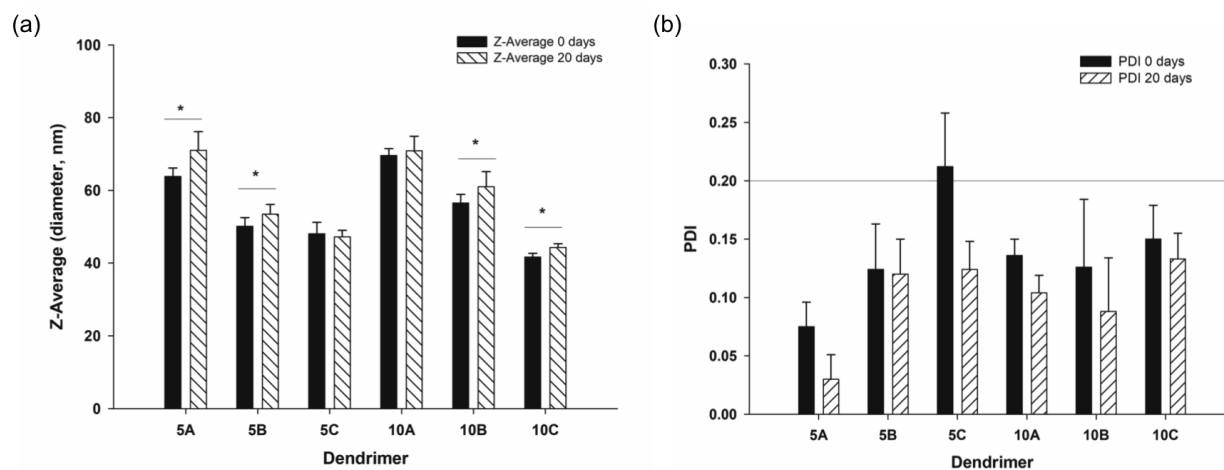
Figure 4.21 Time stability of small assemblies. (a) Z-Average and (b) PDI variation (by DLS). *significant difference by paired t-test at *p*-value ⩽ 0.05. Dendrimers nomenclature: 5, [G-1] dendrimers; 10, [G-2] dendrimers; A, ethylene glycol as the core; B, triethylene glycol as the core; and C, 1,10-decanediol as the core.
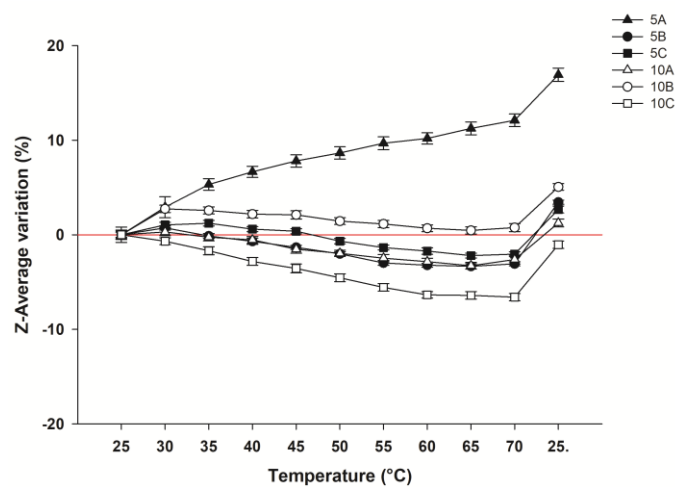
Figure 4.22 Temperature stability of the assemblies reported as a change (%) in Z-average. Dendrimers nomenclature: 5, [G-1] dendrimers; 10, [G-2] dendrimers; A, ethylene glycol as the core; B, triethylene glycol as the core; and C, 1,10-decanediol as the core.

Small assemblies of dendrimer **10A** were also analyzed by atomic force microscopy (AFM), which allowed the observation of isolated structures with concave and convex morphologies in the AFM height images (Figure 4.23a). Profile analysis of an AFM height image is presented in Figure 4.23b. Convex structures with larger dimensions product of assemblies' fusion were observed. All structures presented larger diameters (144.0 ± 21.6 nm) than related heights (4.30 ± 0.91 nm). The diameter values were higher than those calculated by DLS. This morphological characteristic has been previously reported in dried liposomes and it has been attributed to a structural collapse due to the evaporation of water from vesicle interior and the adsorption on the substrate, which leaves a circular shape with a rim similar to a deflated soccer ball [74,75]. This characteristic was also observed in dendrimersomes, as reported by Giustini et al. [31]. Considering the apparent height of the higher outline of the structures (4.30 ± 0.91 nm) that compares with the typical dendrimersome bilayer thickness (5 to 8 nm) [3,31,76], it can be deduced that this value corresponds to the membrane thickness of the assemblies. The AFM phase images (Figure 4.23c) showed a dark area in the center of the assemblies (negative phase shift) and a bright area in their contour (positive phase shift), indicating differences in the surface properties of the samples. Ruozi et al. [74] reported that this variation could be affected by the hydration degree of the bilayer and consequently by the local surface properties of vesicles. The negative phase shift, identified in the depressed central portion of the structure, can be related to a flattened layer of lipids with high viscosity. On the other hand, the positive phase shift observed in the higher outline of the structure suggests that the lipids were still hydrated with a relatively low viscosity environment [74,77]. Although AFM images

allowed the identification of dendrimersomes, one limitation of this study is that assemblies were analyzed as dried samples. Other techniques, including environmental scanning electron microscopy (ESEM) [74,78] and liquid-cell transmission electron microscopy (LCTEM) [73], can be used for the visualization of small assemblies in the hydrated state. Nonetheless, unlike AFM, the resolution of ESEM do not provide detailed information related to the surface and architecture of the small vesicles [74], and LCTEM has to be improved and it may not be accessible to researchers due to its short time development [79].
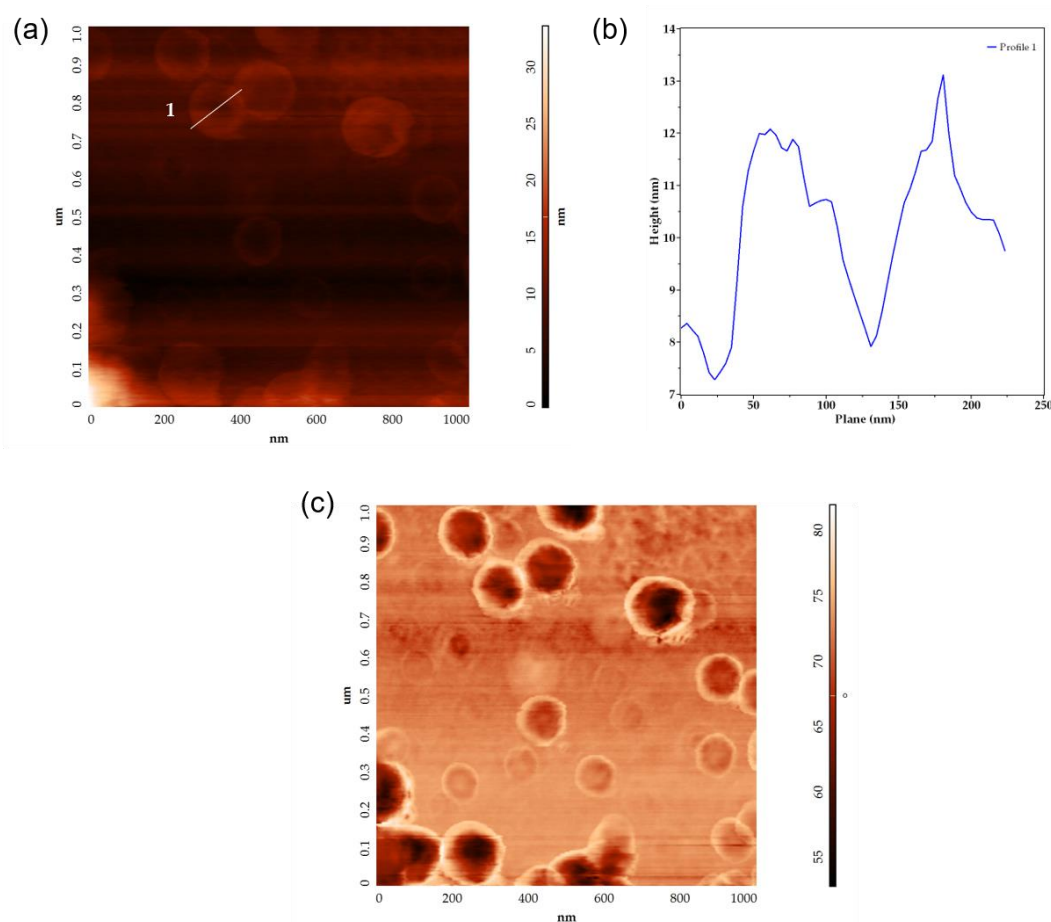
Figure 4.23 Atomic force microscopy (AFM) images of air-dried small assemblies obtained using ethanol injection method. (a) AFM height image and (b) cross-section profile determined from line 1. (c) AFM phase image.

4.3.3 Coarse-grained Molecular Dynamic Simulation of Dendrimer 10A

The self-assembly of dendrimers **10A** in water at different stages of the CG-MD simulation is shown in Figure 4.24. At the beginning of the simulation, the randomly distributed dendrimers self-assembled into clusters, including small disk-like bilayers with a non-zero spontaneous curvature. More complex clusters, formed by several stacked bilayers, were also identified at the early stages of the simulation. Along with simulation, the small clusters continued aggregating to large clusters through hydrophobic interactions.
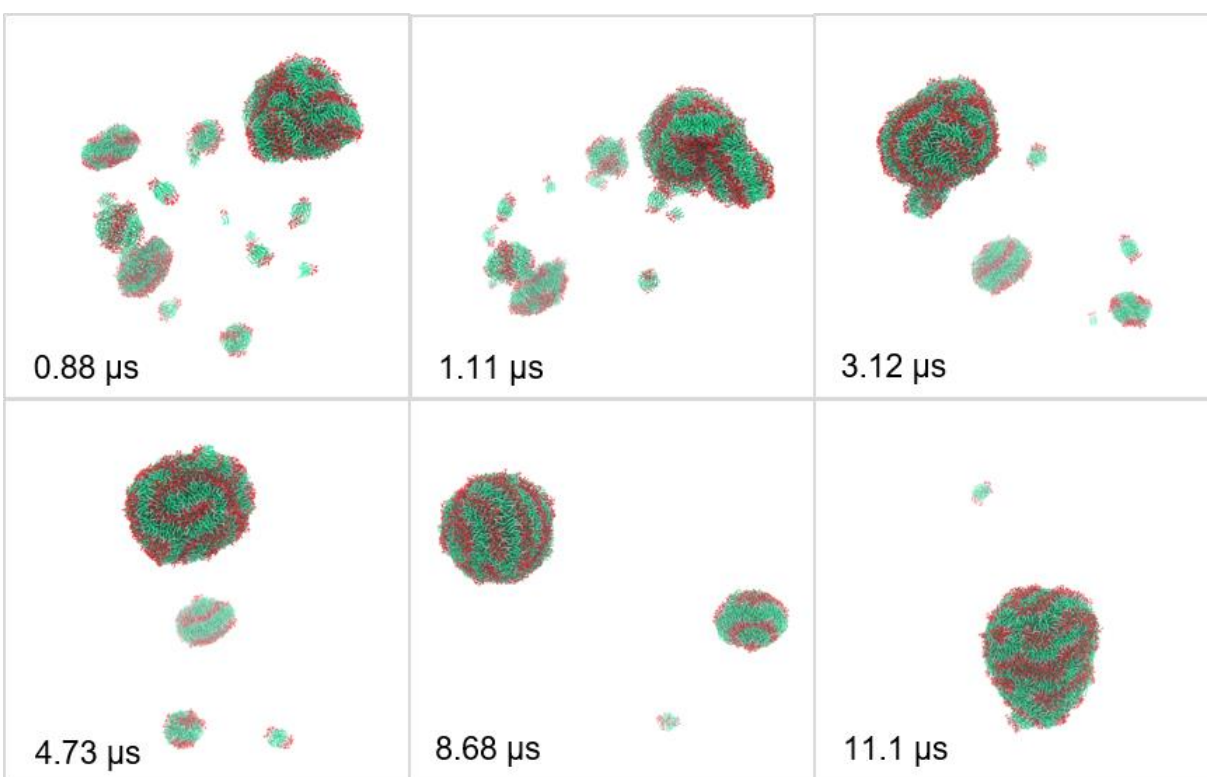
Figure 4.24 Representative images of the self-assembly process of JDs in water at different stages of the coarse-grained molecular dynamics (CG-MD) simulation. Color code: polar head group, red; hydrophobic tails, green; and hydrophilic groups, gray. Water is not shown.

Figure 4.25 presents images taken from the simulation, in which a fusion event between a nanostructure and a disk-like bilayer was observed. At the end of the simulation, the majority of the bilayered assemblies clustered together. The reaching of the equilibrium stage of the system was confirmed by the calculation of solvent accessible surface area (SASA) of the dendrimers during the simulation (Appendix D). After 10 µs of simulation, this parameter remained constant.

At the 13 µs of simulation, a quasi-spherical nanostructure with an average volume of 12.9 nm^3, diameter around 20 nm and aggregation number of 1689 JDs, was obtained (Figure 4.26a). This final structure was constituted by entangled dendrimer bilayers, with hydrophobic sites exposed to aqueous media and did not present dendrimersome morphology as seen in the cross-sectional view of the final structure (Figure 4.27b).
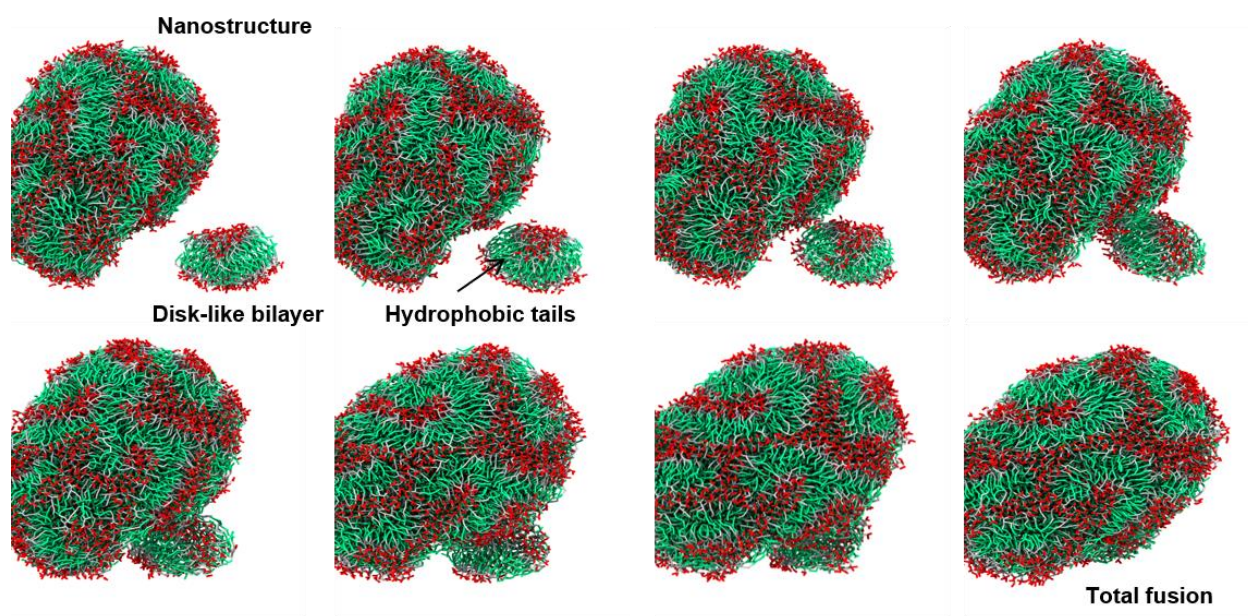
Figure 4.25 Snapshot of fusion mechanism of a disk-like bilayer and a major size nanostructure. Color code: polar head group, red; hydrophobic tails, green; and hydrophilic groups, gray. Water is not shown.
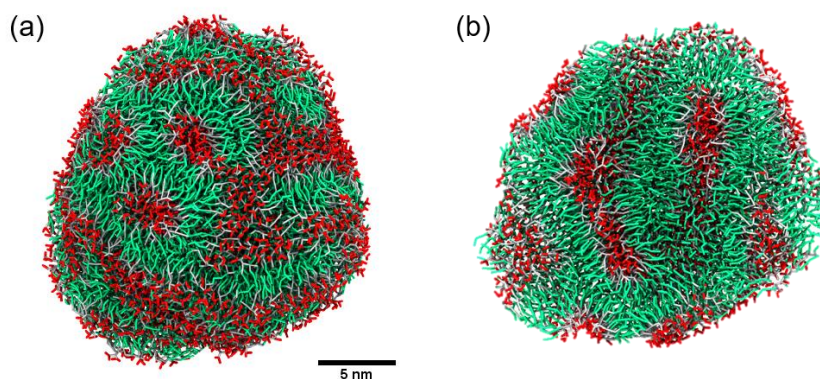
Figure 4.26 (a) Final assembly obtained by coarse-grained molecular dynamics (CG-MD) simulation. (b) A cross-sectional view of the nanostructure. Time of simulation: 13 µs. Color code: polar head group, red; hydrophobic tails, green; and hydrophilic groups, gray. Water is not shown.

The self-assembly behavior of the JDs and its aggregation nanostructure does not coincide with the reported mechanisms for vesicle formation. Reported mechanisms, using computer simulation and macromolecules different to dendrimers (polymers [80,81], cationic-anionic surfactants [35], and phospholipids [82,83]) describe three stages in this process: the nucleating, fusion and curling stages. In the nucleating stage, small clusters of amphiphilic molecules are formed; during the fusion stage, small micelles fuse to form disk-like aggregates; and finally, in the curling stage these disk-like aggregates curl up and close to form vesicles [35]. In contrast, JDs presented aggregation into bilayers rather than micelles, this behavior could be due to the lack of molecules that being able to form the lateral edges of the micelles. The geometrical condition in the molecular structure of the amphiphiles to form that edges in micelles is that their packing parameter factor accomplish $v/a_o l_c < 1/3$, where v is the volume of their hydrocarbon chains, a_o is their optimal area per head group that minimize the free energy and l_c is roughly the length of the hydrocarbon chain [84]. According to this, the

volume of the JDs hydrocarbon chains is too high compared to the polar head group area, causing that they cannot form micelles, in contrast to single-tailed amphiphilic dendrimers, such as PAMAM-G2 derivatives [38].

In accordance with our results, Percec et al. [4] reported differences in resulting structures of CG-MD simulation of an uncharged amphiphilic JD, dependent on the concentration of the initially dispersed molecules. Also, Arai et al. [85] reported this behavior with lipid membrane solutions simulations, where they observed network and sponge morphologies, closer to our results, at higher lipid concentrations. Furthermore, using experimental methods, Fedeli et al. [3] reported the obtaining of aggregates, homogeneous in dimensions and with diameters around 50 nm (observed in TEM images) from a bis-MPA based [G-2] JD with a molecular structure like the JD simulated herein. According to Fedeli et al., these aggregates cannot be explained as formed by individual bilayers and they proposed that the obtained nanospheres are formed from bent and rolled-up bilayer structures. On the other hand, the authors describe the formation of vesicles from higher generation JDs (hydrophobic-hydrophilic block generations: [G-2]-[G-3] and [G-3]-[G-3]). According to this result and previous studies of CG-MD focused on the self-assembly of different generation amphiphilic dendrimers [38], generation of the hydrophilic block influences the morphology of the assemblies and higher dendrimer generation could derive in the formation of vesicles. One limitation of our study is that we did not evaluate different concentrations or compositions of dendrimers in the simulation, to explore other assemblies' morphologies. Nevertheless, to our knowledge, this is the first report where the self-assembly phenomenon of this type of bis-MPA amphiphilic JD was molecularly explored using a CG-MD simulation.

A patch was selected from the final simulation nanostructure. The density profile analysis of the components of this patch (Figure 4.27) displays the decrease of polar head groups and total hydrophilic groups density, as the measured distance approaches the center of the selection. On the contrary, the density of tail end groups and total hydrophobic groups increased in this zone and decreases as the measured distance moves away from the center of the selection. This data confirms that dendrimers tend to arrange into bilayers that are forming the final nanostructure.
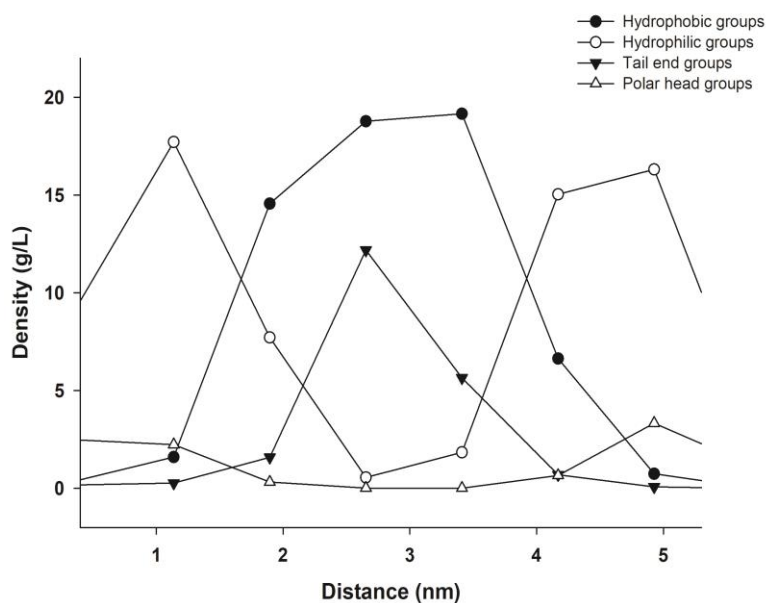
Figure 4.27 Density profile analysis of a selected patch from the final nanostructure. Size of selected patch considered: 6.5 × 5.4 × 7.4 nm^3.

A bilayer thickness of 4.1 nm with a hydrophobic part length of 1.8 nm was determined from the selected patch. In addition, a dendrimer length of 2.0 nm with a hydrophobic tail length of 0.7 nm was determined. It is important to note that bilayer thickness and its hydrophobic part length were more than twice as large as the dendrimer and its hydrophobic tail length, respectively. Hence, there was no interdigitation among bilayer components. Interdigitation degree in bilayers is related to the size, hardness, and

stability of aggregates [10]. This parameter is influenced by the length of hydrophobic tails [38] and other factors, such as the formation of hydrogen bonds between the hydrophilic segments of the membrane dendrimers, which prevent the interdigitation [13]. The dendrimer studied here was composed of bis-MPA moieties with hydroxyl groups that form this type of interactions and may be influencing the arrangement of the dendrimers in the bilayers.

Comparing the bilayer thickness determined from the final simulation structure versus the value deducted from AFM height images of small assemblies, a non-significant difference was found (*p*-value > 0.05). However, CG-MD simulation did not represent in totality the results obtained by the experimental methods. In comparison with small assemblies obtained by ethanol injection method, CG-MD simulation assembly presented smaller particle size and different morphology. These differences may be due to experimental variables involved in the method applied for assemblies' formation, such as: stirring speed, injection flow and ethanol concentration [41,86]. These variables were unable to be reproduced by simulation and have an impact on the properties of the assemblies. In addition, the size of experimental results corresponds to the hydrodynamic diameter calculated by DLS. This diameter is indicative of the apparent size of the solvated particle and is greater than the size calculated by other techniques. Furthermore, the initial concentration of the dendrimer and spatial disposition in the simulated system may also influence the morphology of the assemblies. Simulation environment with a high concentration of JD favors the interaction between polar heads of the dendrimers, preventing the formation of disk-like aggregates with larger dimensions and with the ability to curl up to form a vesicle.

Chapter 5

Conclusions

A series of myristylated bis-MPA Janus dendrimers with structural variations in the core and branching pattern were synthesized, and their self-assembly behavior in aqueous media was evaluated using experimental methods and CG-MD simulation.

A relationship between the chemical structure of the synthesized dendrimers and the properties of their assemblies in water was established. The generation number and the core type play a key role in the formation of assemblies and have an effect in the melting transition temperatures of the dendrimers, and in the size and polydispersity index of their assemblies in water.

Dendrimersomes with sizes in nanometric and micrometer scale were obtained by the solvent injection method and microfluidics, respectively. Solvent injection method generated dendrimersomes with sizes below 100 nm and narrow size distribution. With the use of microfluidic techniques, dendrimersomes with a minimal amount of residual solvent within their membranes were produced. In addition, the microfluidic technique enabled the production of large quantities of dendrimersomes with controlled size and composition, in contrast with the thin-film hydration method. Moreover, we showed the possibility to form dendrimersomes with microfluidics, using highly hydrophobic JDs.

The CG-MD simulation allowed us to gain a molecular insight into the mechanism of self-assembly of the dendrimer, in which disk-like bilayers were important intermediates of the assembly obtained at the end of the simulation. This is the first report where a CG

model for the studied bis-MPA dendrimers was developed and the self-assembly phenomenon was explored.

Further research will be focused on the mechanical behavior of dendrimers at interfaces to find the optimal conditions to prepare dendrimersomes. Also, further research on the developing of smart dendrimersomes for controlled drug release should be conducted; taking advantage of the high versatility that gives the use of dendrimers, and the possibility to control the composition of dendrimersomes given by the microfluidic technique.

Appendix A

^{1}H NMR, ^{13}C NMR, and MALDI-TOF MS Data of Dendrons and Dendrimers

Dendron 1

^{1}H NMR (500 MHz, CDCl$_3$) δ 7.40–7.17 (m, 5H, -C<u>H</u>=), 5.14 (s, 2H, -O-CO-C<u>H</u>$_2$-C-), 4.31 – 4.11 (m, 4H, -C<u>HH'</u>-O-CO- [G-1] non-polar block), 2.21 (t, *J* = 7.6 Hz, 4H, -O-CO-C<u>H</u>$_2$-CH$_2$-(CH$_2$)$_{10}$-), 1.57–1.47 (m, 4H, -O-CO-CH$_2$-C<u>H</u>$_2$-(CH$_2$)$_{10}$-), 1.36–1.05 (m, ~43H, -C-C<u>H</u>$_3$ and -O-CO-CH$_2$-CH$_2$-(C<u>H</u>$_2$)$_{10}$-), 0.86 (t, *J* = 7.0 Hz, 6H, -(CH$_2$)$_{10}$-C<u>H</u>$_3$).^{13}C NMR (126 MHz, CDCl$_3$) δ 173.24, 172.65, 135.64, 128.55, 128.30, 128.05, 66.75, 65.33, 46.41, 34.07, 31.91, 29.67, 29.64, 29.60, 29.46, 29.34, 29.24, 29.11, 24.84, 22.67, 17.79, 14.08. MALDI-TOF MS (m/z) [M+Na]$^+$ calcd. for C$_{40}$H$_{68}$NaO$_6$: 667.95; found: 669.90.

Dendron 2

^{1}H NMR (500 MHz, CDCl$_3$) δ 4.36–4.12 (m, 4H, -C<u>HH'</u>-O-CO- [G-1] non-polar block), 2.31 (t, *J* = 7.6 Hz, 4H, -O-CO-C<u>H</u>$_2$-CH$_2$-(CH$_2$)$_{10}$-), 1.69–1.47 (m, 4H, -O-CO-CH$_2$-C<u>H</u>$_2$-(CH$_2$)$_{10}$-), 1.35–1.15 (m, 43H, -C-C<u>H</u>$_3$ and -O-CO-CH$_2$-CH$_2$-(C<u>H</u>$_2$)$_{10}$-), 0.88 (t, *J* = 7.0 Hz, 6H, -(CH$_2$)$_{10}$-C<u>H</u>$_3$). ^{13}C NMR (126 MHz, CDCl$_3$) δ 178.37, 173.31, 65.00, 46.19, 34.13, 31.94, 29.70, 29.67, 29.63, 29.49, 29.37, 29.27, 29.14, 24.89, 22.70, 17.78, 14.10. MALDI-TOF MS (m/z) [M+Na]$^+$ calcd. for C$_{33}$H$_{62}$NaO$_6$: 577.83; found: 578.82.

Dendron 3A

^{1}H NMR (500 MHz, CDCl$_3$) δ 4.35–4.18 (m, 6H, -C<u>HH'</u>-O-CO- [G-1] non-polar block and -CO-O-C<u>H</u>$_2$-CH$_2$-OH), 3.79 (s, 2H, -CO-O-CH$_2$-C<u>H</u>$_2$-OH), 2.30 (t, *J* = 7.6 Hz, 4H, -O-CO-

C$\underline{H}_2$-CH$_2$-(CH$_2$)$_{10}$-), 1.66–1.52 (m, 4H, -O-CO-CH$_2$-C$\underline{H}_2$-(CH$_2$)$_{10}$-), 1.38–1.16 (m, 43H, -C-C$\underline{H}_3$ and -O-CO-CH$_2$-CH$_2$-(C$\underline{H}_2$)$_{10}$-), 0.88 (t, *J* = 6.9 Hz, 6H, -(CH$_2$)$_{10}$-C$\underline{H}_3$). ^{13}C NMR (126 MHz, CDCl$_3$) δ 173.46, 173.00, 66.95, 65.34, 60.96, 46.72, 34.19, 31.94, 29.69, 29.66, 29.62, 29.49, 29.37, 29.26, 29.15, 24.92, 22.70, 17.82, 14.10. MALDI-TOF MS (m/z) [M+Na]$^+$ calcd. for C$_{35}$H$_{66}$NaO$_7$: 621.88; found: 623.51.

Dendron 3B

^{1}H NMR (500 MHz, CDCl$_3$) δ 4.34–4.05 (m, 6H, -O-CO-C$\underline{H}_2$-CH$_2$-O- and -C$\underline{H}$H'-O-CO-[G-1] non-polar block), 3.74–3.69 (m, 2H, -O-CH$_2$-C$\underline{H}_2$-OH), 3.69–3.57 (m, 8H, -CO-O-CH$_2$-C$\underline{H}_2$-, -O-C$\underline{H}_2$-C$\underline{H}_2$-O-C$\underline{H}_2$-), 2.27 (t, *J* = 7.6 Hz, 4H, -O-CO-C$\underline{H}_2$-CH$_2$-(CH$_2$)$_{10}$-), 1.64–1.47 (m, 4H, -O-CO-CH$_2$-C$\underline{H}_2$-(CH$_2$)$_{10}$-), 1.39–1.11 (m, 43H, -C-C$\underline{H}_3$ and -O-CO-CH$_2$-CH$_2$-(C$\underline{H}_2$)$_{10}$-), 0.86 (t, *J* = 7.0 Hz, 6H, -(CH$_2$)$_{10}$-C$\underline{H}_3$). ^{13}C NMR (126 MHz, CDCl$_3$) δ 173.31, 172.74, 72.56, 70.67, 70.40, 68.92, 65.21, 64.06, 61.80, 46.35, 34.13, 33.95, 31.91, 29.67, 29.63, 29.60, 29.47, 29.34, 29.25, 29.13, 24.88, 22.67, 17.76, 14.08. MALDI-TOF MS (m/z) [M+K]$^+$ calcd. for C$_{39}$H$_{74}$KO$_9$: 726.09; found: 728.07.

Dendron 3C

^{1}H NMR (500 MHz, CDCl$_3$) δ 4.27–4.17 (m, 4H, -C$\underline{H}$H'-O-CO- [G-1] non-polar block), 4.11 (t, *J* = 6.7 Hz, 2H, -CO-O-C$\underline{H}_2$-(CH$_2$)$_9$-), 3.64 (t, *J* = 6.6 Hz, 2H, -CO-O-(CH$_2$)$_9$-C$\underline{H}_2$-OH), 2.29 (t, *J* = 7.6 Hz, 4H, -O-CO-C$\underline{H}_2$-CH$_2$-(CH$_2$)$_{10}$-), 1.66–1.53 (m, 8H, -O-CO-CH$_2$-C$\underline{H}_2$-(CH$_2$)$_{10}$-, -CO-O-CH$_2$-C$\underline{H}_2$-(CH$_2$)$_8$- and -CO-O-(CH$_2$)$_8$-C$\underline{H}_2$-CH$_2$-OH), 1.42–1.11 (m, ~55H, -C-C$\underline{H}_3$, -O-CO-CH$_2$- CH$_2$-(C$\underline{H}_2$)$_{10}$- and -CO-O-CH$_2$-CH$_2$-(C$\underline{H}_2$)$_6$-CH$_2$-CH$_2$-OH), 0.88 (t, *J* = 7.0 Hz, 6H, -(CH$_2$)$_{10}$-C$\underline{H}_3$). ^{13}C NMR (126 MHz, CDCl$_3$) δ 173.28, 172.86, 65.34, 65.26, 63.02, 46.30, 34.15, 32.79, 31.91, 29.67, 29.64, 29.60, 29.47, 29.40,

29.36, 29.34, 29.25, 29.16, 29.13, 28.52, 25.81, 25.71, 24.90, 22.67, 17.85, 14.08.

MALDI-TOF MS (m/z) [M+Na]$^+$ calcd. for $C_{43}H_{82}NaO_7$: 734.10; found: 736.72.

Dendron 5A

^{1}H NMR (500 MHz, CDCl$_3$): δ 4.37 (s, 4H, -C$\underline{H}_2$-O-CO- [G-1] non-polar block), 4.22 (q, *J* = 11.1 Hz, 4H, -O-CO-C$\underline{H}_2$-C$\underline{H}_2$-O-CO-), 3.87 (d, *J* = 11.2 Hz, 2H, -C$\underline{H}$H'-OH), 3.74 (d, *J* = 11.3 Hz, 2H, -CH$\underline{H}$'-OH), 2.30 (t, *J* = 7.6, 4H, -O-CO-C$\underline{H}_2$-CH$_2$-(CH$_2$)$_{10}$-), 1.62–1.49 (m, 4H, -O-CO-CH$_2$-C$\underline{H}_2$-(CH$_2$)$_{10}$-), 1.44–1.14 (m, 43H, -C-C$\underline{H}_3$ and -O-CO-CH$_2$-CH$_2$-(C$\underline{H}_2$)$_{10}$-), 1.08 (s, 3H, -C-C$\underline{H}_3$), 0.88 (t, *J* = 6.8, 6H, -(CH$_2$)$_{10}$-C$\underline{H}_3$). ^{13}C NMR (126 MHz, CDCl$_3$): δ 175.51, 173.45, 172.72, 68.14, 68.12, 65.18, 62.80, 62.54, 49.43, 46.43, 34.13, 31.93, 29.69, 29.66, 29.62, 29.49, 29.36, 29.27, 29.14, 24.88, 22.69, 17.71, 17.17, 14.12. MALDI-TOF MS (m/z) [M+Na]$^+$ calcd. for $C_{40}H_{74}NaO_{10}$: 738.00; found 740.78.

Dendron 5B

^{1}H NMR (500 MHz, CDCl$_3$): δ 4.38 – 4.32 (m, 2H, -C$\underline{H}$H'-O-CO- [G-1] non-polar block), 4.31 – 4.17 (m, 6H, -CH$\underline{H}$'-O-CO- [G-1] non-polar block and -CO-O-C$\underline{H}_2$-CH$_2$-O-), 3.83 (d, *J* = 11.4 Hz, 2H, -C$\underline{H}$H'-OH), 3.73 (d, *J* = 11.5 Hz, 2H, -CH$\underline{H}$'-OH), 3.70 – 3.65 (m, 4H, -CO-O-CH$_2$-C$\underline{H}_2$-O-CH$_2$-), 3.62 (s, 4H, -O-C$\underline{H}_2$-C$\underline{H}_2$-O-), 2.29 (t, *J* = 7.6, 4H, -O-CO-C$\underline{H}_2$-CH$_2$-(CH$_2$)$_{10}$-), 1.64 – 1.53 (m, 4H, -O-CO-CH$_2$-C$\underline{H}_2$-(CH$_2$)$_{10}$-), 1.34 – 1.19 (m, 43H, -C-C$\underline{H}_3$ and -O-CO-CH$_2$-CH$_2$-(C$\underline{H}_2$)$_{10}$-), 1.11 (s, 3H, -C-C$\underline{H}_3$), 0.88 (t, *J* = 6.9, 6H, -(CH$_2$)$_{10}$-C$\underline{H}_3$). ^{13}C NMR (126 MHz, CDCl$_3$): δ 175.62, 173.31, 172.72, 70.51, 70.34, 68.94, 68.83, 67.76, 65.16, 64.02, 63.31, 49.67, 46.31, 34.12, 31.91, 29.67, 29.64,

29.60, 29.47, 29.34, 29.26, 29.12, 26.22, 25.13, 24.89, 22.67, 17.78, 17.07, 14.10. MALDI-TOF MS (m/z) [M+Na]$^+$ calcd. for $C_{44}H_{82}NaO_{12}$: 826.10; found 829.67.

Dendron 5C

^{1}H NMR (500 MHz, CDCl$_3$) δ 4.28–4.09 (m, 8H, -C<u>HH'</u>-O-CO- [G-1] non-polar block and -CO-O-C<u>H$_2$</u>-(CH$_2$)$_8$-), 3.92 (d, *J* = 11.3 Hz, 2H, -C<u>H</u>H'-OH), 3.73 (d, *J* = 11.3 Hz, 2H, -CH<u>H'</u>-OH), 2.30 (t, *J* = 7.6 Hz, 4H, -O-CO-C<u>H$_2$</u>-CH$_2$-(CH$_2$)$_{10}$-), 1.71–1.58 (m, 8H, -O-CO-CH$_2$-C<u>H$_2$</u>-(CH$_2$)$_{10}$- and -CO-O-CH$_2$-C<u>H$_2$</u>-(CH$_2$)$_8$-), 1.47–1.21 (m,~ 55H, -C-C<u>H$_3$</u>, -O-CO-CH$_2$-CH$_2$-(C<u>H$_2$</u>)$_{10}$- and -O-CH$_2$-CH$_2$-(C<u>H$_2$</u>)$_6$-), 1.08 (s, 3H, -C-C<u>H$_3$</u>), 0.89 (t, *J* = 6.8 Hz, 6H, -(CH$_2$)$_{10}$-C<u>H$_3$</u>). ^{13}C NMR (126 MHz, CDCl$_3$): δ 176.02, 173.31, 172.88, 68.54, 65.34, 65.27, 65.19, 49.10, 46.30, 34.18, 31.93, 29.69, 29.66, 29.63, 29.49, 29.42, 29.36, 29.28, 29.19, 29.18, 29.15, 28.55, 25.85, 25.84, 24.92, 22.70, 17.88, 17.15, 14.12. MALDI-TOF MS (m/z) [M+K]$^+$ calcd. for $C_{48}H_{90}KO_{10}$: 866.32; found 869.61.

Dendron 6

^{1}H-NMR (500 MHz, CDCl$_3$) δ 7.45–7.28 (m, ~5H, -C<u>H</u>=), 5.15 (s, 2H, -O-CO-C<u>H$_2$</u>-C-), 4.30–4.23 (m, 4H, -C<u>HH'</u>-O-CO- [G-1] non-polar block), 4.18–4.10 (m, ~8H, -C<u>HH'</u>-O-CO- [G-2] non-polar block), 2.27 (t, *J* = 7.6 Hz, 8H, -O-CO-C<u>H$_2$</u>-CH$_2$-(CH$_2$)$_{10}$-), 1.64–1.42 (m, 8H, -O-CO-C<u>H$_2$</u>-CH$_2$-(CH$_2$)$_{10}$-), 1.35–1.20 (m, ~83H, -C-C<u>H$_3$</u> and -O-CO-CH$_2$-CH$_2$-(C<u>H$_2$</u>)$_{10}$-), 1.16 (s, 6H, -C-C<u>H$_3$</u>), 0.88 (t, *J* = 6.9 Hz, 12H, -(CH$_2$)$_{10}$-C<u>H$_3$</u>). ^{13}C-NMR (126 MHz, CDCl$_3$) δ 173.17, 172.10, 172.00, 135.42, 128.69, 128.50, 128.36, 67.13, 65.76, 65.03, 46.75, 46.44, 34.17, 34.06, 31.94, 29.71, 29.68, 29.67, 29.65, 29.51, 29.37, 29.31, 29.16, 24.89, 22.70, 17.72, 17.58, 14.11. MALDI-TOF MS (*m/z*) [M-H+2Na]$^+$ calcd. for $C_{78}H_{135}Na_2O_{14}$: 1342.88; found 1342.29.

Dendron 7

^{1}H-NMR (500 MHz, CDCl$_3$) δ 4.30–4.15 (m, 12H, -C$\underline{HH}$'-O-CO- [G-1] non-polar block, -C$\underline{HH}$'-O-CO- [G-2] non-polar block), 2.29 (t, *J* = 7.6 Hz, 8H, -O-CO-C$\underline{H}_2$-CH$_2$-(CH$_2$)$_{10}$-), 1.66–1.52 (m, 8H, -O-CO-CH$_2$-C$\underline{H}_2$-(CH$_2$)$_{10}$-), 1.35–1.17 (m, 89H, -C-C$\underline{H}_3$ and -O-CO-CH$_2$-CH$_2$-(C$\underline{H}_2$)$_{10}$-), 0.88 (t, *J* = 6.9 Hz, 12H, -(CH$_2$)$_{10}$-C$\underline{H}_3$).^{13}C-NMR (126 MHz, CDCl$_3$) δ 175.33, 173.33, 173.31, 172.04, 65.67, 65.14, 65.11, 46.47, 46.35, 34.08, 31.94, 29.71, 29.69, 29.67, 29.66, 29.52, 29.37, 29.31, 29.17, 24.89, 22.70, 17.77, 17.54, 14.11. MALDI-TOF MS (*m/z*) [M-H+2Na]$^+$ calcd. for C$_{71}$H$_{129}$Na$_2$O$_{14}$: 1252.76; found 1251.96.

Dendron 8A

^{1}H-NMR (500 MHz, CDCl$_3$) δ 4.40–4.08 (m, 14H, -C$\underline{HH}$'-O-CO- [G-1] non-polar block, -C$\underline{HH}$'-O-CO- [G-2] non-polar block and -CO-O-C$\underline{H}_2$-CH$_2$-OH), 3.89–3.76 (m, 2H, -CO-O-CH$_2$-C$\underline{H}_2$-OH), 2.29 (t, *J* = 7.6 Hz, 8H, -O-CO-C$\underline{H}_2$-CH$_2$-(CH$_2$)$_{10}$-), 1.62–1.54 (m, 8H, -O-CO-CH$_2$-C$\underline{H}_2$-(CH$_2$)$_{10}$-), 1.34–1.20 (m, 89H, -C-C$\underline{H}_3$ and -O-CO-CH$_2$-CH$_2$-(C$\underline{H}_2$)$_{10}$-), 0.88 (t, *J* = 6.8, 12H, -(CH$_2$)$_{10}$-C$\underline{H}_3$). ^{13}C-NMR (126 MHz, CDCl$_3$) δ 173.32, 172.46, 172.18, 67.09, 65.92, 65.04, 60.77, 46.77, 46.47, 34.05, 33.93, 31.91, 29.68, 29.65, 29.62, 29.48, 29.34, 29.27, 29.13, 24.85, 22.67, 17.77, 17.61, 14.08. MALDI-TOF MS (*m/z*) [M-H+2Na]$^+$ calcd. for C$_{73}$H$_{133}$Na$_2$O$_{15}$: 1296.81; found: 1296.75.

Dendron 8B

^{1}H NMR (500 MHz, CDCl$_3$) δ 4.31–4.25 (m, 6H, -CO-O-C$\underline{H}_2$-CH$_2$-O- and -C$\underline{HH}$'-O-CO- [G-1] non-polar block), 4.25–4.16 (m, 8H, -C$\underline{HH}$'-O-CO- [G-2] non-polar block), 3.76–3.58 (m, 10H, -O-CH$_2$-C$\underline{H}_2$-OH, -CO-O-CH$_2$-C$\underline{H}_2$- and -O-C$\underline{H}_2$-C$\underline{H}_2$-O-C$\underline{H}_2$-), 2.30 (t,

J = 7.6 Hz, 8H, -O-CO-C$\underline{H_2}$-CH$_2$-(CH$_2$)$_{10}$-), 1.64–1.53 (m, 8H, -O-CO-CH$_2$-C$\underline{H_2}$-(CH$_2$)$_{10}$-),

1.41–1.16 (m, ~89H, -C-C$\underline{H_3}$ and -O-CO-CH$_2$-CH$_2$-(C$\underline{H_2}$)$_{10}$-), 0.89 (t, J = 6.9 Hz, 12H,

-(CH$_2$)$_{10}$-C$\underline{H_3}$). ^{13}C NMR (126 MHz, CDCl$_3$) δ 173.17, 172.10, 172.07, 72.50, 70.58,

70.38, 68.82, 65.68, 65.00, 64.24, 61.76, 46.64, 46.42, 34.03, 33.96, 31.91, 29.68,

29.64, 29.62, 29.48, 29.34, 29.28, 29.14, 24.86, 22.66, 17.77, 17.52, 14.07. MALDI-

TOF MS (m/z) [M+2Na]$^+$ calcd. for C$_{77}$H$_{142}$Na$_2$O$_{17}$: 1385.92; found: 1385.50.

Dendron 8C

^{1}H NMR (500 MHz, CDCl$_3$) δ 4.29–4.14 (m, 12H, -C$\underline{HH'}$-O-CO- [G-1] non-polar block,

-C$\underline{HH'}$-O-CO-[G-2] non-polar block), 4.10 (t, J = 6.8 Hz, 2H, -CO-O-C$\underline{H_2}$-(CH$_2$)$_9$-OH),

3.63 (t, J = 6.6 Hz, 2H, -CO-O-(CH$_2$)$_9$-C$\underline{H_2}$-OH), 2.29 (t, J = 7.6 Hz, 8H, -O-CO-C$\underline{H_2}$-

CH$_2$-(CH$_2$)$_{10}$-), 1.62–1.53 (m, 12H, -O-CO-CH$_2$-C$\underline{H_2}$-(CH$_2$)$_{10}$-, -CO-O-CH$_2$-C$\underline{H_2}$-(CH$_2$)$_8$-

and -CO-O-(CH$_2$)$_8$-C$\underline{H_2}$-CH$_2$-OH), 1.35–1.20 (m, 101H, -C-C$\underline{H_3}$, -O-CO-CH$_2$-CH$_2$-

(C$\underline{H_2}$)$_{10}$- and -CO-O-CH$_2$-CH$_2$-(C$\underline{H_2}$)$_6$-CH$_2$-CH$_2$-OH), 0.88 (t, J = 6.9 Hz, 12H, -(CH$_2$)$_{10}$-

C$\underline{H_3}$). ^{13}C NMR (126 MHz, CDCl$_3$) δ 173.32, 172.29, 172.24, 65.91, 65.73, 65.18, 63.17,

46.76, 46.59, 34.20, 32.96, 32.08, 29.85, 29.83, 29.81, 29.79, 29.66, 29.53, 29.51,

29.45, 29.33, 29.31, 28.68, 26.00, 25.88, 25.03, 22.84, 17.95, 14.25. MALDI-TOF MS

(m/z) [M-H+2Na]$^+$ calcd. for C$_{81}$H$_{149}$Na$_2$O$_{15}$: 1409.02; found: 1409.26.

Dendrimer 10A

^{1}H-NMR (500 MHz, CDCl$_3$) 4.43 (d, J = 11.1 Hz, 2H, -C$\underline{H}$H'-O-[G-1] polar block), 4.39–

4.09 (m, 18H, -O-CO-C$\underline{H_2}$-C$\underline{H_2}$-O-CO-, -CH$\underline{H'}$-O-[G-1] polar block, -C$\underline{HH'}$-O-[G-1] non-

polar block and -C$\underline{HH'}$-O-CO-[G-2] non-polar block), 3.87–3.77 (m, 4H, -C$\underline{H}$H'-OH),

3.76–3.64 (m, 4H, -CH$\underline{H'}$-OH), 2.29 (t, J = 7.6 Hz, 8H, -O-CO-C$\underline{H_2}$-CH$_2$-(CH$_2$)$_{10}$-), 1.64–

1.51 (m, 8H, -O-CO-CH$_2$-C$\underline{H}_2$-(CH$_2$)$_{10}$-), 1.34–1.20 (m, 92H, -C-C$\underline{H}_3$ and -O-CO-CH$_2$-CH$_2$-(C$\underline{H}_2$)$_{10}$-), 1.06 (s, 6H, -C-C$\underline{H}_3$), 0.88 (t, *J* = 6.9 Hz, 12H, -(CH$_2$)$_{10}$-C$\underline{H}_3$). ^{13}C-NMR (126 MHz, CDCl$_3$) δ 175.18, 173.42, 173.41, 172.79, 172.27, 172.08, 68.25, 68.19, 66.09, 65.78, 65.22, 65.17, 65.00, 62.99, 62.95, 49.94, 46.87, 46.70, 46.66, 46.62, 34.20, 32.07, 29.84, 29.81, 29.80, 29.78, 29.65, 29.50, 29.44, 29.42, 29.30, 25.02, 22.82, 18.13, 17.92, 17.77, 17.63, 17.25, 14.23. MALDI-TOF MS (*m/z*) [M+2Na]$^+$ calcd. for C$_{88}$H$_{158}$Na$_2$O$_{24}$: 1646.16; found 1648.92.

Dendrimer 10B

^{1}H NMR (500 MHz, CDCl$_3$) δ 4.41 (d, *J* = 11.0 Hz, 2H, -C$\underline{H}$H'-O-CO- [G-1] polar block), 4.34 - 4.23 (m, 10H, -CO-O-C$\underline{H}_2$-CH$_2$-O-, -CH$\underline{H}$'-O-CO- [G-1] polar block and -C$\underline{H}$H'-O-CO- [G-1] non-polar block), 4.18 (q, *J* = 11.3 Hz, 8H, -C$\underline{H}$H'-O-CO- [G-2] non-polar block), 3.81 (d, *J* = 11.5 Hz, 4H, -C$\underline{H}$H'-OH), 3.77 - 3.65 (m, 8H, -CH$\underline{H}$'-OH and -CO-O-CH$_2$-C$\underline{H}_2$-O-CH$_2$-), 3.62 (s, 4H, -O-C$\underline{H}_2$-C$\underline{H}_2$-O), 2.28 (t, *J* = 7.6 Hz, 8H, -O-CO-C$\underline{H}_2$-CH$_2$-(CH$_2$)$_{10}$-), 1.64 – 1.52 (m, 8H, -O-CO-CH$_2$-C$\underline{H}_2$-(CH$_2$)$_{10}$-), 1.36- 1.17 (m, 92H, -C-C$\underline{H}_3$ and -O-CO-CH$_2$-CH$_2$-(C$\underline{H}_2$)$_{10}$-), 1.06 (s, 6H, -C-C$\underline{H}_3$), 0.87 (t, *J* = 6.7 Hz, 12H, -(CH$_2$)$_{10}$-C$\underline{H}_3$). ^{13}C NMR (126 MHz, CDCl$_3$) δ 175.07, 173.23, 173.20, 172.10, 172.08, 70.43, 68.91, 68.82, 67.96, 67.88, 65.60, 64.98, 64.95, 64.31, 64.21, 49.78, 46.62, 46.49, 46.40, 34.04, 31.92, 29.69, 29.67, 29.65, 29.63, 29.50, 29.35, 29.29, 29.15, 24.86, 22.68, 18.04, 17.79, 17.54, 17.13, 14.10. MALDI-TOF MS (m/z) [M+2Na]$^+$ calcd. for C$_{92}$H$_{166}$Na$_2$O$_{26}$: 1734.27; found: 1737.63.

Dendrimer 10C

^{1}H NMR (500 MHz, CDCl$_3$) δ 4.44 (d, *J* = 11.1 Hz, 2H, -C<u>H</u>H'-O-CO- [G-1] polar block), 4.32 – 4.06 (m, 18H, -CO-O-C<u>H$_2$</u>-(CH$_2$)$_8$-, -CH<u>H</u>'-O-CO- [G-1] polar block, -C<u>H</u>H'-O-CO- [G-1] non-polar block and -C<u>H</u>H'-O-CO- [G-2] non-polar block), 3.88 – 3.77 (m, ~4H, -C<u>H</u>H'-OH), 3.74 – 3.59 (m, 4H, -C<u>H</u>H'-OH), 2.28 (t, *J* = 7.6 Hz, 8H, -O-CO-C<u>H$_2$</u>-CH$_2$-(CH$_2$)$_{10}$-), 1.67 – 1.53 (m, 12H, -O-CO-CH$_2$-C<u>H$_2$</u>-(CH$_2$)$_{10}$- and CO-O-CH$_2$-C<u>H$_2$</u>-(CH$_2$)$_6$-), 1.39 – 1.12 (m, 109H, -O-CH$_2$-CH$_2$-(C<u>H$_2$</u>)$_6$- and -C-C<u>H$_3$</u> and -O-CO-CH$_2$-CH$_2$-(C<u>H$_2$</u>)$_{10}$-), 1.05 (s, ~6H, -C-C<u>H$_3$</u>), 0.87 (t, *J* = 6.8 Hz, 12H, -(CH$_2$)$_{10}$-C<u>H$_3$</u>). ^{13}C NMR (126 MHz, CDCl$_3$) δ 175.27, 173.34, 173.14, 172.29, 172.23, 68.23, 65.85, 65.79, 65.71, 65.16, 65.04, 63.14, 49.84, 48.80, 46.72, 46.62, 46.55, 46.52, 34.27, 34.18, 32.92, 32.06, 29.83, 29.81, 29.80, 29.78, 29.64, 29.59, 29.50, 29.43, 29.35, 29.34, 29.29, 28.68, 28.66, 25.99, 25.86, 25.01, 22.83, 18.28, 17.93, 17.90, 17.76, 17.53, 17.25, 14.25. MALDI-TOF MS (m/z) [M+2Na]$^+$ calcd. for C$_{96}$H$_{174}$Na$_2$O$_{24}$: 1758.38; found: 1762.01.

Appendix B

General Linear Model: Z-AVE vs. Gen, Core

```
Factor   Type   Levels   Values
Gen      Fixed      2    1, 2
Core     Fixed      3    A, B, C


Analysis of Variance for Z-AVE, using Adjusted SS for Tests

Source      DF        SS     Adj SS     Adj MS   F-Value   P-Value
Gen          1    132.06      46.54      46.54      8.78     0.005
Core         2   4046.31    3835.08    1917.54    361.89     0.000
Gen*Core     2    461.12     461.12     230.56     43.51     0.000
Error       47    249.04     249.04       5.30
Total       52   4888.53


S = 2.30190    R-sq = 94.91%    R-sq(adj) = 94.36%
```
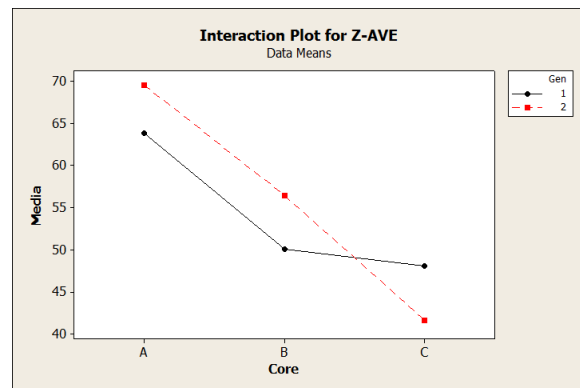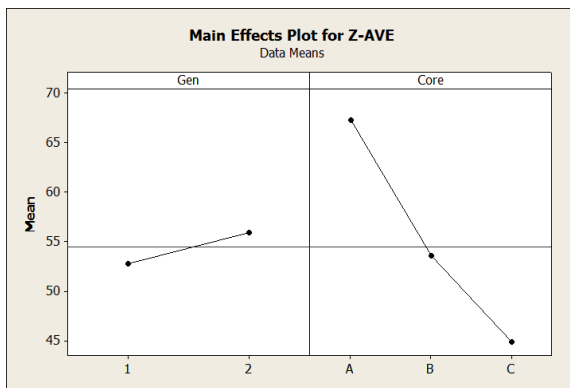


```
Assumptions for ANOVA
```
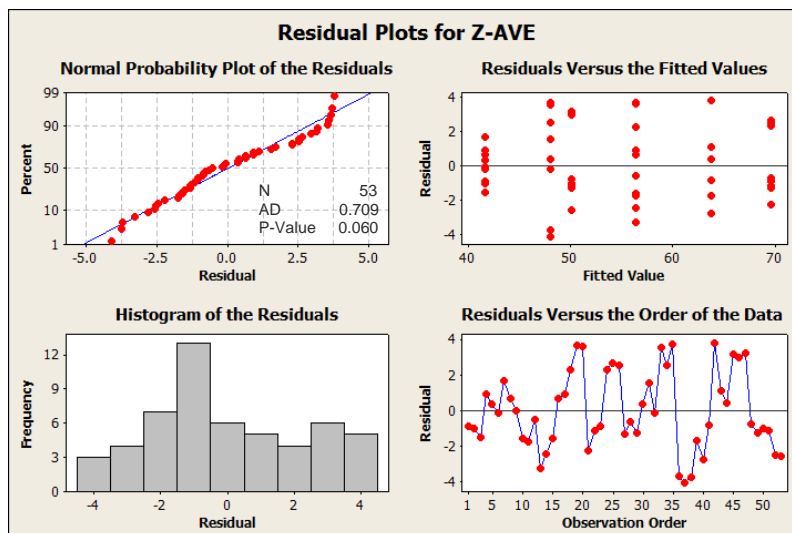
```
Tukey 95% Simultaneous Confidence Intervals
Response Variable Z-AVE
All Pairwise Comparisons among Levels of Gen


Gen = 1  subtracted from:


Gen     Lower    Center    Upper    -+---------+---------+---------+-----
2      0.6120    1.905     3.199    (----------------*------------------)
                                    -+---------+---------+---------+-----
                                    0.70      1.40      2.10      2.80


Tukey Simultaneous Test
Response Variable Z-AVE
All Pairwise Comparisons among Levels of Gen


Gen = 1  subtracted from:


       Difference      SE of               Adjusted
Gen     of Means    difference   T-Value   P-Value
2          1.905       0.6429     2.964     0.0048


Tukey 95% Simultaneous Confidence Intervals
Response Variable Z-AVE
All Pairwise Comparisons among Levels of Core


Core = A  subtracted from:


Core    Lower    Center    Upper    ----+---------+---------+---------+--
B      -15.33    -13.40    -11.47              (--*--)
C      -23.81    -21.84    -19.87   (--*--)
                                    ----+---------+---------+---------+--
                                    -21.0     -14.0     -7.0      0.0


Core = B  subtracted from:


Core    Lower    Center    Upper    ----+---------+---------+---------+--
C      -10.25    -8.437    -6.625                         (--*--)
                                    ----+---------+---------+---------+--
                                    -21.0     -14.0     -7.0      0.0
Tukey Simultaneous Test
Response Variable Z-AVE
All Pairwise Comparisons among Levels of Core


Core = A  subtracted from:


       Difference      SE of               Adjusted
Core    of Means    difference   T-Value   P-Value
B         -13.40       0.7972    -16.81     0.0000
C         -21.84       0.8138    -26.83     0.0000


Core = B  subtracted from:


       Difference      SE of               Adjusted
Core    de Means    difference   T-Value   P-Value
C         -8.437       0.7497    -11.26     0.0000
```

Appendix C

General Linear Model: PDI vs. Gen, Core

```
Factor  Type  Levels  Values
Gen     Fixed      2  1, 2
Core    Fixed      3  A, B, C

Analysis of Variance for PDI, using Adjusted SS for Tests

Source      DF        SS     Adj SS     Adj MS  F-Value  P-Value
Gen          1  0.000877   0.000002   0.000002     0.00    0.974
Core         2  0.045767   0.051441   0.025721    16.60    0.000
Gen*Core     2  0.030709   0.030709   0.015354     9.91    0.000
Error       47  0.072819   0.072819   0.001549
Total       52  0.150172


S = 0.0393616   R-sq = 51.51%   R-sq(adj) = 46.35%
```
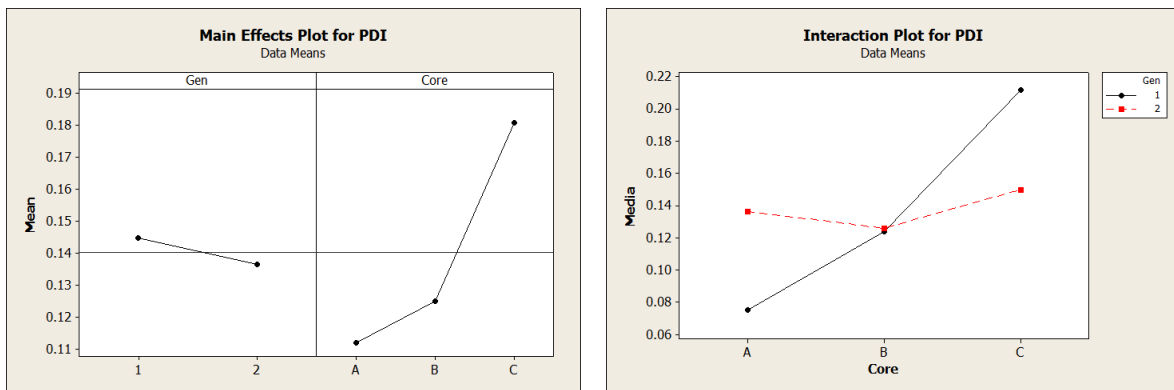


```
Assumptions for ANOVA
```
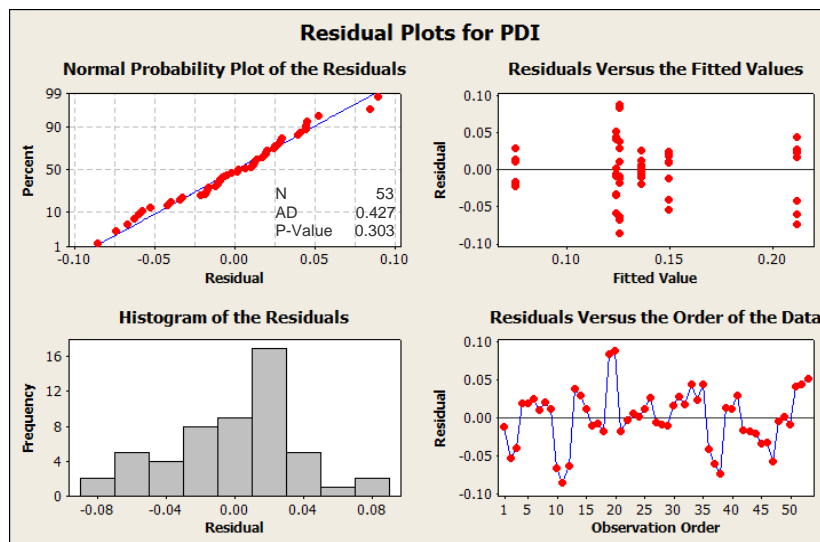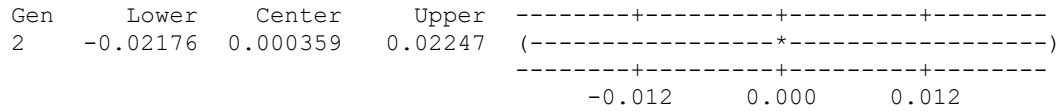
```
Tukey 95% Simultaneous Confidence Intervals
Response Variable PDI
All Pairwise Comparisons among Levels of Gen


Gen = 1  subtracted from:


Gen    Lower    Center    Upper  --------+---------+---------+--------
2    -0.02176  0.000359  0.02247  (----------------*------------------)
                                  --------+---------+---------+--------
                                     -0.012      0.000      0.012




Tukey Simultaneous Test
Response Variable PDI
All Pairwise Comparisons among Levels of Gen


Gen = 1  subtracted from:


       Difference       SE of              Adjusted
Gen     of Means    difference  T-Value    P-Value
2        0.000359      0.01099  0.03262     0.9741




Tukey 95% Simultaneous Confidence Intervals
Response Variable PDI
All Pairwise Comparisons among Levels of Core


Core = A  subtracted from:


Core    Lower    Center    Upper  ----+---------+---------+---------+--
B     -0.01382  0.01915  0.05212  (--------*---------)
C      0.04148  0.07514  0.10879               (--------*---------)
                                  ----+---------+---------+---------+--
                                   0.000     0.035     0.070     0.105


Core = B  subtracted from:


Core    Lower    Center    Upper  ----+---------+---------+---------+--
C      0.02499  0.05599  0.08699            (--------*--------)
                                  ----+---------+---------+---------+--
                                   0.000     0.035     0.070     0.105


Tukey Simultaneous Test
Response Variable PDI
All Pairwise Comparisons among Levels of Core


Core = A  subtracted from:


       Difference       SE of              Adjusted
Gen     of Means    difference  T-Value    P-Value
B        0.01915      0.01363    1.405      0.3467
C        0.07514      0.01392    5.399      0.0000


Core = B  subtracted from:


       Difference       SE of              Adjusted
Gen     of Means    difference  T-Value    P-Value
C        0.05599      0.01282    4.368      0.0002
```
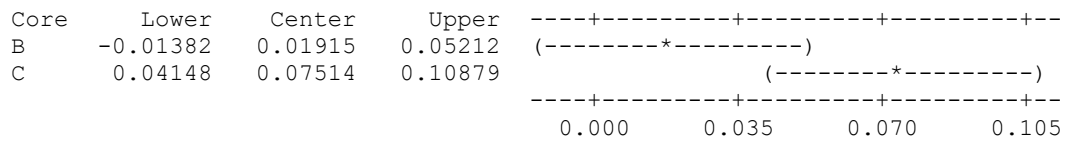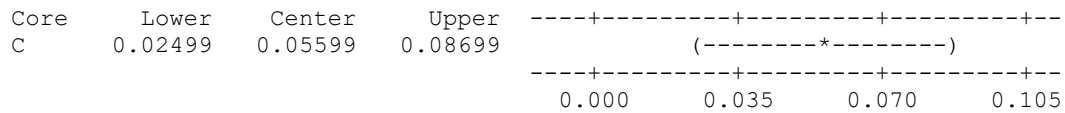
Appendix D

Solvent Accessible Surface Area (SASA) of the Dendrimers During the Simulation
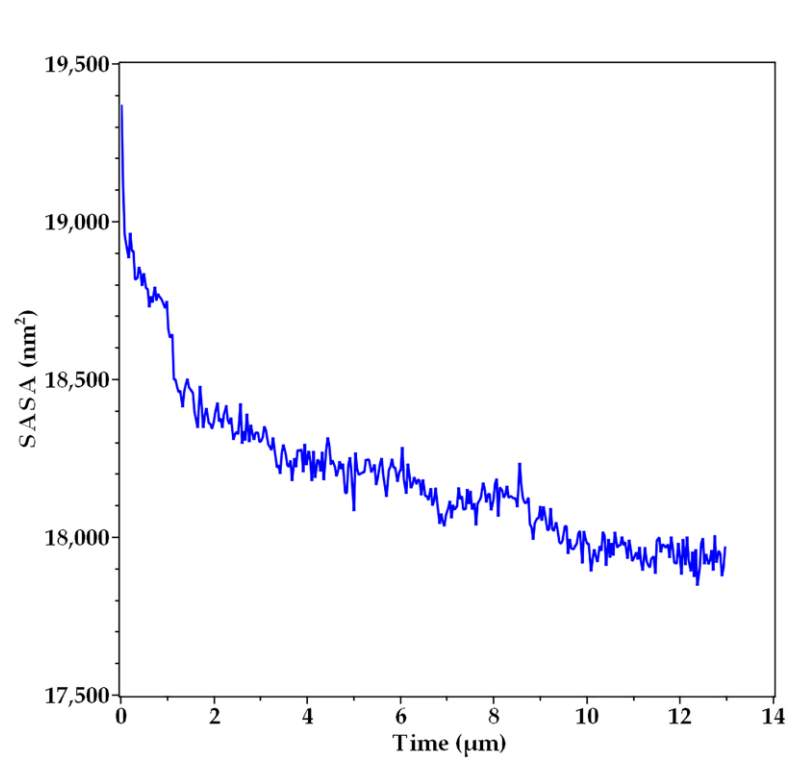
References

1. Gillies, E. R.; Fre, J. M. J. Synthesis and Self-Assembly of Supramolecular Dendritic " Bow-Ties ": Effect of Peripheral Functionality on Association Constants. **2004**, 46–53.

2. Kalhapure, R. S.; Kathiravan, M. K.; Akamanchi, K. G.; Govender, T. Dendrimers - from organic synthesis to pharmaceutical applications: an update. *Pharm. Dev. Technol.* **2013**, *20*, 22–40, doi:10.3109/10837450.2013.862264.

3. Fedeli, E.; Lancelot, A.; Serrano, J. L.; Calvo, P.; Sierra, T. Self-assembling amphiphilic Janus dendrimers: mesomorphic properties and aggregation in water. *New J. Chem.* **2015**, *39*, 1960–1967, doi:10.1039/c4nj02071e.

4. Percec, V.; Wilson, D. A.; Leowanawat, P.; Wilson, C. J.; Hughes, A. D.; Kaucher, M. S.; Hammer, D. A.; Levine, D. H.; Kim, A. J.; Bates, F. S.; Davis, K. P.; Lodge, T. P.; Klein, M. L.; DeVane, R. H.; Aqad, E.; Rosen, B. M.; Argintaru, A. O.; Sienkowska, M. J.; Rissanen, K.; Nummelin, S.; Ropponen, J. Self-assembly of Janus dendrimers into uniform dendrimersomes and other complex architectures. *Science* **2010**, *328*, 1009–14, doi:10.1126/science.1185547.

5. Sikwal, D. R.; Kalhapure, R. S.; Govender, T. An emerging class of amphiphilic dendrimers for pharmaceutical and biomedical applications: Janus amphiphilic dendrimers. *Eur. J. Pharm. Sci.* **2017**, *97*, 113–134, doi:10.1016/j.ejps.2016.11.013.

6. Filippi, M.; Patrucco, D.; Martinelli, J.; Botta, M.; Castro-Hartmann, P.; Tei, L.; Terreno, E. Novel stable dendrimersome formulation for safe bioimaging applications. *Nanoscale* **2015**, *7*, 12943–12954, doi:10.1039/c5nr02695d.

7. Filippi, M.; Martinelli, J.; Mulas, G.; Ferraretto, M.; Teirlinck, E.; Botta, M.; Tei, L.; Terreno, E. Dendrimersomes: a new vesicular nano-platform for MR-molecular imaging applications. *Chem. Commun. (Camb).* **2014**, *50*, 3453–6, doi:10.1039/c3cc49584a.

8. Filippi, M.; Catanzaro, V.; Patrucco, D.; Botta, M.; Tei, L.; Terreno, E. First in vivo MRI study on theranostic dendrimersomes. *J. Control. Release* **2017**, *248*, 45–52, doi:10.1016/j.jconrel.2017.01.010.

9. Nazemi, A.; Gillies, E. R. Dendrimersomes with photodegradable membranes for triggered release of hydrophilic and hydrophobic cargo. *Chem. Commun. (Camb).* **2014**, *50*, 11122–5, doi:10.1039/c4cc05161k.

10. Peterca, M.; Percec, V.; Leowanawat, P.; Bertin, A. Predicting the size and properties of dendrimersomes from the lamellar structure of their amphiphilic Janus dendrimers. *J. Am. Chem. Soc.* **2011**, *133*, 20507–20, doi:10.1021/ja208762u.

11. Liu, X.; Zhou, J.; Yu, T.; Chen, C.; Cheng, Q.; Sengupta, K.; Huang, Y.; Li, H.; Liu, C.; Wang, Y.; Posocco, P.; Wang, M.; Cui, Q.; Giorgio, S.; Fermeglia, M.; Qu, F.; Pricl, S.; Shi, Y.; Liang, Z.; Rocchi, P.; Rossi, J. J.; Peng, L. Adaptive amphiphilic dendrimer-based nanoassemblies as robust and versatile siRNA delivery systems. *Angew. Chemie - Int. Ed.* **2014**, *53*, 11822–11827, doi:10.1002/anie.201406764.

12. Nummelin, S.; Selin, M.; Legrand, S.; Ropponen, J.; Seitsonen, J.; Nykänen, A.; Koivisto, J.; Hirvonen, J.; Kostiainen, M. A.; Bimbo, L. M. Modular synthesis of self-assembling Janus-dendrimers and facile preparation of drug-loaded dendrimersomes. *Nanoscale* **2017**, *9*, 7189–7198, doi:10.1039/C6NR08102A.

13. Zhang, S.; Sun, H. J.; Hughes, A. D.; Draghici, B.; Lejnieks, J.; Leowanawat, P.; Bertin, A.; Otero De Leon, L.; Kulikov, O. V.; Chen, Y.; Pochan, D. J.; Heiney, P. A.; Percec, V. "Single-Single" Amphiphilic Janus Dendrimers Self-Assemble into Uniform Dendrimersomes with Predictable Size. *ACS Nano* **2014**, *8*, 1554–1565.

14. Zhang, S.; Sun, H. J.; Hughes, A. D.; Moussodia, R. O.; Bertin, A.; Chen, Y.; Pochan, D. J.; Heiney, P. A.; Klein, M. L.; Percec, V. Self-assembly of amphiphilic Janus dendrimers into uniform onion-like dendrimersomes with predictable size and number of bilayers. *Proc. Natl. Acad. Sci. U. S. A.* **2014**, *111*, 9058–63, doi:10.1073/pnas.1402858111.

15. Ihre, H.; Hult, A.; Fréchet, J. M. J.; Gitsov, I. Double-Stage Convergent Approach for the Synthesis of Functionalized Dendritic Aliphatic Polyesters Based on 2,2-Bis(hydroxymethyl)propionic Acid. *Macromolecules* **1998**, *31*, 4061–4068, doi:10.1021/ma9718762.

16. Caminade, A.; Yan, D.; Smith, D. K.; Buhleier, E.; Wehner, W.; Vögtle, F.; Tomalia, D. A.; Baker, H.; Dewald, J.; Hall, M.; Kallos, G.; Martin, S.; Roeck, J.;

Ryder, J.; Smith, P.; Newkome, G. R.; Yao, Z.; Baker, G. R.; Gupta, V. K.; Flory, P. J. Dendrimers and hyperbranched polymers. *Chem. Soc. Rev.* **2015**, *44*, 3870–3873, doi:10.1039/C5CS90049B.

17.   Bugno, J.; Hsu, H.-J.; Hong, S. Recent advances in targeted drug delivery approaches using dendritic polymers. *Biomater. Sci.* **2015**, *3*, 1025–1034, doi:10.1039/C4BM00351A.

18.   Hawker, C. J.; Fréchet, J. M. J. Preparation of Polymers with Controlled Molecular Architecture. A New Convergent Approach to Dendritic Macromolecules. *J. Am. Chem. Soc.* **1990**, *112*, 7638–7647, doi:10.1021/ja00177a027.

19.   Venkataraman, S.; Hedrick, J. L.; Ong, Z. Y.; Yang, C.; Ee, P. L. R.; Hammond, P. T.; Yang, Y. Y. The effects of polymeric nanostructure shape on drug delivery. *Adv. Drug Deliv. Rev.* **2011**, *63*, 1228–1246, doi:10.1016/j.addr.2011.06.016.

20.   Park, C.; Lee, J.; Kim, C. Functional supramolecular assemblies derived from dendritic building blocks. *Chem. Commun.* **2011**, *47*, 12042, doi:10.1039/c1cc11531f.

21.   Caminade, A.-M.; Laurent, R.; Delavaux-Nicot, B.; Majoral, J.-P. "Janus" dendrimers: syntheses and properties. *New J. Chem.* **2012**, *36*, 217, doi:10.1039/c1nj20458k.

22.   Pan, J.; Wen, M.; Yin, D.; Jiang, B.; He, D.; Guo, L. Design and synthesis of novel amphiphilic Janus dendrimers for bone-targeted drug delivery. *Tetrahedron* **2012**, *68*, 2943–2949, doi:10.1016/j.tet.2012.02.040.

23.   Gillies, E. R.; Fréchet, J. M. J. Designing macromolecules for therapeutic applications: polyester dendrimer-poly(ethylene oxide) "bow-tie" hybrids with tunable molecular weight and architecture. *J. Am. Chem. Soc.* **2002**, *124*, 14137–46.

24.   Ropponen, J.; Nummelin, S.; Rissanen, K. Bisfunctionalized Janus molecules. *Org. Lett.* **2004**, *6*, 2495–7, doi:10.1021/ol049555f.

25.   Peterca, M.; Percec, V.; Leowanawat, P.; Bertin, A. Predicting the size and properties of dendrimersomes from the lamellar structure of their amphiphilic janus dendrimers. *J. Am. Chem. Soc.* **2011**, *133*, 20507–20, doi:10.1021/ja208762u.

26. Kalhapure, R. S.; Akamanchi, K. G. Oleodendrimers: a novel class of multicephalous heterolipids as chemical penetration enhancers for transdermal drug delivery. *Int. J. Pharm.* **2013**, *454*, 158–66, doi:10.1016/j.ijpharm.2013.07.028.

27. Shao, S.; Si, J.; Tang, J.; Sui, M.; Shen, Y. Jelly fish-Shaped Amphiphilic Dendrimers: Synthesis and Formation of Extremely Uniform Aggregates. **2014**.

28. Nazemi, A.; Schon, T. B.; Gillies, E. R. Synthesis and Degradation of Backbone Photodegradable Polyester Dendrimers. **2013**, 12–15.

29. Tuuttila, T.; Lahtinen, M.; Kuuloja, N.; Huuskonen, J.; Rissanen, K. Synthesis and thermal behavior of Janus dendrimers, part 1. *Thermochim. Acta* **2010**, *497*, 101–108, doi:10.1016/j.tca.2009.08.018.

30. Tuuttila, T.; Lahtinen, M.; Huuskonen, J.; Rissanen, K. Synthesis and thermal behavior of Janus dendrimers, part 2. *Thermochim. Acta* **2010**, *497*, 109–116, doi:10.1016/j.tca.2009.08.019.

31. Giustini, M.; Bellinazzo, C.; Galantini, L.; Mallardi, A.; Palazzo, G.; Sennato, S.; Bordi, F.; Rissanen, K. Incorporation of the bacterial reaction centre into dendrimersomes. *Colloids Surfaces A Physicochem. Eng. Asp.* **2012**, *413*, 38–43, doi:10.1016/j.colsurfa.2012.01.040.

32. Grayson, S. M.; Frechet, J. M. J. Synthesis and surface functionalization of aliphatic polyether dendrons. *J. Am. Chem. Soc.* **2000**, *122*, 10335–10344, doi:10.1021/ja001903v.

33. Prabakaran, P.; Prasad, E. Janus Dendrimer from Poly(Aryl Ether) Linked PAMAM for Supergelation and Guest Release. *ChemistrySelect* **2016**, *1*, 5561–5568, doi:10.1002/slct.201601335.

34. Modular Synthesis of Amphiphilic Janus Glycodendrimers and Their Self Assembly into Glycodendrimersomes and Other Complex Architectures with Bioactivity to Biomedically Relevant Lectins 2014.

35. Wang, P.; Ma, Y.; Liu, Z.; Yan, Y.; Sun, X.; Zhang, J. Vesicle formation of catanionic mixtures of CTAC/SDS induced by ratio: a coarse-grained molecular dynamic simulation study. *RSC Adv.* **2016**, *6*, 13442–13449, doi:10.1039/C5RA26051E.

36. Marrink, S. J.; de Vries, A. H.; Mark, A. E. Coarse Grained Model for Semiquantitative Lipid Simulations. *J. Phys. Chem. B* **2004**, *108*, 750–760, doi:10.1021/jp036508g.

37. Thota, N.; Luo, Z.; Hu, Z.; Jiang, J. Self-Assembly of Amphiphilic Peptide (AF)6H5K15 : Coarse-Grained Molecular Dynamics Simulation. *J Phys Chem B* **2013**, *117*, 9690–8, doi:10.1021/jp4059752.

38. Márquez-Miranda, V.; Araya-Durán, I.; Camarada, M. B.; Comer, J.; Valencia-Gallegos, J. A.; González-Nilo, F. D. Self-Assembly of Amphiphilic Dendrimers: The Role of Generation and Alkyl Chain Length in siRNA Interaction. *Sci. Rep.* **2016**, *6*, 29436, doi:10.1038/srep29436.

39. Ianiro, A.; Patterson, J.; González García, A.; van Rijt, M. M. J.; Hendrix, M. M. R. M.; Sommerdijk, N. A. J. M.; Voets, I. K.; Esteves, A. C. C.; Tuinier, R. A roadmap for poly(ethylene oxide)-block-poly-ε-caprolactone self-assembly in water: Prediction, synthesis, and characterization. *J. Polym. Sci. Part B Polym. Phys.* **2018**, *56*, 330–339, doi:10.1002/polb.24545.

40. Rodriguez, N.; Pincet, F.; Cribier, S. Giant vesicles formed by gentle hydration and electroformation: A comparison by fluorescence microscopy. *Colloids Surfaces B Biointerfaces* **2005**, *42*, 125–130, doi:10.1016/j.colsurfb.2005.01.010.

41. Garcia-Manrique, P.; Matos, M.; Gutierrez, G.; Estupiñan, O. R.; Blanco-Lopez, M. C.; Pazos, C. Using Factorial Experimental Design to Prepare Size-Tuned Nanovesicles. *Ind. Eng. Chem. Res.* **2016**, *55*, 9164–9175, doi:10.1021/acs.iecr.6b01552.

42. Xiao, Q.; Rubien, J. D.; Wang, Z.; Reed, E. H.; Hammer, D. A.; Sahoo, D.; Heiney, P. A.; Yadavalli, S. S.; Goulian, M.; Wilner, S. E.; Baumgart, T.; Vinogradov, S. A.; Klein, M. L.; Percec, V. Self-sorting and coassembly of fluorinated, hydrogenated, and hybrid Janus dendrimers into dendrimersomes. *J. Am. Chem. Soc.* **2016**, *138*, 12655–12663, doi:10.1021/jacs.6b08069.

43. Gentine, P.; Bubel, A.; Crucifix, C.; Bourel-Bonnet, L.; Frisch, B. Manufacture of liposomes by isopropanol injection: characterization of the method. *J. Liposome Res.* **2012**, *22*, 18–30, doi:10.3109/08982104.2011.584318.

44. Kaminski, T. S.; Scheler, O.; Garstecki, P. Droplet microfluidics for microbiology:

techniques, applications and challenges. *Lab Chip* **2016**, *16*, 2168–2187, doi:10.1039/C6LC00367B.

45. Zhao, C.-X. Multiphase flow microfluidics for the production of single or multiple emulsions for drug delivery. *Adv. Drug Deliv. Rev.* **2013**, *65*, 1420–1446, doi:10.1016/j.addr.2013.05.009.

46. Baroud, C. N.; Gallaire, F.; Dangla, R. Dynamics of microfluidic droplets. *Lab Chip* **2010**, *10*, 2032–2045, doi:10.1039/c001191f.

47. Walde, P.; Cosentino, K.; Engel, H.; Stano, P. Giant vesicles: preparations and applications. *Chembiochem* **2010**, *11*, 848–65, doi:10.1002/cbic.201000010.

48. Meure, L. A.; Foster, N. R.; Dehghani, F. Conventional and dense gas techniques for the production of liposomes: a review. *AAPS PharmSciTech* **2008**, *9*, 798–809, doi:10.1208/s12249-008-9097-x.

49. Gentine, P.; Bourel-Bonnet, L.; Frisch, B. Modified and derived ethanol injection toward liposomes: development of the process. *J. Liposome Res.* **2013**, *23*, 11–9, doi:10.3109/08982104.2012.717298.

50. Moore, J. S.; Stupp, S. I. Room Temperature Polyesterification. *Macromolecules* **1990**, *23*, 65–70.

51. Appel, R.; Fuchs, J.; Tyrrell, S. M.; Korevaar, P. A.; Stuart, M. C. A.; Voets, I. K.; Schönhoff, M.; Besenius, P. Steric Constraints Induced Frustrated Growth of Supramolecular Nanorods in Water. *Chem. - A Eur. J.* **2015**, *21*, 19257–19264, doi:10.1002/chem.201503616.

52. Schindelin, J.; Arganda-Carreras, I.; Frise, E.; Kaynig, V.; Longair, M.; Pietzsch, T.; Preibisch, S.; Rueden, C.; Saalfeld, S.; Schmid, B.; Tinevez, J.-Y.; White, D. J.; Hartenstein, V.; Eliceiri, K.; Tomancak, P.; Cardona, A. Fiji: an open-source platform for biological-image analysis. *Nat Meth* **2012**, *9*, 676–682.

53. Kim, S.-H.; Kim, J. W.; Cho, J.-C.; Weitz, D. A. Double-emulsion drops with ultra-thin shells for capsule templates. *Lab Chip* **2011**, *11*, 3162–3166, doi:10.1039/c1lc20434c.

54. Arriaga, L. R.; Datta, S. S.; Kim, S. H.; Amstad, E.; Kodger, T. E.; Monroy, F.; Weitz, D. A. Ultrathin shell double emulsion templated giant unilamellar lipid vesicles with controlled microdomain formation. *Small* **2014**, *10*, 950–956,

doi:10.1002/smll.201301904.

55. Abràmoff, M. D.; Magalhães, P. J.; Ram, S. J. Image processing with ImageJ. *Biophotonics Int.* **2004**, *11*, 36–41, doi:10.1117/1.3589100.

56. Griffin, W. C. Calculation of HLB values of non-ionic surfactants. *J. Soc. Cosmet. Chem.* **1954**, *5*, 249–256.

57. Griffin, W. C. Classification of surface-active agents by "HLB." *J. Soc. Cosmet. Chem.* **1949**, *1*, 311–326.

58. Marrink, S. J.; Risselada, H. J.; Yefimov, S.; Tieleman, D. P.; de Vries, A. H. The MARTINI Force Field : Coarse Grained Model for Biomolecular Simulations. *J. Phys. Chem. B* **2007**, *111*, 7812–7824, doi:10.1021/jp071097f.

59. Periole, X.; Marrink, S.-J. The Martini Coarse-Grained Force Field. In *Biomolecular Simulations. Methods in Molecular Biology (Methods and Protocols)*; Monticelli, L., Salonen, E., Eds.; Humana Press: Totowa, NJ, 2013; Vol. 924, pp. 533–565 ISBN 978-1-62703-016-8.

60. Bradley, R.; Radhakrishnan, R. Coarse-grained models for protein-cell membrane interactions. *Polymers (Basel).* **2013**, *5*, 890–936, doi:10.3390/polym5030890.

61. Bussi, G.; Donadio, D.; Parrinello, M. Canonical sampling through velocity rescaling. *J. Chem. Phys.* **2007**, *126*, 14101, doi:10.1063/1.2408420.

62. Thota, N.; Jiang, J. Self-assembly of amphiphilic peptide (AF)6H5K 15 derivatives: Roles of hydrophilic and hydrophobic residues. *J. Phys. Chem. B* **2014**, *118*, 2683–2692, doi:10.1021/jp500406p.

63. Essmann, U.; Perera, L.; Berkowitz, M. L.; Darden, T.; Lee, H.; Pedersen, L. G. A smooth particle mesh Ewald method. *J Chem Phys* **1995**, *103*, 8577–8593, doi:10.1063/1.470117.

64. Humphrey, W.; Dalke, A.; Schulten, K. VMD: Visual molecular dynamics. *J. Mol. Graph.* **1996**, *14*, 33–38, doi:10.1016/0263-7855(96)00018-5.

65. Ali, S.; Minchey, S.; Janoff, A.; Mayhew, E. A differential scanning calorimetry study of phosphocholines mixed with paclitaxel and its bromoacylated taxanes. *Biophys. J.* **2000**, *78*, 246–256, doi:10.1016/S0006-3495(00)76588-X.

66. Demetzos, C. Differential Scanning Calorimetry (DSC): A tool to study the thermal behavior of lipid bilayers and liposomal stability. *J. Liposome Res.* **2008**, *18*, 159–

173, doi:10.1080/08982100802310261.

67. Tsumoto, K.; Matsuo, H.; Tomita, M.; Yoshimura, T. Efficient formation of giant liposomes through the gentle hydration of phosphatidylcholine films doped with sugar. *Colloids Surfaces B Biointerfaces* **2009**, *68*, 98–105, doi:10.1016/j.colsurfb.2008.09.023.

68. Erb, R. M.; Obrist, D.; Chen, P. W.; Studer, J.; Studart, A. R. Predicting sizes of droplets made by microfluidic flow-induced dripping. *Soft Matter* **2011**, *7*, 8757–8761, doi:10.1039/c1sm06231j.

69. Zhao, C. X.; Chen, D.; Hui, Y.; Weitz, D. A.; Middelberg, A. P. J. Controlled generation of ultrathin-shell double emulsions and studies on their stability. *ChemPhysChem* **2017**, *18*, 1393–1399, doi:10.1002/cphc.201601334.

70. Hayward, R. C.; Utada, A. S.; Dan, N.; Weitz, D. A. Dewetting instability during the formation of polymersomes from block-copolymer-stabilized double emulsions. *Langmuir* **2006**, *22*, 4457–4461, doi:10.1021/la060094b.

71. do Nascimento, D. F.; Arriaga, L. R.; Eggersdorfer, M.; Ziblat, R.; Marques, M. de F. V.; Reynaud, F.; Koehler, S. A.; Weitz, D. A. Microfluidic fabrication of pluronic vesicles with controlled permeability. *Langmuir* **2016**, *32*, 5350–5355, doi:10.1021/acs.langmuir.6b01399.

72. Taabache, S.; Bertin, A. Vesicles from amphiphilic dumbbells and Janus dendrimers: Bioinspired self-assembled structures for biomedical applications. *Polymers (Basel).* 2017, *9*, 280.

73. Parent, L. R.; Bakalis, E.; Ramírez-Hernández, A.; Kammeyer, J. K.; Park, C.; De Pablo, J.; Zerbetto, F.; Patterson, J. P.; Gianneschi, N. C. Directly Observing Micelle Fusion and Growth in Solution by Liquid-Cell Transmission Electron Microscopy. *J. Am. Chem. Soc.* **2017**, *139*, 17140–17151, doi:10.1021/jacs.7b09060.

74. Ruozi, B.; Belletti, D.; Tombesi, A.; Tosi, G.; Bondioli, L.; Forni, F.; Vandelli, M. A. AFM, ESEM, TEM, and CLSM in liposomal characterization: a comparative study. *Int. J. Nanomedicine* **2011**, *6*, 557–563, doi:10.2147/IJN.S14615.

75. Antonietti, M.; Förster, S. Vesicles and Liposomes: A Self-Assembly Principle Beyond Lipids. *Adv. Mater.* **2003**, *15*, 1323–1333, doi:10.1002/adma.200300010.

76. Luman, N. R.; Grinstaff, M. W. Synthesis and aqueous aggregation properties of amphiphilic surface-block dendrimers. *Org. Lett.* **2005**, *7*, 4863–6, doi:10.1021/ol051583q.

77. Ruozi, B.; Tosi, G.; Tonelli, M.; Bondioli, L.; Mucci, A.; Forni, F.; Vandelli, M. A. AFM phase imaging of soft-hydrated samples: A versatile tool to complete the chemical-physical study of liposomes. *J. Liposome Res.* **2009**, *19*, 59–67, doi:10.1080/08982100802584071.

78. Bibi, S.; Kaur, R.; Henriksen-Lacey, M.; McNeil, S. E.; Wilkhu, J.; Lattmann, E.; Christensen, D.; Mohammed, A. R.; Perrie, Y. Microscopy imaging of liposomes: From coverslips to environmental SEM. *Int. J. Pharm.* **2011**, *417*, 138–150, doi:10.1016/j.ijpharm.2010.12.021.

79. Liao, H.-G.; Zheng, H. Liquid Cell Transmission Electron Microscopy. *Annu. Rev. Phys. Chem.* **2016**, *67*, 719–747, doi:10.1146/annurev-physchem-040215-112501.

80. Han, M.; Hong, M.; Sim, E. Influence of the block hydrophilicity of AB2 miktoarm star copolymers on cluster formation in solutions. *J. Chem. Phys.* **2011**, *134*, 204901, doi:10.1063/1.3586804.

81. Yamamoto, S.; Maruyama, Y.; Hyodo, S. Dissipative particle dynamics study of spontaneous vesicle formation of amphiphilic molecules. *J. Chem. Phys.* **2002**, *116*, 5842, doi:10.1063/1.1456031.

82. Wang, Z.; He, X. Dynamics of vesicle formation from lipid droplets: Mechanism and controllability. *J. Chem. Phys.* **2009**, *130*, 94905, doi:10.1063/1.3079097.

83. Shinoda, W.; Devane, R.; Klein, M. L. Zwitterionic lipid assemblies: Molecular dynamics studies of monolayers, bilayers, and vesicles using a new coarse grain force field. *J. Phys. Chem. B* **2010**, *114*, 6836–6849, doi:10.1021/jp9107206.

84. Israelachvili, J. N.; Mitchell, D. J.; Ninham, B. W. Theory of self-assembly of hydrocarbon amphiphiles into micelles and bilayers. *J. Chem. Soc. Faraday Trans. 2* **1976**, *72*, 1525, doi:10.1039/f29767201525.

85. Arai, N.; Yoshimoto, Y.; Yasuoka, K.; Ebisuzaki, T. Self-assembly behaviours of primitive and modern lipid membrane solutions: a coarse-grained molecular simulation study. *Phys. Chem. Chem. Phys.* **2016**, *18*, 19426–19432, doi:10.1039/C6CP02380K.

86. Kremer, J. M.; Esker, M. W.; Pathmamanoharan, C.; Wiersema, P. H. Vesicles of Variable Diameter Prepared by a Modified Injection Method. *Biochemistry* **1977**, *16*, 3932–3935, doi:10.1021/bi00636a033.

Published papers

molecules

Article

Self-Assembly Behavior of Amphiphilic Janus Dendrimers in Water: A Combined Experimental and Coarse-Grained Molecular Dynamics Simulation Approach

Mariana E. Elizondo-García [1,*], **Valeria Márquez-Miranda** [2], **Ingrid Araya-Durán** [2],
Jesús A. Valencia-Gallegos [1,*] **and Fernando D. González-Nilo** [2,3]

[1] Escuela de Ingeniería y Ciencias, Tecnológico de Monterrey, Av. Eugenio Garza Sada 2501 Sur, Monterrey 64849, Mexico

[2] Center for Bioinformatics and Integrative Biology (CBIB), Facultad de Ciencias Biológicas, Universidad Andrés Bello, Av. República 330, Santiago 8370186, Chile; valeria.marquez.m@gmail.com (V.M.-M.); ingrid.araya.duran@gmail.com (I.A.-D.); fernando.gonzalez@unab.cl (F.D.G.-N.)

[3] Centro Interdisciplinario de Neurociencia de Valparaíso, Facultad de Ciencias, Universidad de Valparaíso, Gran Bretaña 1111, Playa Ancha, Valparaíso 2360102, Chile

* Correspondence: mariana.elizndo@gmail.com (M.E.E.-G); valencia@itesm.mx (J.A.V.-G); Tel.: +52-818-358-2000 (ext. 4511) (J.A.V.-G)

check for updates

Abstract: Amphiphilic Janus dendrimers (JDs) are repetitively branched molecules with hydrophilic and hydrophobic components that self-assemble in water to form a variety of morphologies, including vesicles analogous to liposomes with potential pharmaceutical and medical application. To date, the self-assembly of JDs has not been fully investigated thus it is important to gain insight into its mechanism and dependence on JDs' molecular structure. In this study, the aggregation behavior in water of a second-generation bis-MPA JD was evaluated using experimental and computational methods. Dispersions of JDs in water were carried out using the thin-film hydration and ethanol injection methods. Resulting assemblies were characterized by dynamic light scattering, confocal microscopy, and atomic force microscopy. Furthermore, a coarse-grained molecular dynamics (CG-MD) simulation was performed to study the mechanism of JDs aggregation. The obtaining of assemblies in water with no interdigitated bilayers was confirmed by the experimental characterization and CG-MD simulation. Assemblies with dendrimersome characteristics were obtained using the ethanol injection method. The results of this study establish a relationship between the molecular structure of the JD and the properties of its aggregates in water. Thus, our findings could be relevant for the design of novel JDs with tailored assemblies suitable for drug delivery systems.

Keywords: Janus dendrimers; amphiphilic; self-assembly; coarse-grained molecular dynamics

---

1. Introduction

Amphiphilic Janus dendrimers (JDs) are molecules composed of polar (hydrophilic) and non-polar (hydrophobic) dendritic blocks [1]. This characteristic is the key factor that favors the spontaneous self-assembly of JDs in water into complex supramolecular structures [2]. The variation in the chemical structure of JDs allows achieving a rich palette of morphologies in water, such as cubosomes, disks, tubular vesicles, helical ribbons and bilayered vesicles, termed as dendrimersomes [3].

Curriculum Vitae

Mariana Estefanía Elizondo García was born in Monterrey, México, on September 9, 1988. She earned her BSc in Industrial Chemistry from the *Universidad Autónoma de Nuevo León* in December 2009 and her MSc in Biotechnology from the *Instituto Tecnológico y de Estudios Superiores de Monterrey*, Monterrey Campus in May 2012. She was accepted in the graduate program in Biotechnology in January 2014, working under the supervision of Dr. Jesús A. Valencia Gallegos. This thesis represents the termination of her Doctoral studies.

This document was typed in using Microsoft Word by Mariana E. Elizondo García